Optimization Study of a Trans-Atlantic Abort for the U.S. Space Shuttle Using a Pseudospectral Legendre Method

by

Christine P. Taylor
B.S. Mechanical and Aerospace Engineering, Cornell University, 2001

Submitted to the Department of Aeronautics and Astronautics
in partial fulfillment of the requirements for the degree of
Master of Science in Aeronautics and Astronautics
at the
MASSACHUSETTS INSTITUTE OF TECHNOLOGY
September 2003

Author .....
Department of Aeronautics and Astronautics
August 22, 2003

Certified by .....
Anil V. Rao, Ph.D.
Senior Member of the Technical Staff
The Charles Stark Draper Laboratory, Inc.
Technical Supervisor

Certified by .....
Jonathan P. How, Ph.D.
Professor, Department of Aeronautics and Astronautics
Thesis Advisor

Accepted by .....
Edward M. Greitzer, Ph.D.
H.N. Slater Professor of Aeronautics and Astronautics
Chair, Committee on Graduate Students

[This page intentionally left blank.]

Optimization Study of a Trans-Atlantic Abort for the U.S. Space Shuttle Using a Pseudospectral Legendre Method

by

Christine P. Taylor

Submitted to the Department of Aeronautics and Astronautics
on August 22, 2003, in partial fulfillment of the
requirements for the degree of
Master of Science in Aeronautics and Astronautics

Abstract

The problem of performance optimization for a trans-atlantic shuttle abort is considered. At five points during the second stage of ascent, a failure of a main engine occurs, which necessitates an abort from the nominal mission. The abort trajectories generated initiate from the current state at the time of abort and terminate at the TAEM interface for a landing site. The abort trajectories consist of three regimes, or phases of flight, and each phase has a different dynamic model governing the motion of the vehicle. To ensure a solution is obtained for each abort, additional constraints on the vehicle are formulated as soft constraints in the penalty function. In particular, the third phase cost functional consists of a weighted combination of heating rate, dynamic pressure and sensed acceleration. Thus, the problem formulation is one of a multiple phase optimal control problem. A Pseudospectral Legendre Method is used to discretize the optimal control problem into a nonlinear programming problem, which is then solved using a sparse nonlinear optimizer. The first study conducted compares the trajectories generated to each landing site for various combinations of third phase cost functional weighting factors. A cost calculation is developed to compare each optimized abort trajectory. The second study evaluates the significance of the improvements due to the chosen weighting factor combination with that of an entry aerodynamic model uncertainty.

Technical Supervisor: Anil V. Rao, Ph.D.
Title: Senior Member of the Technical Staff
The Charles Stark Draper Laboratory, Inc.

Thesis Advisor: Jonathan P. How, Ph.D.
Title: Professor, Department of Aeronautics and Astronautics

[This page intentionally left blank.]

Acknowledgments

I would like to thank everyone who made the completion of my Master's degree possible. First, I would like to thank the Charles Stark Draper Laboratory for providing me with the funding and support necessary to complete my degree. I am especially grateful to the GCB2 staff and the Education Office. In particular, I would like to thank individually Ron Proulx and Anil Rao. Ron, I learned a lot from you and it is too bad that we never got to go to Mars together. Anil, I want to offer you a special thanks for sharing your insights and understanding with me and for helping me with my thesis. I will miss the coffee breaks and corny jokes.

I would like to thank the MIT professors and Aero/Astro staff. In my two years at MIT, I have had the privilege of studying under some of the brightest men and women in the field. I would especially like to thank Professor How for his guidance on my thesis research and for being my qualifying exam advocate. I would also like to thank Professor Murman for being my mentor and for helping me to realize my goals while keeping my sanity.

To my friends at MIT, these past two years have been filled with such excitement and frustration and it has been wonderful to share both with all of you. I will always remember the 'forget your lunch Fridays' group and all of the good times shared. Jen, thanks for the Friday breakfasts that made coming to work bearable. Geoff, thanks for bar golf and taco nights. Dave, thanks for riding with me on the T to parties, for feeding Sasha and for my wonderful wok. Heidi, thanks for the lunches, shopping and eating Indian food with me. To Daveed, thanks for cleaning up on Thursday nights, for the math tutoring sessions, but most of all, for being such a wonderful friend. Kim, thanks for the bathroom breaks, the late night popcorn, the shopping trips, but most of all, thanks for being my girl. For the first year Draper fellows, I wish you all the best in your future endeavors and for all those taking the qualifying exam, Good Luck!

I would also like to thank my friends and family who got me through this

process by providing me with support and distractions. Chris, thanks for the late night talks and for conversations about the ever-shrinking world we live in. Sarah, thanks for listening to my gripes and playing darts with me. Erica and Allison, thanks for taking my mind off of my work and making me laugh. Alex, thanks for DJ'ing that Saturday night over a year ago. This past year has been the most wonderful because of you. Thanks for keeping me going when I ran out of steam, for always having confidence in me and for showing me what love really is. Last, but most important, I would like to thank my parents. Thanks for always believing in me, even when I didn't, for supporting me through all of the challenges that have past and all that lie ahead. Without your love and support I would never have made it as far as I have. Thank you.

This thesis was prepared at The Charles Stark Draper Laboratory, Inc., under Internal Research and Development, Project Advanced Guidance and Trajectory Design, 15253.

Christine P. Taylor .....

[This page intentionally left blank.]

[This page intentionally left blank.]

Contents

List of Figures

List of Tables

Nomenclature

α	=	Angle of attack
β	=	Thrust angle of attack
χ	=	Heading angle
ϕ	=	Latitude
γ	=	Flight path angle
θ	=	Longitude
ψ	=	Euler pitch angle
ζ	=	Euler roll angle
σ	=	Bank angle
$\mathbf{r}$	=	Position
r	=	Radius
h	=	Altitude
$\mathbf{v}$	=	Velocity
v	=	Speed
M	=	Mach number
B	=	Ballistic coefficient
R_e	=	Earth radius
ρ	=	Density
m	=	mass
$\mathbf{g}$	=	Gravitational acceleration
$\mathbf{L}$	=	Lift acceleration
L	=	Magnitude of lift acceleration
C_L	=	Lift coefficient
$\mathbf{D}$	=	Drag acceleration
D	=	Magnitude of drag acceleration
D_L	=	Drag coefficient
$\mathbf{T}$	=	Thrust

AOA = Abort once around

ATO = Abort to orbit

ET = External tank

ME = Main engine

$NASA$ = National aeronautics and space administration

OMS = Orbital maneuvering system

RCS = Reaction control system

RLV = Reusable launch vehicle

$RTLS$ = Return to launch site

TAL = Drag coefficient

$TAEM$ = Terminal area energy management

Chapter 1

Introduction

1.1 Motivation

In the wake of the recent U.S. Space Shuttle tragedy there is a renewed interest in redesigning current space flight vehicles to take advantage of recent technological developments. The current methods for space shuttle travel use circa 1970's flight computers, which rely on loaded trajectories that are computed prior to launch. The loaded trajectories require intensive pre-flight design and restrict the vehicle to tight flight corridors which reduce robustness to changing flight conditions and environmental factors [14]. The next generation of reusable launch vehicles under consideration is looking to improve the current ascent and entry procedures by using technological developments to redesign the associated guidance algorithms [9, 28]. The ability to rapidly generate trajectories would reduce pre-flight design time and costly mission delays.

Along with redesigning the nominal mission planning and guidance, the next generation space flight vehicle should have an increased ability to handle an abort. Currently, all abort contingencies are pre-defined and loaded into the computer, which severely limits the recovery of a vehicle if the conditions at the time of an abort do not coincide with the pre-programmed trajectories. Currently, NASA has four abort contingencies that provide for recovery of the crew and vehicle. The four abort procedures are: return to launch site (RTLS), trans-

atlantic abort (TAL), abort to orbit (ATO) and abort once around (AOA). Each of these abort procedures are chosen based on a timer. That is, once the decision to abort is made, the mode of abort chosen is determined by the time into flight. However, choosing the abort trajectory in this manner does not allow the current state information to be taken into account, which can severely limit the recovery of the vehicle in the event of an off-nominal failure.

The ability to have an on-board autonomous abort planner would allow the accurate assessment of the current state and conditions and determine the best course of action. An autonomous abort planner would have a two level decision cycle. At the bottom level, a trajectory optimization scheme would calculate the control necessary to move the vehicle from the current state to a specified landing site using the available information. At the top level, the computer would analyze different trajectories computed to various landing sites and determine which is the best route to follow. This cycle may be repeated during the abort to ensure a safe return of the crew and vehicle.

The ability to perform an autonomous abort requires the real time optimization of an abort trajectory. Although, real time optimization of an abort is not currently available, the method for trajectory optimization used in this research has shown promise in this area. Nonetheless, the ability to optimize a trajectory that has multiple parts or phases with different nonlinear dynamics in each phase and subject to stressing conditions throughout is a necessary first step.

1.2 Mission Design Problem

The particular problem under consideration in this thesis is a Space Shuttle abort due to the failure of a single Space Shuttle main engine. The abort initiates at various points along the second stage ascent trajectory and terminates at one of the trans-atlantic abort landing sites. At specified times along the nominal ascent, an engine failure occurs and from this point, a trajectory is generated to the chosen landing site using the initial state information as well as the limited

thrust capacity. Terminal conditions at the TAEM interface for a landing site are imposed.

To appropriately model a trans-atlantic abort of a shuttle, certain constraints on the vehicle must be imposed. Since an abort initiates before main engine cutoff, the vehicle must drop the external tank at some point during the abort, which changes the vehicle model. Also, at high-altitudes, aerodynamic forces are negligible, which increases the vehicle's maneuverability. Finally, the vehicle is un-powered as it approaches the terminal conditions. To naturally model the changes in the vehicle's structure and capability, the abort problem is split into three phases of flight, where each phase corresponds to a different vehicle model. Thus, a different dynamic model with the corresponding vehicle model is used describe the motion of the vehicle over different segments of flight.

Although, there are many constraints on the vehicle during these three phases of flight, the desire to create a trajectory is primary. Thus, flight constraints such as heating rate, dynamic pressure and sensed acceleration are not imposed. Instead, these constraints are included in the cost functional for the third phase as penalty functions and the trajectory is optimized such that the violation of these constraints is minimized. Weighting factors are assigned to each term in the third phase cost functional and an optimal trajectory is computed for different values of the weighting factors. For each initial condition and for each set of weighting factors a trajectory is computed to two different landing sites, Spain and Senegal.

The abort trajectory planning problem stated above constitutes an optimal control problem. This optimal control problem is nonlinear and is solved using a numerical method. Although, there are many numerical methods available for solving optimal control problems, the complexity of a multiple phase optimal control problem severely limits this choice. A method that has come into prominence recently, is the Pseudospectral Legendre method. This method allows for the discretization of the multiple phase optimal control problem to occur naturally and yields a solution for the problem as a whole. In this thesis,

the Pseudospectral Legendre method is applied to the problem of shuttle abort trajectory generation.

1.3 Research Objectives

This thesis seeks to demonstrate the application of the Pseudospectral Legendre method to the problem of shuttle abort trajectory optimization. All trajectories are computed and compared to determine which landing site and which third phase cost functional weighting factor combination is best for a given initial condition. Essential characteristics of the trajectory are analyzed and the trajectory is evaluated to determine how 'flyable' it is. To evaluate the usefulness of varying the weighting factors, a study is performed that compares the effects on a trajectory due to model uncertainties with that of the chosen weighting factor combination for each abort.

1.4 Thesis Overview

Chapter 2 gives a basic description of the shuttle components, mission procedures and abort methods. The first part of Chapter 3 describes the vehicle model used in each phase of the trajectory. The second half of Chapter 3 presents the coordinate reference frame and dynamic equations that describe the motion of the vehicle during the different phases of flight. Chapter 4 describes the abort considered in this research and defines the additional constraints on the problem. Chapter 5 discusses the optimization criteria selection and describes the resulting optimal control problem. Chapter 6 presents an overview of various solution methods for optimal control problems. Then, a detailed description of the solution method chosen, the Pseudospectral Legendre method, is given followed by the extensions of this method to a multiple phase optimal control problem. Chapter 7 presents the results obtained by applying the Pseudospectral Legendre method to the abort problem. The characteristics of the abort trajectories as

well as the selection of the best weighting factor combination for each abort is presented. An evaluation of the effectiveness of the selected optimization criteria follows. Finally, Chapter 8 provides a summary of the material presented in this thesis and the conclusions obtained.

[This page intentionally left blank.]

Chapter 2

Shuttle Overview

The purpose of this chapter is to give a general description of the shuttle and detail the current NASA abort procedures. All information pertaining to the shuttle and the NASA mission procedures in this chapter is taken from the Shuttle Reference Manual [35] and presented here for completeness. First, a physical description of the shuttle is given followed by an overview of nominal mission procedures. Then, a description of the current procedures for an abort are presented.

2.1 Physical Description of Shuttle

The four main components of the shuttle are the orbiter, the two solid rocket boosters (SRB), the external tank (ET), and three Space Shuttle main engines (ME). The orbiter is a reusable vehicle that houses the crew and carries the payload to orbit. The orbiter houses the Orbital Maneuvering System (OMS) engines and the primary Reaction Control System (RCS) engines along with the fuel supply for both. The two OMS engines each provide 6000 lbs of thrust and are used for orbit insertion, velocity maneuvers in orbit and deorbit. The thirty-eighty primary RCS engines maintain the vehicle's attitude during external tank separation from the orbiter and maintain attitude in orbit. The orbiter is covered by a thermal heat shield which protects the vehicle and crew from the intense temperatures

during entry.

The two solid rocket boosters are attached to the external tank and provide the bulk of thrust for lift off. Each booster has a sea level thrust of approximately $3,300,000$ lbs. Each solid rocket booster is 149.16 ft long and 12.17 ft in diameter and each weighs approximately $1,300,000$ lbs at launch.

The external tank houses the fuel for the Space Shuttle main engines. The external tank is 153.8 ft long and 27.6 ft in diameter and weighs $1,655,600$ lbs fully loaded ($66,000$ lbs of dry weight). The external tank is connected to the shuttle at one forward point and two aft points. At the aft connections, umbilicals carry fluids, gases, electrical signals and power between the orbiter and the external tank.

The three Space Shuttle main engines provide the thrust after solid rocket booster depletion and detachment. Each main engine weighs 7000 lbs and is attached to the orbiter. The main engine fuel is a combination of liquid hydrogen fuel and liquid oxygen oxidizer, which provides each engine with $470,000$ lbs of vacuum thrust.

2.2 Nominal Mission Description

The shuttle takes off from either Kennedy Space Center in Florida or Vandenberg Air Force Base in California, depending on the desired nominal orbit inclination. For an equatorial orbit, the shuttle is launched from Kennedy Space Center. On the launch pad, the orbiter is facing nose up and is attached to the external tank, as shown in Figure 2-1. All weight rests on the solid rocket boosters which are bolted to the launch pad until takeoff. The main engines are fired first, to assure that all engines are operating properly. The solid rocket boosters are then lit and the bolts holding the boosters to the launch pad are released and the shuttle lifts off. After about two minutes, the solid rocket boosters have expended all fuel and are released from the external tank, which ends the first phase of ascent. The boosters fall into the ocean to be recovered and reused.

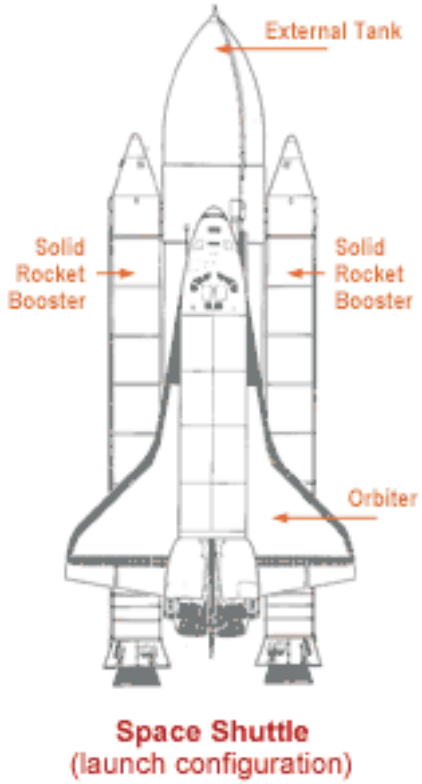

Figure 2-1: Space Shuttle Launch Configuration

The main engines provide the thrust for the second stage of ascent. At the end of ascent, the external tank is dropped and follows a ballistic trajectory into the ocean. To avoid collision between the external tank and orbiter, the primary RCS engines are used to maintain the orbiter's attitude. The OMS engines are fired to place the shuttle into the nominal orbit.

At the end of the mission, the primary RCS engines are fired to rotate the tail of the vehicle in the direction of velocity. The OMS engines are then used to deorbit the vehicle and begin reentry. During reentry, the vehicle glides to the landing site using bank angle maneuvers to remove energy. The vehicle must dissipate enough energy to meet the requirements of the TAEM interface, which removes the remaining excess energy. The vehicle is then captured by the Auto-landing interface and glides to rest on a runway. The possible landing sites for a nominal reentry include Edwards Air Force Base, California, White Sands, New Mexico, Vandenberg Air Force Base, California, and Kennedy Space Center,

Florida.

2.3 Shuttle Abort Procedures

There are four abort procedures used during the shuttle's second stage ascent and exo-atmospheric flight phases: Return to launch site (RTLS), Trans-atlantic abort (TAL), Abort to orbit (ATO), and Abort once around (AOA). All four of these abort techniques recover the crew and vehicle intact.

If the need to abort occurs sometime within the first 4 min and 20 seconds into flight, the shuttle is commanded to return to Kennedy Space Center once the solid rocket boosters have separated. To maneuver the vehicle off of its nominal ascent path to orbit and redirect it to Kennedy Space Center, the shuttle performs a pitch-around, thrust-back maneuver so that it is aligned to perform a landing similar to one performed at entry. The thrusting maneuver allows the vehicle to burn the remaining fuel and drop the external tank before entry. The OMS engine fuel is burned in order to achieve the proper center of gravity and weight for landing. The vehicle proceeds to the TAEM interface where the final approach to the runway is determined.

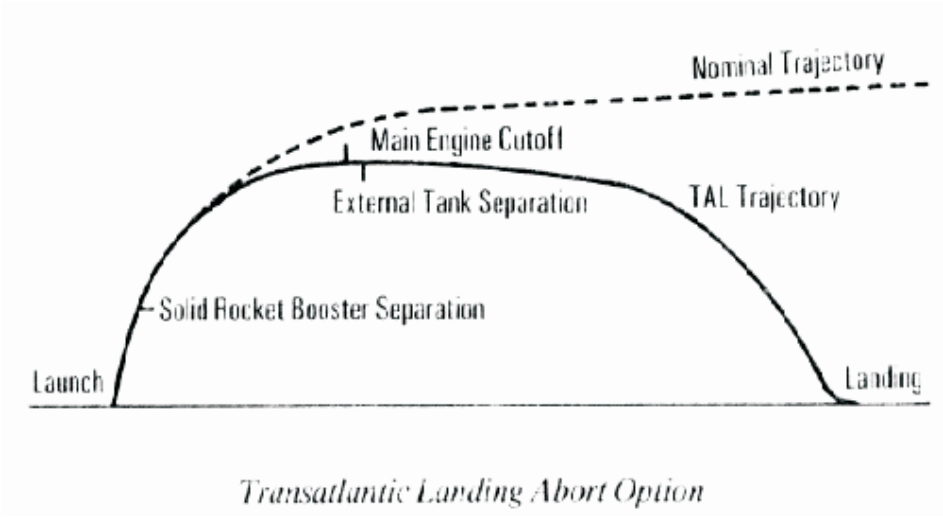

Figure 2-2: Diagram of a Trans-Atlantic Abort

If the need to abort occurs sometime after the first 4 min and 20 seconds

into flight, but before main engine cut-off, the shuttle is commanded to perform a trans-atlantic abort. In this mode, the landing site is chosen by its proximity to the nominal ascent groundtrack position, which is pre-determined before flight. Possible landing sites are Moron, Spain, Dakar, Senegal, or Ben Guerir, Morocco. For this type of abort, the shuttle continues to thrust with both the main engines and OMS engines while properly aligning itself with the TAEM interface at the appropriate landing site. Again, the shuttle depletes the fuel necessary in order to drop the external tank and meet the center of gravity and weight requirements for entry. The shuttle performs a low-altitude entry and reaches the TAEM interface, where the procedures for landing are determined.

If the need to abort occurs after main engine cutoff, or if the speed at main engine cutoff is below the required speed to make the mission orbit, the shuttle will perform an abort to orbit. During an abort to orbit, the OMS engines are used to place the shuttle into a lower circular orbit. Once the appropriate conditions are set for reentry the OMS engines will deorbit the vehicle and the shuttle will perform a nominal reentry.

If the need to abort occurs after main engine cutoff and the OMS engines cannot provide the necessary thrust to perform an abort to orbit, or there is a system failure that requires a quick landing, an abort once around is performed. In this case, the OMS engines perform a sequence of thrusting maneuvers to adjust the initial orbit and then deorbit the vehicle. The shuttle circles the Earth once and performs a nominal reentry.

[This page intentionally left blank.]

Chapter 3

Vehicle Model

The problem under consideration in this thesis is the optimization of a trans-atlantic abort for the U.S. Space Shuttle. Since the purpose of this research is to optimize the path taken by the shuttle during an abort, only the translational motion of the center of mass of the vehicle is modeled. The duration of time for an abort is short enough that the effect of the rotation of the Earth can be neglected. A hybrid dynamic model consisting of three phases is used to simulate a trans-atlantic abort. For the first phase (ME burn) an atmospheric model with the appropriate aerodynamic and control model, is used. During the second phase (high-altitude thrust) an exo-atmospheric model is used with the corresponding control model. In the third phase (entry) an atmospheric model is used with the corresponding aerodynamic and control model. The model is designed with the interest of maintaining the complexity and limitations of a manned RLV, but without making the model the focus of the research. Thus, certain simplifying assumptions have been made and will be noted where appropriate.

3.1 Vehicle Model for Main Engine Burn

Main engine burn is the most difficult phase to model due to all of the constraints imposed on the vehicle. During this phase, the external tank (ET) is still attached to the vehicle, limiting the vehicle's maneuverability and significantly

increasing the weight. During ME burn, aerodynamic forces act on the vehicle and the vehicle can thrust using both of the two remaining main engines and OMS engines.

3.1.1 Aerodynamic Model for Main Engine Burn

The aerodynamic model used for the first phase is taken from Reference 2. This paper defines the x-body axis in the direction of the thrust vector. The x-body axis, $\mathbf{x}_B$, forms a constant 13 degree offset with the vector lying along the nose of the vehicle, $\mathbf{x}_N$, as shown in Figure 3-1.

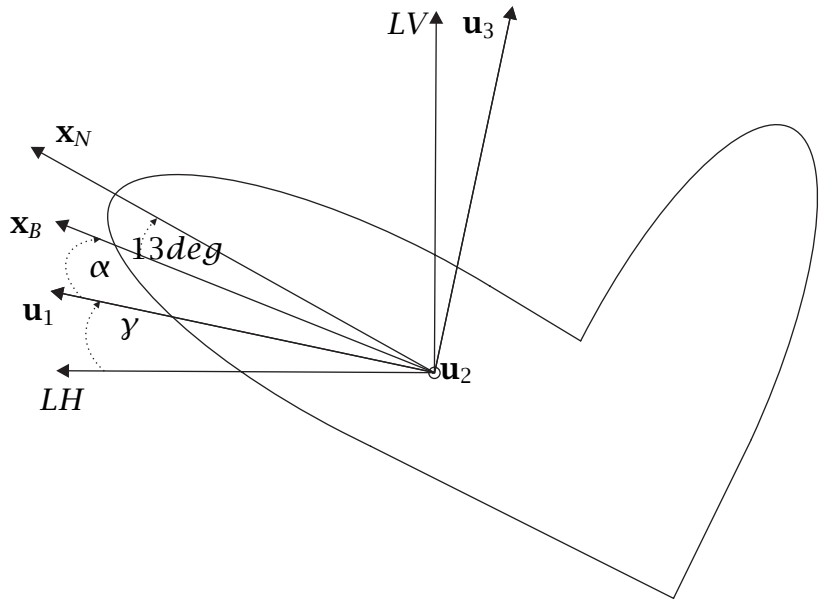

Figure 3-1: Definition of Angle of Attack (α) During ME Burn

The angle of attack, α, is defined as the angle between the unit vector in the direction of velocity ($\mathbf{u}_1$) and $\mathbf{x}_B$. The coefficients of lift and drag, C_L and C_D, are obtained by rotating the trimmed axial and normal coefficients, taken from the Shuttle Design Aerodynamic Data book [33],through the angle of attack plus the 13 degree bias. The expressions for the aerodynamic coefficients are

approximated by trigonometric fits in angle of attack [2].

$$\begin{aligned} C_L &= (C_{L_1} + C_{L_2}M + C_{L_3}M^2) + (C_{L_4} + C_{L_5}M + C_{L_6}M^2)\sin\alpha \\ &\quad + (C_{L_7} + C_{L_8}M + C_{L_9}M^2)\cos\alpha \\ C_D &= (C_{D_1} + C_{D_2}M + C_{D_3}M^2) + (C_{D_4} + C_{D_5}M + C_{D_6}M^2)\sin\alpha \\ &\quad + (C_{D_7} + C_{D_8}M + C_{D_9}M^2)\cos\alpha \end{aligned} \tag{3.1}$$

Since we are assuming that there is a sensible atmosphere at these altitudes, the Mach number, M, is the ratio of the Earth-relative speed to the speed of sound. For simplicity, the speed of sound is assumed to have a constant value of 372.5 m/s. The values of $C_{L_{1-9}}$ and $C_{D_{1-9}}$ are listed in Equation A.1 and Equation A.2, respectively. The aerodynamic coefficients are evaluated and used to calculate the magnitude of the lift and drag accelerations, L and D, respectively. The density is approximated by an exponential model in altitude (h).

$$\begin{aligned} L &= Bv^2C_L\exp(-h/H) \\ D &= Bv^2C_L\exp(-h/H) \end{aligned} \tag{3.2}$$

where

$$\begin{aligned} B &= \frac{\rho_0 S}{2m} \\ h &= r - R_e \end{aligned}$$

Here, B is the ballistic coefficient, h is the altitude above the surface of the earth ($R_e = 6378$ km), H is a constant with a value of 7000 m, ρ_0 is the sea level density ($\rho_0 = 1.225$ kg/m^3), m is the total mass, and S is the cross-sectional area ($S = 250$ m^2). The lift and drag accelerations in Equation 3.2 are defined in this manner to alleviate some numerical difficulties.

3.1.2 Control Model for Main Engine Burn

The control model used for the first phase is chosen to achieve a smooth control. The thrust for the first phase is provided by the two main engines and the OMS engines. Each contribution to the thrust from the main engines and the OMS

engines has a different fuel supply and a different thrust capability. However, the engines thrust in the same direction, so the thrust magnitude is the sum of the two components and is modeled as a total thrust vector, **T**.

The thrust provided by the main engines is taken as twice the thrust provided by a single engine. The thrust magnitude, T_1, may be varied between zero and twice the maximum value of vacuum thrust provided by a single engine, while neglecting ambient pressure. The vacuum thrust for each engine is $2 * 10^6$ N and each engine has a specific impulse, I_{sp_1} of 455.15 seconds [2].

The thrust provided by the OMS engines, T_2, is twice the value of a single thruster and the thrust level may be varied between zero and two times the maximum force of one engine ($T_{max} = 26689$ N). The engines have a specific impulse, I_{sp_2} of 313 seconds [35].

The angle of attack determines the magnitude of the lift and drag accelerations. To limit the rate of change of the angle of attack, an additional state for α is included in the dynamic model and the rate of change of angle of attack is equal to a pseudo-control, w_1.

$$\dot{\alpha} = w_1$$

A pseudo-control allows the rate of change of the angle of attack to be bounded and thus a smoother control profile is achieved.

The direction of the aerodynamic forces and thrust is determined by the cosine and sine components of the bank angle and thrust angle of attack. Defining u_1 through u_4 as given in Equation 3.3 achieves a smoother control profile.

$$\begin{aligned} u_1 &= \cos\sigma \\ u_2 &= \sin\sigma \\ u_3 &= \cos\beta \\ u_4 &= \sin\beta \end{aligned} \tag{3.3}$$

By defining the control in this manner, a constraint for each angle must be added that requires the sum of the squares of the components of the angle equal one.

3.2 Vehicle Model for High-Altitude Thrust

The vehicle model for high-altitude thrust is easier to define. Since the vehicle is required to be above 60 km during this phase, the aerodynamic forces are neglected. The high altitude maintained during flight allows for greater maneuverability. The only two forces acting on the vehicle are thrust and the gravitational force.

3.2.1 Control Model for High-Altitude Thrust

The thrust magnitude and direction provide the control for the second phase. During high-altitude thrust, the thrust is provided by the OMS engines. The engines thrust with the remaining fuel from the first phase and maneuver the vehicle into the position for entry.

The Euler pitch and roll angles, ζ and ψ, respectively, define the thrust direction for this phase. To ensure a smooth control profile, the products of the sines and cosines of the angles and not the individual components are the control and thus enter the equations of motional linearly.

$$\begin{aligned} u_5 &= \cos\zeta\cos\psi \\ u_6 &= \sin\zeta\cos\psi \\ u_7 &= \sin\psi \end{aligned}$$

3.3 Vehicle Model for Entry

During the third phase, the vehicle is descending into the lower atmosphere to reach the TAEM interface for a particular landing site. The TAEM interface conditions enforce a final value on the radius, speed, and flight path angle, as well as a narrow range in longitude and latitude. During entry, the vehicle does not have any thrust capability and must maneuver to the terminal interface using only the aerodynamic forces acting on the vehicle.

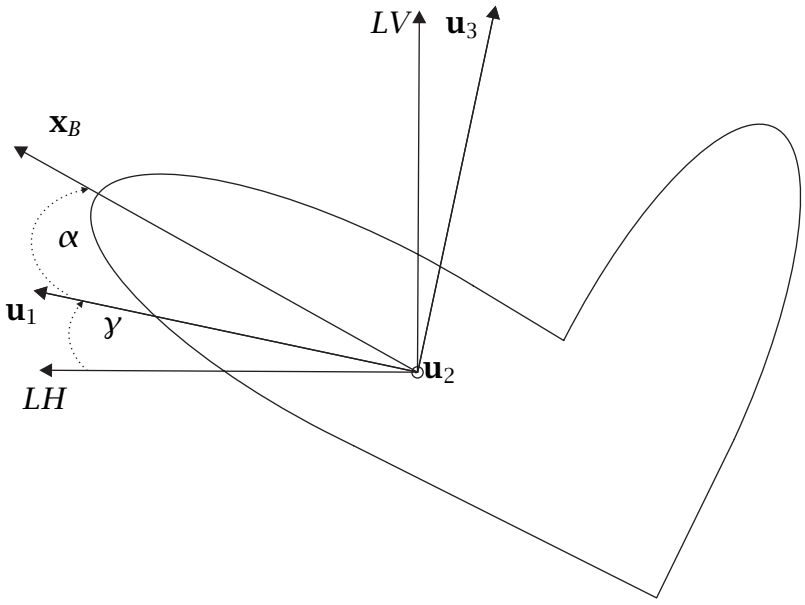

Figure 3-2: Definition of Angle of Attack (α) During Entry

3.3.1 Aerodynamic Model for Entry

The aerodynamic model for entry is taken from Reference 39. During entry, the angle of attack, α, is defined as the angle between the x-body axis and the unit vector in the direction of velocity ($\mathbf{u}_1$), as shown in Figure 3-2.

The x-body axis is defined to lie along the nose of the vehicle and pass through the center of mass. The expressions for the aerodynamic coefficients, C_L and C_D, respectively, are approximated by polynomic fits in angle of attack [39].

$$\begin{aligned} C_L &= C_{L_0} + C_{L_1}\alpha \\ C_D &= C_{D_0} + C_{D_1}\alpha + C_{D_2}\alpha^2 \end{aligned} \tag{3.4}$$

The values for $C_{L_{0-1}}$ and $C_{D_{0-2}}$ are listed in Equation A.3 and Equation A.4, respectively. The aerodynamic coefficients are evaluated and used to calculate the magnitude of the lift and drag accelerations, L and D, respectively using the same relations as in Equation 3.2.

3.3.2 Control Model for Entry

The control model for entry, is chosen to produce a smooth control. In order to limit the rate of change of the angle of attack, an additional state for α is added. The corresponding differential equation sets the rate of change of angle of attack equal to a pseudo-control, w_2.

$$\dot{\alpha} = w_2$$

Bounds are imposed on the pseudo-control, which limits the rate of change of α and thus a smoother control profile is achieved.

The bank angle enters the control as the cosine and sine component of the bank angle, u_8 and u_9, respectively.

$$\begin{aligned} u_8 &= \cos\sigma \\ u_9 &= \sin\sigma \end{aligned}$$

By defining the control in this manner a constraint on the sum of the squares of the components of the bank angle is required.

3.4 Coordinate Systems

The first step in defining a dynamic model is to choose a coordinate system. For this problem, a rotating-radial coordinate system is chosen and the equations of motion are given in spherical coordinates. The spherical coordinate equations of motion are derived as follows. Suppose we are given an Earth-centered inertial (ECI) coordinate system as shown in Figure 3-3 where, r is the radius, θ is the longitude and ϕ is the latitude. As shown, the $\{\mathbf{E}_x, \mathbf{E}_y\}$ plane coincides with the equatorial plane and the $\mathbf{E}_x$-direction passes through the equator along the line of zero longitude. The position is given in Cartesian coordinates as

$$\mathbf{r} = x\mathbf{E}_x + y\mathbf{E}_y + z\mathbf{E}_z$$

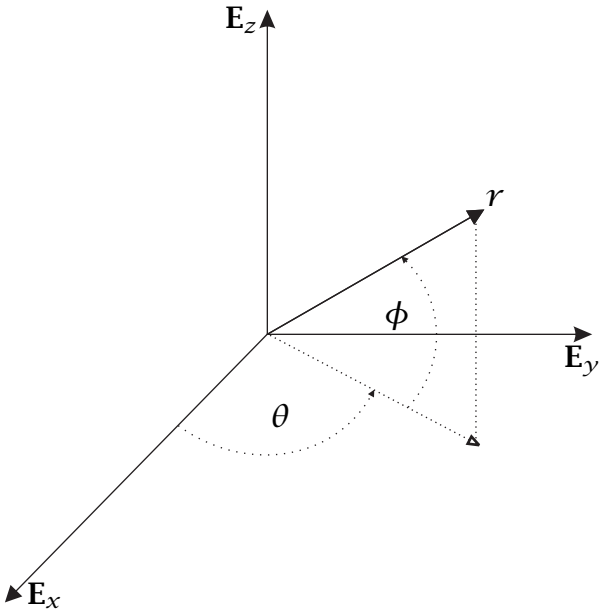

Figure 3-3: Position Defined in an ECI Coordinate System

In terms of r, θ and ϕ the position can be written as

$$\mathbf{r} = r\cos\theta\cos\phi\mathbf{E}_x + r\sin\theta\cos\phi\mathbf{E}_y + r\sin\phi\mathbf{E}_z \tag{3.5}$$

In terms of **r** the coordinate system described in Figure 3-4 can be defined as:

$$\begin{aligned}
\mathbf{e}_r &= \frac{\mathbf{r}}{\|\mathbf{r}\|} = \frac{\mathbf{r}}{r} \\
\mathbf{e}_\theta &= \frac{\mathbf{E}_z \times \mathbf{r}}{\|\mathbf{E}_z \times \mathbf{r}\|} \\
\mathbf{e}_\phi &= \mathbf{e}_r \times \mathbf{e}_\theta
\end{aligned}$$

The transformation between the coordinate system $\{\mathbf{e}_r, \mathbf{e}_\theta, \mathbf{e}_\phi\}$ and $\{\mathbf{E}_x, \mathbf{E}_y, \mathbf{E}_z\}$ is given in Equation 3.6.

$$[\mathbf{e}_r \;\; \mathbf{e}_\theta \;\; \mathbf{e}_\phi] = \begin{bmatrix} \cos\theta\cos\phi & \sin\theta\cos\phi & \sin\phi \\ -\sin\theta & \cos\theta & 0 \\ -\cos\theta\sin\phi & -\sin\theta\sin\phi & \cos\phi \end{bmatrix} [\mathbf{E}_x \;\; \mathbf{E}_y \;\; \mathbf{E}_z] \tag{3.6}$$

Suppose now, that we define two angles, γ and χ that are measured relative

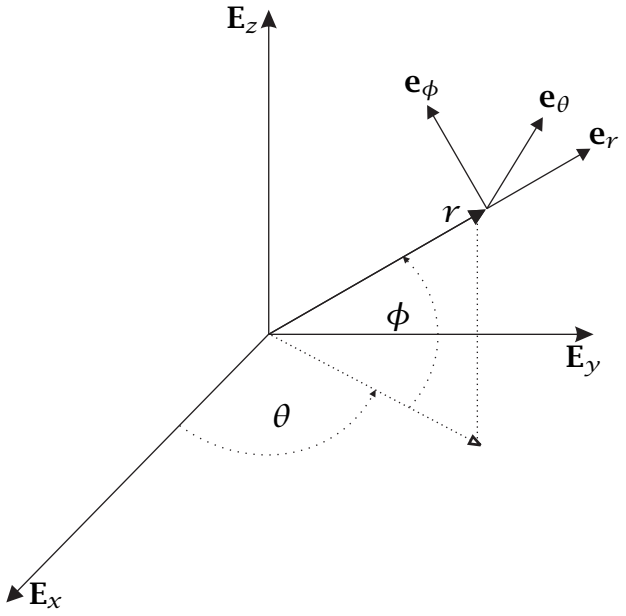

Figure 3-4: Rotating Radial Coordinate System

to the coordinate system $\{\mathbf{e}_r, \mathbf{e}_\theta, \mathbf{e}_\phi\}$ as shown in Figure 3-5. Then the velocity of the vehicle is given as

$$\mathbf{v} = v \sin\gamma \mathbf{e}_r + v \cos\gamma \cos\chi \mathbf{e}_\theta + v \cos\gamma \sin\chi \mathbf{e}_\phi \tag{3.7}$$

where $v = \|\mathbf{v}\|$ is the speed of the vehicle, γ is the flight path angle and χ is the heading angle.

For convenience, the forces are defined in a body-centered velocity coordinate system, as shown in Figure 3-6, and transformed into an Earth-centered frame. To define the body-centered velocity coordinate system, we define the first principle direction, $\mathbf{u}_1$, as the unit vector in the direction of the velocity vector. The second principle direction, $\mathbf{u}_2$, is defined by the unit vector in the direction of specific angular momentum. The third direction, $\mathbf{u}_3$ is chosen to complete a right-handed system as described in Equation 3.8

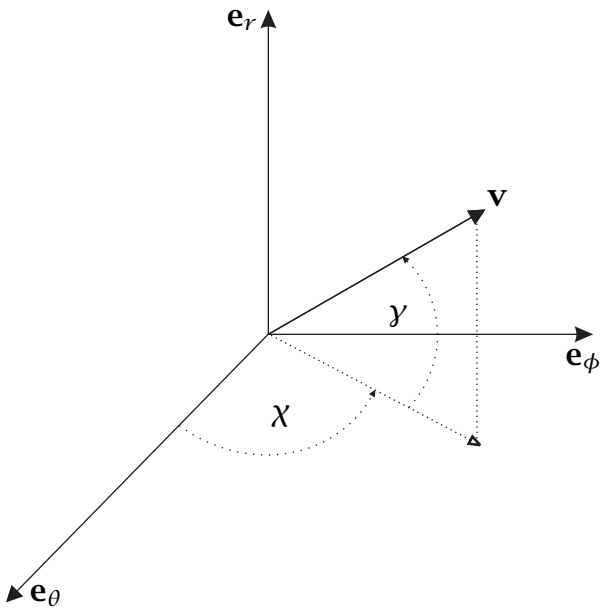

Figure 3-5: Velocity in the $\{\mathbf{e}_r, \mathbf{e}_\theta, \mathbf{e}_\phi\}$ Coordinate System

$$\begin{aligned} \mathbf{u}_1 &= \frac{\mathbf{v}}{\|\mathbf{v}\|} \\ \mathbf{u}_2 &= \frac{\mathbf{r}\times\mathbf{v}}{\|\mathbf{r}\times\mathbf{v}\|} \\ \mathbf{u}_3 &= \mathbf{u}_1\times\mathbf{u}_2 \end{aligned} \tag{3.8}$$

The transformation matrix from the $\{\mathbf{e}_r, \mathbf{e}_\theta, \mathbf{e}_\phi\}$ coordinate system to the $\{\mathbf{u}_1, \mathbf{u}_2, \mathbf{u}_3\}$ coordinate system is

$$[\mathbf{u}_1 \;\; \mathbf{u}_2 \;\; \mathbf{u}_3] = \begin{bmatrix} \sin\gamma & \cos\gamma\cos\chi & \cos\gamma\sin\chi \\ 0 & -\sin\chi & \cos\chi \\ \cos\gamma & -\sin\gamma\cos\chi & -\sin\gamma\sin\chi \end{bmatrix} [\mathbf{e}_r \;\; \mathbf{e}_\theta \;\; \mathbf{e}_\phi]$$

3.5 Equations of Motion

The $\{\mathbf{u}_1, \mathbf{u}_2, \mathbf{u}_3\}$ coordinate system is chosen in order to simplify the decomposition of the forces acting on the vehicle. During atmospheric flight, the forces on the body are lift, $m\mathbf{L}$, drag, $m\mathbf{D}$, thrust, $\mathbf{T}$ and the gravitational force $m\mathbf{g}$. In exo-atmospheric flight, the only two forces acting on the vehicle are thrust and the

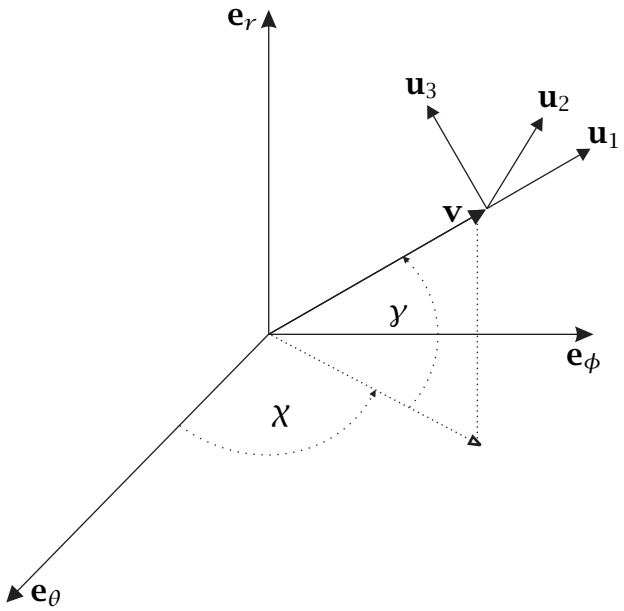

Figure 3-6: The $\{\mathbf{u}_1, \mathbf{u}_2, \mathbf{u}_3\}$ coordinate system

gravitational force. Thus, there are two dynamic models for this problem. The derivation of these models is similar to that presented in Reference 38, which should be referred to for a complete derivation.

3.5.1 Kinematics

The kinematics for the dynamic models are derived by defining the velocity as in Equation 3.7 and equating this expression with the time derivative of position. When defining the time derivative of position, the coordinate system with which the velocity is expressed is very important. To represent velocity in the $\{\mathbf{e}_r, \mathbf{e}_\theta, \mathbf{e}_\phi\}$ coordinate system, the rotation of the frame with respect to the inertial frame must be taken into account. Referring to Figure 3-4 the rotation, $\boldsymbol{\omega}$, is the sum of the rotation about the $\mathbf{e}_\theta$ axis as viewed by an observer in the $\{\mathbf{E}_z, \mathbf{r}\}$ plane and the rotation about the $\mathbf{E}_z$ axis as viewed by an observer in the inertial frame.

$$\boldsymbol{\omega} = \dot{\theta} \sin\phi \mathbf{e}_r - \dot{\phi}\mathbf{e}_\theta + \dot{\theta} \cos\phi \mathbf{e}_\phi \tag{3.9}$$

For a non-rotating Earth, the Earth-relative velocity is the same as the inertial velocity and for convenience will be referred to as simply velocity. The velocity is defined as the time derivative of the radius as represented within the rotating frame plus the cross-product of the angular velocity of the frame and the radius.

$$\mathbf{v} = \left(\frac{\partial \mathbf{r}}{\partial t}\right)_B + \boldsymbol{\omega} \times \mathbf{r}$$

The above calculation produces an expression for velocity in terms of the time derivatives of radius ($\dot{r}$), longitude ($\dot{\theta}$), and latitude ($\dot{\phi}$).

$$\mathbf{v} = \dot{r}\mathbf{e}_r + \dot{\theta} r \cos\phi \mathbf{e}_\theta + \dot{\phi} r \mathbf{e}_\phi \tag{3.10}$$

Equating the corresponding directions of Equation 3.7 and Equation 3.10 produces three differential equations.

$$\begin{aligned} \dot{r} &= v \sin\gamma \\ \dot{\theta} &= \frac{v \cos\gamma \cos\chi}{r \cos\phi} \\ \dot{\phi} &= \frac{v \cos\gamma \sin\chi}{r} \end{aligned} \tag{3.11}$$

These three scalar equations are the kinematics.

3.5.2 Kinetics for Atmospheric Flight

Consider the system at a given time, t. During atmospheric flight, the vehicle is subject to aerodynamic forces, the gravitational force, and the propulsive force, due to the expenditure of fuel. At any time t, Newton's second law ($\sum \mathbf{F} = m\mathbf{a}$) can be applied to the system that consists of the dry mass of the vehicle and the mass of the fuel contained inside the fuel tanks[25].

The kinetics for atmospheric flight are derived by equating the forces acting on the body during atmospheric flight with the mass times the absolute acceleration. During atmospheric flight, there are four forces acting on the body, as

shown in Figure 3-7.

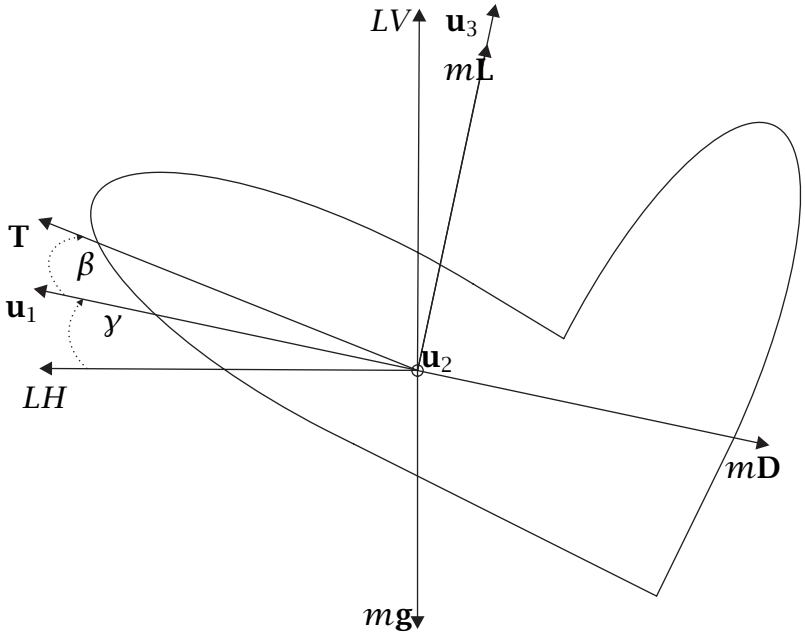

Figure 3-7: Free Body Diagram of the Shuttle During Atmospheric Flight

The drag , $m\mathbf{D}$, is in the opposite direction of $\mathbf{u}_1$. The lift, $m\mathbf{L}$, is perpendicular to drag and has components in the $\mathbf{u}_2$ and $\mathbf{u}_3$ directions, as shown in Figure 3-8. The lift direction is defined by the bank angle, σ.

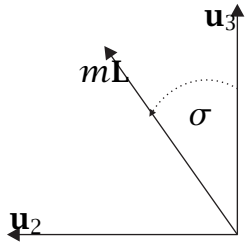

Figure 3-8: Diagram of Lift During Atmospheric Flight in the $\{\mathbf{u}_2, \mathbf{u}_3\}$ Frame

The thrust, $\mathbf{T}$, is in the lift-drag plane as described in Figure 3-9. The direction $\mathbf{u}_L$ is the unit vector in the direction of lift and β is the thrust angle of attack. Since the direction of thrust is determined by the orientation of the vehicle, defining the thrust direction in this manner ensures coordinated flight. The gravitational force, $m\mathbf{g}$, is pointed towards the center of the Earth and is thus decomposed into the $\{\mathbf{u}_1, \mathbf{u}_2, \mathbf{u}_3\}$ frame as shown in Figure 3-10. The sum of the

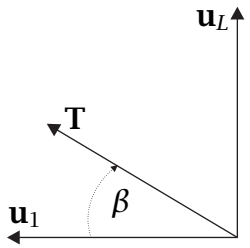

Figure 3-9: Diagram of Thrust During Atmospheric Flight in the $\{\mathbf{u}_1, \mathbf{u}_L\}$ Frame

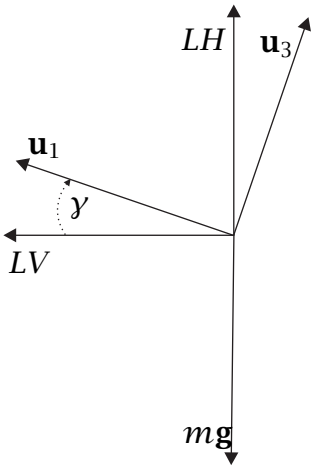

Figure 3-10: Diagram of Gravitational Force in the $\{\mathbf{u}_1, \mathbf{u}_3\}$ Frame

forces in the body-centered velocity frame is

$$\begin{aligned} \sum \mathbf{F} \cdot \mathbf{u}_1 &= -Dm + T\cos\beta - mg\sin\gamma \\ \sum \mathbf{F} \cdot \mathbf{u}_2 &= Lm\sin\sigma + T\sin\beta\sin\sigma \\ \sum \mathbf{F} \cdot \mathbf{u}_3 &= Lm\cos\sigma + T\sin\beta\cos\sigma - mg\cos\gamma \end{aligned} \tag{3.12}$$

To apply Newton's second law, $\sum \mathbf{F} = m\mathbf{a}$, to the atmospheric forces, we must derive the absolute acceleration. For a non-rotating Earth, the absolute acceleration vector is defined as the time rate of change of the velocity vector with respect to the $\{\mathbf{e}_r, \mathbf{e}_\theta, \mathbf{e}_\phi\}$ frame plus the cross product of angular velocity,

$\boldsymbol{\omega}$ with the velocity as expressed in Equation 3.7.

$$\begin{aligned}
\mathbf{a} &= \left(\frac{d\mathbf{v}}{dt}\right)_B + \boldsymbol{\omega} \times \mathbf{v} \\
\mathbf{a} &= \left(\dot{v}\sin\gamma + \dot{\gamma}v\cos\gamma - \frac{v^2}{r}\cos^2\gamma\right)\mathbf{e}_r \\
&\quad + \left(\dot{v}\cos\gamma\cos\chi - \dot{\gamma}v\sin\gamma\cos\chi - \dot{\chi}v\cos\gamma\sin\chi + \frac{v^2}{r}\sin\gamma\cos\gamma\cos\chi\right. \\
&\quad \left. - \frac{v^2}{r}\cos^2\gamma\sin\chi\cos\chi\tan\phi\right)\mathbf{e}_\theta \\
&\quad + \left(\dot{v}\cos\gamma\sin\chi - \dot{\gamma}v\sin\gamma\sin\chi + \dot{\chi}v\cos\gamma\cos\chi + \frac{v^2}{r}\cos^2\gamma\cos^2\chi\tan\phi\right. \\
&\quad \left. + \frac{v^2}{r}\cos\gamma\sin\gamma\sin\chi\right)\mathbf{e}_\phi
\end{aligned} \tag{3.13}$$

Equation 3.13 is the absolute acceleration represented in the $\{\mathbf{e}_r, \mathbf{e}_\theta, \mathbf{e}_\phi\}$ coordinate system.

To obtain the three kinetic equations for atmospheric flight, the forces are transformed into the $\{\mathbf{e}_r, \mathbf{e}_\theta, \mathbf{e}_\phi\}$ coordinate system by applying the transformation matrix from the $\{\mathbf{u}_1, \mathbf{u}_2, \mathbf{u}_3\}$ coordinate system to the $\{\mathbf{e}_r, \mathbf{e}_\theta, \mathbf{e}_\phi\}$ coordinate system. For convenience, the forces are divided by mass, and are equated to the corresponding directions of acceleration. Through mathematical manipulation, the kinetic equations for atmospheric flight are obtained.

$$\begin{aligned}
\dot{v} &= -D + \frac{T}{m}\cos\beta - g\sin\gamma \\
\dot{\gamma} &= \frac{L\cos\sigma}{v} + \frac{T\sin\beta\cos\sigma}{mv} - \left(\frac{g}{v} - \frac{v}{r}\right)\cos\gamma \\
\dot{\chi} &= \frac{L\sin\sigma}{v\cos\gamma} + \frac{T\sin\beta\sin\sigma}{mv\cos\gamma} - \frac{v}{r}\cos\gamma\cos\chi\tan\phi
\end{aligned} \tag{3.14}$$

The model used to account for the expenditure of fuel is

$$\dot{m} = -\frac{T}{I_{sp}g_0} \tag{3.15}$$

where, T is the magnitude of the thrust, I_{sp} is the specific impulse which is a characteristic of the engine and the fuel burned and g_0 is the acceleration due

to gravity at sea level.

3.5.3 Kinetics for Exo-Atmospheric Flight

Once again, the system under consideration is the dry mass of the vehicle and the mass of the fuel contained in the fuel tanks at an instant in time, t. Exo-atmospheric flight is easier to model, with only two forces acting on the vehicle, thrust and weight. For exo-atmospheric flight, the thrust is defined using Euler angles since atmospheric effects are neglected. Without atmospheric effects, the vehicle has more maneuverability and a greater ability to orientate itself in the desired direction. However, we have assumed that the vehicle remains sub-orbital and therefore does not have the freedom to orientate the body in any desired direction, hence a limitation on the thrust direction is imposed.

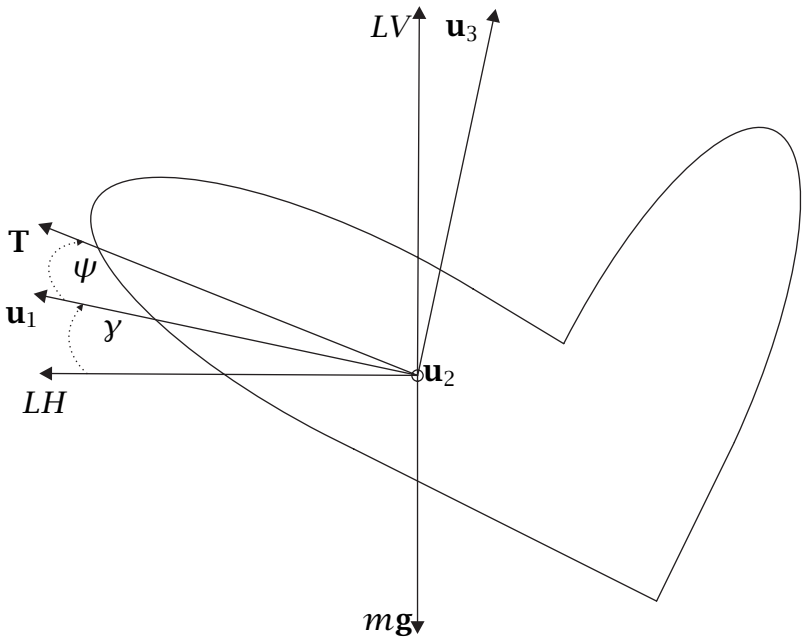

Figure 3-11: Free Body Diagram of the Shuttle During Exo-Atmospheric Flight

As shown in the Figure 3-11, there are two forces acting on the vehicle: thrust and the gravitational force. The forces are then decomposed into the $\{\mathbf{u}_1, \mathbf{u}_2, \mathbf{u}_3\}$ coordinate system. The gravitational force is decomposed as shown in Figure 3-10. The thrust direction is defined by the Euler pitch and roll angles, ζ, and ψ,

respectively, as shown in Figure 3-12. The sum of the forces in each of the three

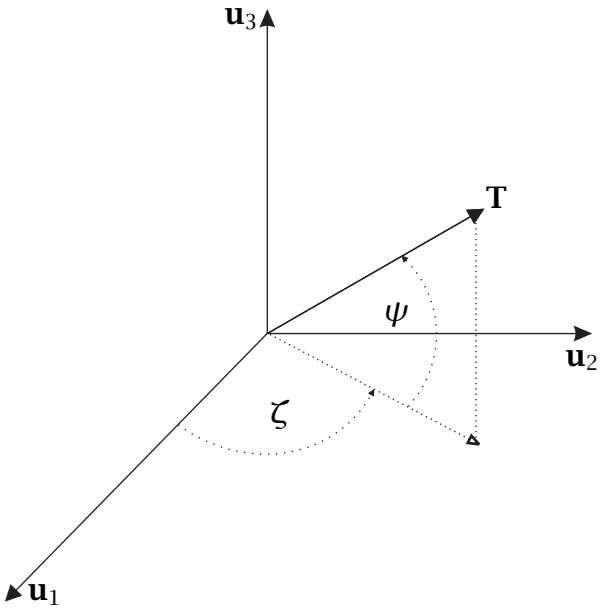

Figure 3-12: Thrust Direction of OMS Engines Using Euler Angles

body-centered directions are

$$\begin{aligned} \sum \mathbf{F} \cdot \mathbf{u}_1 &= T \cos\zeta \cos\psi - mg \sin\gamma \\ \sum \mathbf{F} \cdot \mathbf{u}_2 &= T \sin\zeta \cos\psi \\ \sum \mathbf{F} \cdot \mathbf{u}_3 &= T \sin\psi - mg \cos\gamma \end{aligned} \tag{3.16}$$

The kinetics for exo-atmospheric flight are derived in the same manner as for atmospheric flight, substituting the force components listed in Equation 3.16. The force components are divided by mass and transformed into the $\{\mathbf{e}_r, \mathbf{e}_\theta, \mathbf{e}_\phi\}$ frame. By applying Newton's Law and setting the appropriate components equal to the acceleration components, as defined in Equation 3.13, the kinetics for exo-atmospheric flight are determined.

$$\begin{aligned} \dot{v} &= \frac{T}{m} \cos\zeta \cos\psi - g \sin\gamma \\ \dot{\gamma} &= \frac{T \sin\psi}{mv} - \left(\frac{g}{v} - \frac{v}{r}\right) \cos\gamma \\ \dot{\chi} &= \frac{T \sin\beta \cos\psi}{mv \cos\gamma} - \frac{v}{r} \cos\gamma \cos\chi \tan\phi \end{aligned} \tag{3.17}$$

Once again, the model used to account for the expenditure of fuel is

$$\dot{m} = -\frac{T}{I_{sp} g_0} \tag{3.18}$$

where, T is the magnitude of the thrust, I_{sp} is the specific impulse which is a characteristic of the engine and the fuel burned and g_0 is the acceleration due to gravity at sea level.

3.5.4 Dynamic Model for Main Engine Burn

Using the ME burn vehicle model and the atmospheric dynamics, the full mathematical description for the motion of the shuttle during the first phase is given below.

$$\begin{aligned}
\dot{r} &= v \sin\gamma \\
\dot{\theta} &= \frac{v \cos\gamma \cos\chi}{r \cos\phi} \\
\dot{\phi} &= \frac{v \cos\gamma \sin\chi}{r} \\
\dot{v} &= -D + \frac{T u_3}{m} - g \sin\gamma \\
\dot{\gamma} &= \frac{L u_1}{v} + \frac{T u_1 u_4}{m v} - \left(\frac{g}{v} - \frac{v}{r}\right) \cos\gamma \\
\dot{\chi} &= \frac{L u_2}{v \cos\gamma} + \frac{T u_2 u_4}{m v \cos\gamma} - \frac{v}{r} \cos\gamma \cos\chi \tan\phi \\
\dot{m}_1 &= -\frac{T_1}{I_{sp_1} g_0} \\
\dot{m}_2 &= -\frac{T_2}{I_{sp_2} g_0} \\
\dot{\alpha} &= w_1
\end{aligned} \tag{3.19}$$

3.5.5 Dynamic Model for High-Altitude Thrust

Using the high-altitude thrust model and the exo-atmospheric dynamics, the full mathematical description for the motion of the shuttle during the second phase

is given below.

$$\begin{aligned}
\dot{r} &= v \sin\gamma \\
\dot{\theta} &= \frac{v \cos\gamma \cos\chi}{r \cos\phi} \\
\dot{\phi} &= \frac{v \cos\gamma \sin\chi}{r} \\
\dot{v} &= \frac{T_2 u_5}{m} - g \sin\gamma \\
\dot{\gamma} &= \frac{T_2 u_7}{mv} - \left(\frac{g}{v} - \frac{v}{r}\right) \cos\gamma \\
\dot{\chi} &= \frac{T_2 u_6}{mv \cos\gamma} - \frac{v}{r} \cos\gamma \cos\chi \tan\phi \\
\dot{m} &= -\frac{T_2}{I_{sp_2} g_0}
\end{aligned} \tag{3.20}$$

3.5.6 Dynamic Model for Entry

Using the entry vehicle model and the atmospheric dynamics, the full mathematical description for the motion of the shuttle during the third phase is given below.

$$\begin{aligned}
\dot{r} &= v \sin\gamma \\
\dot{\theta} &= \frac{v \cos\gamma \cos\chi}{r \cos\phi} \\
\dot{\phi} &= \frac{v \cos\gamma \sin\chi}{r} \\
\dot{v} &= -D - g \sin\gamma \\
\dot{\gamma} &= \frac{L u_8}{v} - \left(\frac{g}{v} - \frac{v}{r}\right) \cos\gamma \\
\dot{\chi} &= \frac{L u_9}{v \cos\gamma} - \frac{v}{r} \cos\gamma \cos\chi \tan\phi \\
\dot{m} &= 0 \\
\dot{\alpha} &= w_2
\end{aligned} \tag{3.21}$$

[This page intentionally left blank.]

Chapter 4

Abort Problem Formulation

The abort problem under consideration is the loss of one main engine during a nominal ascent to orbit of a manned RLV. It is assumed that the loss of one main engine during the second stage of ascent necessitates an abort from the nominal mission. From the point of abort, the vehicle is to fly an alternate trajectory, either to Spain or to Senegal. The abort trajectory terminates at a point where the vehicle can be controlled by the terminal area energy management (TAEM) interface and subsequently the auto-landing interface at the chosen landing site. This chapter details a full description of the problem from the time of an abort to the TAEM interface. The corresponding mathematical model is then given for a complete problem formulation.

4.1 Description of Abort

For the purposes of this research, the abort problem under investigation is a single main engine failure during a nominal ascent to orbit of a shuttle after solid rocket booster ejection but before main engine cutoff. The failure of a main engine is chosen as the abort trigger because of the difficulty it presents to flying a trans-atlantic trajectory with a significant loss of thrusting capability. Consequently, the resulting trajectories stress the vehicle's limitations during flight.

At the point of abort, the ET is still attached to the vehicle, which allows the two remaining main engines to thrust using the fuel reserve in the ET. In addition, the OMS engines may be turned on at this point since the fuel reserve is no longer needed to maneuver the vehicle in orbit. The vehicle is still within the atmosphere and subject to aerodynamic forces which impact the vehicle's capability.

At an undetermined point, the vehicle must drop the external tank which contains any remaining main engine fuel. At this point, the vehicle must have a positive flight path angle so that the vehicle is not descending when the ET is dropped. Having the vehicle increase its altitude avoids the possibility of collision with the ET.

Once the ET is dropped, the vehicle may continue to thrust using the OMS engines. In fact, it must do so, if more than 20 percent of the OMS engine fuel remains. This condition ensures that the vehicle achieves the proper center of gravity and weight distribution needed to land. If the OMS engines are thrusting after the ET is dropped, the vehicle must be at a high altitude (above 60 km). Consequently, the aerodynamic forces acting on the vehicle are neglected. Although the vehicle is flying at a high-altitude, it is assumed to remain sub-orbital at all times, which creates increased, but limited, maneuverability.

Once the vehicle has burned at least 80 percent of the fuel, it may turn off the OMS engines and enter the atmosphere using only the aerodynamic forces to maneuver to the terminal manifold. To meet the energy restrictions at the TAEM interface, the vehicle must have a specific radius, speed and flight path angle. The vehicle also must be within a 118 mile long box centered at the chosen landing site to ensure it reaches the runway.

4.2 Abort Problem Formulation

The problem as stated above has many different components. There are three different regimes of flight from the point of abort to the TAEM interface. During

each of these regimes, or phases, the vehicle has different properties and different forces are acting on the vehicle. To model the vehicle throughout the abort, three different dynamic models were defined in Chapter 3. The remainder of this section details the additional constraints imposed on the abort problem.

4.2.1 Path Constraints

A path constraint is a restriction imposed on the vehicle during a certain time segment of flight. Since the vehicle has a different dynamic model for each segment of flight, the restrictions on the vehicle change. For this problem, the path constraint imposed on the vehicle occurs during the second phase, high-altitude thrust.

During the second phase, the vehicle's maneuverability is increased and atmospheric effects are neglected. This assumption is only reasonable at high altitudes where the air density is low. Thus, the vehicle must maintain an altitude greater than 60 km during this segment of flight. However, the vehicle may choose to burn the required amount of OMS engine fuel while the ET is still attached and neglect the second phase. To accommodate this choice, the path constraint is only enforced if the vehicle chooses to use the dynamics prescribed in the second phase (i.e. if the vehicle spends time in the second phase). If the vehicle chooses to enter directly after dropping the external tank, it can neglect the dynamics of the second phase and remain at a low altitude.

The mathematical description of this statement results in a logical argument imposed on the path constraint.

$$(t_f - t_0 > \epsilon)\,(h - h_{min}) \geq 0 \tag{4.1}$$

Here, h is the altitude of the vehicle, and h_{min} is the minimum value of altitude, 60 km. The logical argument can take on either a value of zero or one, depending on whether the condition is met. If the final time, t_f, is greater than the initial time, t_0, to within some value of machine accuracy (ϵ), then the logical condition

is true (equal to one), and the solution has a second phase and consequently, the constraint is imposed. If the vehicle does not spend time in the second phase, the logical argument is false (equal to zero) and the path constraint is neglected.

4.2.2 Boundary Conditions

The abort trajectory begins at the point at which one of the main engines fails during a nominal ascent. This point is varied from the beginning to the end of a nominal ascent. At the time of an abort, t_{abort}, the corresponding state of the vehicle at that time is the initial state for the abort trajectory.

$$\begin{aligned} r\left(t_{abort}\right) &= r_0 \\ \theta\left(t_{abort}\right) &= \theta_0 \\ \phi\left(t_{abort}\right) &= \phi_0 \\ v\left(t_{abort}\right) &= v_0 \\ \gamma\left(t_{abort}\right) &= \gamma_0 \\ \chi\left(t_{abort}\right) &= \chi_0 \\ m\left(t_{abort}\right) &= m_0 \end{aligned} \tag{4.2}$$

At the terminal manifold, the vehicle must meet a final radius, speed and flight path angle constraint.

$$\begin{aligned} r\left(t_f\right) &= r_f \\ v\left(t_f\right) &= v_f \\ \gamma\left(t_f\right) &= \gamma_f \end{aligned} \tag{4.3}$$

In addition, limits are imposed on the vehicle's geographic distance from the landing site. Equation 4.4 bounds the final longitude and latitude to be within an acceptable region.

$$\begin{aligned} \theta_{min}\left(t_f\right) \leq \theta_f \leq \theta_{max}\left(t_f\right) \\ \phi_{min}\left(t_f\right) \leq \phi_f \leq \phi_{max}\left(t_f\right) \end{aligned} \tag{4.4}$$

4.2.3 Interior Point Constraints

Interior point constraints occur at a single point in time along the trajectory. The time at which the constraint is imposed is not specified before hand, but determined by the problem formulation. At the end of ME burn, the vehicle drops the external tank, which creates a discontinuity in mass between the end of ME burn and the beginning of high-altitude thrust. If we refer to the time at the end of ME burn as t_1^- and the time at the beginning of high-altitude thrust as t_1^+, than the mathematical expression for the mass difference is

$$m\left(t_1^-\right) - \left(m_{ET} + m_{MEfuel}\right) = m\left(t_1^+\right) \tag{4.5}$$

where $m\left(t_1^-\right)$ is the total mass at the end of ME burn, m_{ET} is the dry mass of the external tank, m_{MEfuel} is the amount of main engine fuel remaining at the end of ME burn, and $m\left(t_1^+\right)$ is the total mass at the beginning of high-altitude thrust.

At the end of ME burn, the vehicle is required to ascend to avoid collision with the external tank. Thus, we constrain the flight path angle, γ, to be non-negative at the end of this phase of flight. Equation 4.6 represents the mathematical expression for this condition.

$$\gamma\left(t_1^-\right) \geq 0 \tag{4.6}$$

Although the constraint is applied at the end of ME burn, by continuity, it will hold for the beginning of high-altitude thrust.

A third interior point constraint arises from the requirement to burn at least 80 percent of the OMS engine fuel (m_{OMS_f}). If we refer to the final time of high-altitude thrust as t_2^-, then Equation 4.7 is the mathematical expression for the mass constraint at the end of the second phase.

$$m_{veh} \leq m\left(t_2^-\right) \leq m_{veh} + .2m_{OMS_f} \tag{4.7}$$

Here, m_{veh} is the dry mass of the vehicle.

[This page intentionally left blank.]

Chapter 5

Optimal Control Problem Formulation

In the previous chapters, we have described the problem formulation for a trans-atlantic abort of the U.S. Space Shuttle due to the failure of a main engine during the second stage of ascent. In particular, Chapter 3 described the dynamic model and Chapter 4 described the path constraints, interior point constraints and boundary conditions imposed on the vehicle during flight. In this chapter, we describe an approach that determines a trajectory and control that steers the vehicle from the initial conditions at main engine failure to a designated landing site.

For any given set of initial conditions, three may exist a control history that is capable of steering the vehicle to a desired landing site. A control that does so, while satisfying all constraints imposed on the problem is a *feasible control*[28]. The abort trajectory, or abort plan that arises from the application of a feasible control is a *feasible abort plan*. However, in practice we often are interested in determining a control that has the most desirable characteristics. If we define a performance measure to account for the desired characteristics, we can minimize the performance measure to determine the most desirable control. A control that minimizes a performance measure, while satisfying all constraints imposed on the problem is a *optimal control*[27]. The abort plan that arises from the application of an optimal control is an *optimal abort plan*.

5.1 Feasible Planning vs. Optimal Planning

Often, though not always, there are many control histories that produce a feasible control. However, as additional constraints are added to the problem formulation, it often becomes more difficult to determine a feasible abort plan. In the extreme, the addition of a constraint can cause the problem to become infeasible.

For the purposes of evaluating an abort planner, we desire a method that obtains a solution. The solution obtained will then be evaluated to determine if the abort plan is desirable. For these reasons, additional constraints are not imposed, since they may cause the problem to become infeasible.

As noted in Reference 8, defining a penalty function is another way to handle additional constraints on the problem. By formulating additional constraints as soft constraints, we ensure that a solution to the problem is obtained and that the control minimizes the violations of the constraints. Thus, the problem considered in this research is formulated as an optimal control problem.

5.1.1 Performance Measure

The abort trajectories in this thesis are developed using three different dynamic models over three different phases of flight. For each of these phases a different performance measure can be chosen. The performance measure selected models the important aspects of flight for each phase.

For the first phase, ME burn, the vehicle is subjected to atmospheric forces, and has the ability to thrust. The sensed acceleration (a), or g-load, is the magnitude of the sum of the lift acceleration, $\mathbf{L}$, the drag acceleration, $\mathbf{D}$, and the thrust acceleration, $\mathbf{T}/m$.

$$a = \|\mathbf{L} + \mathbf{D} + \mathbf{T}/m\|_2$$

Since we are considering a manned RLV, the amount of sensed acceleration on the vehicle should be as small as possible. As such, the performance measure

for the first phase minimizes the square of the ratio of the sensed acceleration to the desired maximum value of sensed acceleration (a_{max}), which is 2.5 g's, over the entire first phase.

During ME burn the vehicle is no longer on a trajectory to orbit, but instead performing a trans-atlantic abort. As such, the vehicle no longer requires the energy needed to boost into orbit, and therefore should limit the amount of energy at the end of ME burn. The final specific energy of the vehicle, e, is calculated by the vis-viva integral [1].

$$e = \frac{v^2}{2} - \frac{\mu}{r}$$

By maximizing the difference between the final energy of a nominal ascent, e_{nom}, and the final energy of ME burn, we can impose this desired condition.

The performance measure for ME burn takes both of these aspects into account.

$$\mathcal{J} = -\frac{e_{nom}(t_1) - e(t_1)}{e_{nom}(t_1)} + \int_{t_0}^{t_1} \left(\frac{a}{a_{max}}\right)^2 dt \tag{5.1}$$

Notice that the condition on the final energy is only computed at the final time for ME burn, t_1, while the condition on sensed acceleration applies throughout the phase. The difference in the final energy is divided by the nominal final energy for scaling purposes. The constraint on sensed acceleration is squared for improved numerical performance.

The second phase of flight, high-altitude thrust, is a much more benign phase, where the dynamics are simple and the stresses on the vehicle are limited. In this problem, the second phase is optional and the vehicle can choose to move directly from the dynamics of ME burn to the dynamics of entry, by setting the initial time for the second phase, t_1, and the final time for the second phase, t_2, equal. Consequently, we have chosen to omit a performance metric in the second phase.

The third phase of flight is a very different case, however, with stressing conditions throughout entry. As the vehicle enters the atmosphere, it heats up.

If the heating rate becomes too large, the vehicle can burn up during entry. The expression for the stagnation point heating rate is

$$\dot{Q} = k_{therm} \left(\frac{\rho}{\rho_0} \right)^{1/2} \left(\frac{v}{v_{circ}} \right)^{3.15}$$

where k_{therm} has a constant value of 2×10^8 W/m^2.

During entry, the dynamic pressure can become very large while the vehicle is traveling at a high speed. The expression for dynamic pressure is

$$q = \frac{\rho V^2}{2}$$

where ρ is the density at the current altitude and is approximated using an exponential model.

Furthermore, as the vehicle enters the atmosphere and heads to the TAEM interface, the vehicle must greatly reduce its altitude and speed by maneuvering through the atmosphere using only aerodynamic forces. Thus, the aerodynamic accelerations can become very large and create large values in the sensed acceleration (a) experienced by the vehicle and crew.

$$a = \|\mathbf{L} + \mathbf{D}\|_2$$

Once again, the sensed acceleration is squared to improve the numerical performance.

By taking the sum of the ratio of each of these parameters to their respective desired maximum values over the entire time for entry, we obtain a penalty function that minimizes these parameters.

$$\mathcal{J} = \int_{t_2}^{t_f} \left[k_1 \left(\frac{\dot{Q}}{\dot{Q}_{max}} \right) + k_2 \left(\frac{q}{q_{max}} \right) + k_3 \left(\frac{a^2}{a_{max}^2} \right) \right] \tag{5.2}$$

The desired maximum value for heating rate ($\dot{Q}_{max}$) is 2.83 MW/m^2, for dynamic pressure (q_{max}) is 16.37 kPa, and sensed acceleration (a_{max}) is 2.5 g's. The val-

ues of k_1, k_2, and k_3 are weighting factors on each of these terms. The weighting factors are included so that the relative importance of each parameter can be varied to determine the effect on the trajectory .

5.2 Form of an Optimal Control Problem

As stated in the previous section, an optimal control problem is one that determines a control history that satisfies all of the constraints on the problem and minimizes the desired performance measure [27]. In general, an optimal control problem has four parts: (1) the dynamic model describing the motion of the vehicle, (2) the path constraints on the vehicle that are enforced over a segment of time, (3) the boundary conditions on the variable at the initial and terminal time points and (4) the performance measure used to optimize the solution. The problem formulation developed in this research is an optimal control problem. However, due to the inherent structure of the problem, the problem is naturally broken up into three segments or phases. Thus, we are looking to solve a single optimal control problem, which contains three phases. Since each phase is a segment of the optimal control problem, there may be a dynamic model, path constraints, boundary conditions and a performance measure in each phase. These phases are then linked together using appropriate constraints to ensure the solution yields a control history, a trajectory and a cost for the entire problem. In this section the general form of an optimal control problem will be examined. The next section will present the form of a multi-phase optimal control problem and detail the steps necessary to properly define a multi-phase optimal control problem.

5.2.1 The Dynamic Model

The mathematical model used to determine the motion of the vehicle is referred to as the equations of motion. When written in state-variable form the differ-

ential equations governing the motion of the vehicle are reduced to a system of first-order ordinary differential equations [20]. The equations of motion are functions of the state of the system, the control input, and a monotonically increasing or decreasing independent variable. For the purposes of this research, the independent variable chosen is time, t. The state of the system, $\mathbf{x}(t)$, is a vector of the components of the state required to define the motion of the vehicle at any point of time.

$$\mathbf{x}(t) = \begin{bmatrix} x_1(t) \\ x_2(t) \\ \vdots \\ x_n(t) \end{bmatrix} \in \mathbb{R}^n \tag{5.3}$$

Equation 5.3 denotes the dimension of the state as n. The control, $\mathbf{u}(t)$ is a vector of the individual components that consist of the inputs to the system.

$$\mathbf{u}(t) = \begin{bmatrix} u_1(t) \\ u_2(t) \\ \vdots \\ u_m(t) \end{bmatrix} \in \mathbb{R}^m \tag{5.4}$$

Equation 5.4 denotes the dimension of the control as m. Thus, the equations of motion used to model the vehicle are a set of nonlinear first-order ordinary differential equations of the general form

$$\dot{\mathbf{x}}(t) = \mathbf{a}(\mathbf{x}(t)\,\mathbf{u}(t), t) \tag{5.5}$$

where $\dot{\mathbf{x}}(t)$ is the time derivative of the state, $\mathbf{x}(t)$, and $\mathbf{a} : \mathbb{R}^n \times \mathbb{R}^m \times \mathbb{R} \to \mathbb{R}^n$.

5.2.2 Path Constraints

Path constraints are additional constraints placed on the dynamic system for an interval of operation. While these constraints are imposed, a solution must also satisfy these additional constraints to remain feasible. Often, path constraints are inequality constraints, such that there is a range of values for which the solution satisfies the additional constraints. The general form of p path constraints is

$$\mathbf{g}_{min} \leq \mathbf{g}\left(\mathbf{x}\left(t\right), \mathbf{u}\left(t\right), t\right) \leq \mathbf{g}_{max} \tag{5.6}$$

where $\mathbf{g}_{min} \in \mathbb{R}^p$, $\mathbf{g}_{max} \in \mathbb{R}^p$ are both vectors of constant values and $\mathbf{g} : \mathbb{R}^n \times \mathbb{R}^m \times \mathbb{R} \rightarrow \mathbb{R}^p$

5.2.3 Boundary Conditions

The boundary conditions describe the initial and final state of the vehicle. At the beginning of the trajectory, the initial conditions specify the state at the initial time, t_0. At the end of the trajectory, the terminal conditions specify the state at the final time, t_f. Referring to the number of initial conditions as q_0 and the number of terminal conditions as q_f, we can express the boundary conditions as

$$\begin{aligned} \mathbf{h}_0\left(\mathbf{x}\left(t_0\right), t_0\right) &= 0 \\ \mathbf{h}_f\left(\mathbf{x}\left(t_f\right), t_f\right) &= 0 \end{aligned} \tag{5.7}$$

where $q_0 \leq n$, $q_f \leq n$ where n is the dimension of the state, $\mathbf{h}_0 : \mathbb{R}^n \times \mathbb{R} \rightarrow \mathbb{R}^{q_0}$ and $\mathbf{h}_f : \mathbb{R}^n \times \mathbb{R} \rightarrow \mathbb{R}^{q_f}$

5.2.4 Performance Measure

The selection of a performance measure, or objective functional, corresponds to creating a mathematical statement, that when minimized or maximized, yields a trajectory and control that enables the system to operate in the best way possible [27]. The term objective functional refers to a mathematical expression that

takes a function or functions as inputs and outputs a scalar quantity. In an optimal control problem the solution is a function that minimizes (or maximizes) the objective functional [27]. The general form of an objective functional has three parts: an initial cost, a terminal cost, and an integrated cost. The initial cost is the value of the cost at the initial time, t_0, and the corresponding initial state, $\mathbf{x}(t_0)$. The terminal cost is the value of the cost at the terminal time, t_f, and the corresponding terminal state, $\mathbf{x}(t_f)$. The integrated cost accumulates over the entire interval of time (from t_0 to t_f) and may be dependent on the state, the control, and the time. The general form of a objective functional is

$$\mathcal{J} = \mathcal{M}(\mathbf{x}(t_0), t_0) + \mathcal{N}(\mathbf{x}(t_f), t_f) + \int_{t_0}^{t_f} \mathcal{L}(\mathbf{x}(t), \mathbf{u}(t), t)\, dt \tag{5.8}$$

where $\mathcal{M} : \mathbb{R}^n \times \mathbb{R} \to \mathbb{R}$, $\mathcal{N} : \mathbb{R}^n \times \mathbb{R} \to \mathbb{R}$ and $\mathcal{L} : \mathbb{R}^n \times \mathbb{R}^m \times \mathbb{R} \to \mathbb{R}$.

5.2.5 General Form of an Optimal Control Problem

Having defined the four parts of an optimal control problem, the general problem statement of an optimal control problem is to find a feasible control history, $\mathbf{u}^*$, and resulting state history, $\mathbf{x}^*$, that minimizes the cost functional

$$\mathcal{J} = \mathcal{M}(\mathbf{x}(t_0), t_0) + \mathcal{N}(\mathbf{x}(t_f), t_f) + \int_{t_0}^{t_f} \mathcal{L}(\mathbf{x}(t), \mathbf{u}(t), t)\, dt \tag{5.9}$$

subject to the dynamic constraints

$$\dot{\mathbf{x}}(t) = \mathbf{a}(\mathbf{x}(t)\,\mathbf{u}(t), t) \tag{5.10}$$

path constraints

$$\mathbf{g}_{min} \leq \mathbf{g}(\mathbf{x}(t), \mathbf{u}(t), t) \leq \mathbf{g}_{max} \tag{5.11}$$

and boundary conditions.

$$\begin{aligned} \mathbf{h}_0\left(\mathbf{x}\left(t_0\right), t_0\right) &= 0 \\ \mathbf{h}_f\left(\mathbf{x}\left(t_f\right), t_f\right) &= 0 \end{aligned} \tag{5.12}$$

5.3 Multiple-Phase Optimal Control Problem

As stated in the previous section, the problem under consideration in this research is naturally modeled as a three-phase optimal control problem due to the different dynamics operating over different segments of flight. A three-phase optimal control problem is an extension of a single phase optimal control problem in the sense that the performance measure(s) are minimized over the entire problem subject to the dynamics, the constraints, and the boundary conditions. In order to define the multiple phase optimal control problem such that the solution is one that satisfies all constraints and is the optimum solution to the entire problem, linkage constraints are added between adjacent phases. In this section, the multiple phase problem is presented and the linkage constraints are defined.

5.3.1 Form of a Multiple Phase Optimal Control Problem

An optimal control problem that is broken up over segments of time due to the nature of the problem is a multi-phase optimal control problem. Since each phase is a segment of the entire optimal control problem, the general description of the optimal control problem formulation applies in each segment [30]. Thus, each segment of the optimal control problem has an associated cost functional, dynamic model, path constraints and boundary conditions. The total cost is the sum of the cost functionals for each phase. The optimal solution is obtained by minimizing the total cost functional subject to the dynamic constraints, path constraints and boundary conditions in each phase [30].

In this research we are considering a three-phase optimal control problem,

where each phase, i, (for $i \in [1,2,3]$), is a segment of the entire optimal control problem. Hence, by the above description, we have three dynamic models, three path constraints and three performance measures. The boundary conditions for a phase at an interior time point ($t_0 \leq t \leq t_f$) correspond to the interior point constraints described in Section 4.2. The linkage constraints are the final component necessary to complete the formulation of a multiple phase optimal control problem.

5.3.2 Linkage Constraints

Linkage constraints are necessary to formulate a multiple phase optimal control problem because they adjoin the adjacent phases of the optimal control problem. By connecting two adjacent phases, the linkage constraints assure that the solution obtained is a solution for the entire problem.

The first linkage constraint is applied to the independent variable, time (t), over two consecutive phases. Since the optimal control problem is split into phases over different times, the final time for a previous phase, $t_f^{(i)}$ and the initial time for the next phase, $t_0^{(i+1)}$ are the same. Hence, the first linkage constraint is

$$t_f^{(i)} - t_0^{(i+1)} = 0, \quad i = 1,2 \tag{5.13}$$

This constraint is applied between two adjacent phases in the optimal control problem, or as is the case in this research, between ME burn and high-altitude thrust, and between high-altitude thrust and entry.

The linkage constraints for the state are defined by the problem formulation. In this particular problem, the first six components of the state are the position and velocity of the vehicle. Since we have constrained the final time of the previous phase and the initial time of the following phase to be the same, the vehicle can not change its position or velocity. Hence, the position and velocity of the vehicle at the end of the previous phase and at the beginning of the next phase must be the same. This translates into six linkage constraints between each set

of adjacent phases.

$$\begin{aligned}
r\left(t_f^{(i)}\right) - r\left(t_0^{(i+1)}\right) &= 0 \\
\theta\left(t_f^{(i)}\right) - \theta\left(t_0^{(i+1)}\right) &= 0 \\
\phi\left(t_f^{(i)}\right) - \phi\left(t_0^{(i+1)}\right) &= 0 \qquad\qquad i = 1,2 \\
v\left(t_f^{(i)}\right) - v\left(t_0^{(i+1)}\right) &= 0 \\
\gamma\left(t_f^{(i)}\right) - \gamma\left(t_0^{(i+1)}\right) &= 0 \\
\chi\left(t_f^{(i)}\right) - \chi\left(t_0^{(i+1)}\right) &= 0
\end{aligned} \tag{5.14}$$

Another linkage constraint is imposed on the value of mass between each phase, however, this constraint differs according to which phases are being linked. Referring to Section 4.1, the vehicle drops the external tank and the remaining fuel it contains. By doing so, there is a discontinuity in the value of mass between the end of the first phase and the beginning of the second phase, which translates into the following linkage constraint.

$$m\left(t_f^{(1)}\right) - (m_{ET} + m_{MEfuel}) - m\left(t_0^{(2)}\right) = 0 \tag{5.15}$$

Here, m is the total mass of the system, m_{ET} is the mass of the external tank, and m_{MEfuel} is the mass of the remaining main engine fuel. Hence, the amount of mass at the beginning of the second phase is only dependent on the amount of OMS engine fuel burned in the first phase.

Between the end of the second phase and the beginning of the third phase, the vehicle's mass remains constant. Thus, the linkage constraint for mass between high-altitude thrust and entry is an equality constraint.

$$m\left(t_f^{(2)}\right) - m\left(t_0^{(3)}\right) = 0 \tag{5.16}$$

5.3.3 Principle of Optimality

The linkage constraints imposed between two consecutive phases serve to reunite the phases to form the original optimal control problem. Although the

linkage constraints are additional constraints in the multiple phase optimal control problem, they are originally present in the problem formulation, since the original problem is a single optimal control problem. Bellman's Principle of Optimality [4] states that

> An optimal policy has the property that whatever the initial state and initial decision are, the remaining decisions must constitute an optimal policy with regard to the state resulting from the frist decision.

The linkage constraints are applied to yield consistency in the value of the state components between two consecutive phases. However, the linkages do not prescribe the value of time at these connections, nor do the linkages constrain the state to be a particular value. The value of the time, state and control at the linkage points is determined by solving the optimal control problem. Any initial, interior or terminal constraints imposed are prescribed in the original problem formulation [30]. Thus the linkage constraints do not violate the Principle of Optimality since they are part of the original problem formulation [30].

5.3.4 General Form of a Multiple Phase Optimal Control Problem

Having fully detailed the form of a general optimal control problem and defined the extensions necessary to create a multiple phase optimal control problem, the general problem statement for the three-phase optimal control is to find a feasible control history, $\mathbf{u}^*$, and resulting state history, $\mathbf{x}^*$, that minimizes the cost functional

$$\sum_{i=1}^{3} \mathcal{J}^{(i)} \tag{5.17}$$

subject to the dynamic constraints

$$\dot{\mathbf{x}}^{(i)}(t) = \mathbf{a}\left(\mathbf{x}^{(i)}\left(t^{(i)}\right)\mathbf{u}^{(i)}\left(t^{(i)}\right), t^{(i)}\right), \quad i = 1,2,3 \quad t^{(i)} \in \left[t_0^{(i)}, t_f^{(i)}\right] \tag{5.18}$$

path constraints

$$\mathbf{g}_{min}^{(i)} \leq \mathbf{g}^{(i)}\left(\mathbf{x}^{(\mathbf{i})}\left(t^{(i)}\right), \mathbf{u}^{(\mathbf{i})}\left(t^{(i)}\right), t^{(i)}\right) \leq \mathbf{g}_{max}^{(i)}, \quad i = 1,2,3, \quad t^{(i)} \in \left[t_0^{(i)}, t_f^{(i)}\right] \tag{5.19}$$

boundary conditions

$$\begin{aligned} \mathbf{h}_0^{(i)}\left(\mathbf{x}^{(\mathbf{i})}\left(t_0^{(i)}\right), t_0^{(i)}\right) &= 0 \\ \mathbf{h}_f^{(i)}\left(\mathbf{x}^{(\mathbf{i})}\left(t_f^{(i)}\right), t_f^{(i)}\right) &= 0 \quad i = 1,2,3 \end{aligned} \tag{5.20}$$

and linkage constraints

$$\begin{aligned} t_f^{(i)} - t_0^{(i+1)} &= 0 \\ r\left(t_f^{(i)}\right) - r\left(t_0^{(i+1)}\right) &= 0 \\ \theta\left(t_f^{(i)}\right) - \theta\left(t_0^{(i+1)}\right) &= 0 \\ \phi\left(t_f^{(i)}\right) - \phi\left(t_0^{(i+1)}\right) &= 0 \qquad i = 1,2 \\ v\left(t_f^{(i)}\right) - v\left(t_0^{(i+1)}\right) &= 0 \\ \gamma\left(t_f^{(i)}\right) - \gamma\left(t_0^{(i+1)}\right) &= 0 \\ \chi\left(t_f^{(i)}\right) - \chi\left(t_0^{(i+1)}\right) &= 0 \end{aligned} \tag{5.21}$$

and

$$\begin{aligned} m\left(t_f^{(1)}\right) - m\left(t_0^{(2))}\right) &= m_{ET} + m_{MEfuel} \\ m\left(t_f^{(2))}\right) - m\left(t_0^{(3))}\right) &= 0 \end{aligned} \tag{5.22}$$

[This page intentionally left blank.]

Chapter 6

Solution Methods of an Optimal Control Problem

As discussed in the previous chapter, the problem formulation presented in this research is an optimal control problem. An optimal control problem can be solved by either an analytic or a numerical method. The problem under consideration is a large scale nonlinear optimal control problem and therefore must be solved numerically. Numerical solutions for optimal control problems fall into two categories: indirect methods and direct methods. In this chapter, a discussion of both indirect and direct methods is given. Next, a description of a type of direct method, the Pseudospectral Legendre method, is given and the details of how this method is extended to solving a multiple phase optimal control problem is discussed. Finally, a brief discussion of the solution method for the resulting nonlinear programming problem is given.

6.1 Numerical Methods for Solving Optimal Control Problems

In general, an optimal control problem cannot be solved analytically, so a numerical method must be employed. Numerical methods for solving optimal control

problems can be categorized as either indirect or direct methods. Indirect methods formulate and solve the necessary conditions for optimality. Direct methods transcribe the optimal control problem into a nonlinear programming problem and minimize the performance index. In this section, a general description of both methods is discussed.

6.1.1 Indirect Methods

Indirect methods involve the derivation of the Hamiltonian boundary-value problem (HBVP) that results from the analytic first order variation of the optimal control problem. Using calculus of variations, the first variation of the objective functional (or augmented objective functional) is set equal to zero. For convenience, the Hamiltonian ($\mathcal{H}$) is defined as

$$\mathcal{H}\left(\mathbf{x}\left(t\right),\mathbf{u}\left(t\right),\lambda\left(t\right),t\right) \doteq \mathcal{L}\left(\mathbf{x}\left(t\right),\mathbf{u}\left(t\right),t\right) + \lambda^{T}\left[a\left(\mathbf{x}\left(t\right),\mathbf{u}\left(t\right),t\right)\right]$$

where $\mathbf{x}\left(t\right)$ is the state vector, $\mathbf{u}\left(t\right)$ is the control vector, $\lambda\left(t\right)$ are the Lagrange multipliers or costate vector, $\mathcal{L}\left(\mathbf{x}\left(t\right),\mathbf{u}\left(t\right),t\right)$ is the function inside the integral of the performance measure, and $a\left(\mathbf{x}\left(t\right),\mathbf{u}\left(t\right),t\right)$ is a general function representing the nonlinear dynamics of the problem [27]. Deriving the first order necessary conditions for optimality, including Pontryagin's minimum principle, leads to the system of differential equations in Equation 6.1.

$$\begin{aligned} \dot{\mathbf{x}}\left(t\right) &= \mathcal{H}_{\lambda} \\ \dot{\lambda}\left(t\right) &= -\mathcal{H}_{\mathbf{x}} \end{aligned} \tag{6.1}$$

The solution to the HBVP is found by making an initial guess of the solution for both the state and costate by estimating the free initial and/or terminal boundary conditions not specified in the necessary conditions. The initial solution is then iterated upon until a better solution to the necessary conditions is obtained. The process continues until the necessary conditions are met to within

a certain tolerance [6].

The benefits of using an indirect method are that the values for the costate are obtained along the trajectory. The accurate costate obtained from the solution to the HBVP allows for an accurate control to be computed [31].

A drawback to indirect methods is that the radius of convergence is very small. Hence, a very good initial guess is needed and determining one is a non-trivial process. If the initial guess is not close to the solution, the system of differential equations can quickly become unstable during integration [7]. An additional drawback to indirect methods occurs if the problem contains path constraints. If path constraints are present, which is a frequent occurrence, an apriori estimate of the constrained arc sequence must be made [6].

6.1.2 Direct Methods for Solving Optimal Control Problems

In contrast to indirect methods, direct methods do not explicitly formulate or solve the necessary conditions for optimality [6]. To employ a direct transcription method, the continuous time optimal control problem must be discretized at specified time points called nodes. The state and control time histories are discretized at these node points. A piecewise continuous interpolating polynomial is used to approximate the state and control time histories. A linear or cubic spline is most often used as the interpolating polynomial [16]. The differential equations are approximated by differences and a quadrature is used to perform an implicit integration. As a consequence, continuity constraints on the value of the state and the slope must be enforced at the boundary of each segment. Once discretized, the differential equations and path constraints form a set of algebraic constraints. The integral in the objective function is replaced by a summation. The initial and terminal constraints define the values of the state at the first and last time point, respectively. Thus, by discretizing the optimal control problem in this manner, we transform the problem into a nonlinear programming problem (NLP) for which a standard NLP solver, such as NPSOL or

SNOPT, may be used to compute the solution [14].

The discretization of the state and control may be accomplished by two different methods: differential inclusion and collocation. In differential inclusion, the control variables are eliminated from the problem formulation by rewriting the controls as a function of the state and state rates. Hence, the bounds on the control are replaced by the bounds on the attainable state rates, which are computed from the Euler implicit integration rule [13]. The benefit to formulating the problem in this manner is that the number of variables in the NLP problem is reduced and consequently, the computation time is reduced. However, differential inclusion is generally limited to problems where the control appears linearly in the differential equations and isolating the control may still be a difficult process [13]. Another difficulty arises with the use of the Euler integration scheme. Since the Euler quadrature rule is the least accurate integration method ($O(h^2)$)[11], the step size must remain small, which increases the number of nodes in the problem, offsetting the gain from the reduction in variables [18].

The method of collocation discretizes the control directly. Thus, the values of the control at each node are added as variables in the NLP. Since the control is explicit in the differential equations, a higher-order quadrature scheme, such as Simpson's rule or a fourth order Runga-Kutta [13], may be used to satisfy the differential equation constraints. The greater accuracy associated with these methods allows for a reduction in step-size which reduces the number of nodes and therefore the total number of variables in the NLP. Another benefit to collocation is that the control is solved for explicitly and does not need to be derived from the solution [13].

Differential inclusion and collocation describe two different methods to formulate the nonlinear programming problem. However, both methods use a local approximation to the function at each node and perform an implicit integration scheme of varying accuracy to solve the problem. There is no guarantee, however, that this approximation is accurate or that the time points for which the solution is obtained will yield a representative trajectory. Thus, once a solution

is obtained its accuracy must be checked, and if necessary, the node points may need to be changed to produce a more accurate solution [6].

The advantages of using a direct method to solve an optimal control problem are many. First, a direct method solves the nonlinear programming problem by optimizing the performance measure. This allows for the solution of a complicated problem with a poor initial guess. In addition, path constraints are handled directly, as additional constraints in the formulation, without having to first specify a constrained arc sequence [7]. However, it is difficult to obtain an accurate co-state for the problem [12].

6.2 Pseudospectral Methods

An alternate method for discretizing the optimal control problem is the use of a spectral collocation method, or pseudospectral method [15, 19]. A pseudospectral method discretizes the state and control at specific node points. These node points coincide with the locations of the knots in the Gaussian quadrature formulas which yield an exact solution at the node points for polynomials of higher order [19]. According to approximation theory, choosing the nodes to correspond to the roots of the orthogonal polynomial trial functions will yield the best approximation [17].

The state and control are approximated by global orthogonal polynomials. Choosing a global orthogonal polynomial is beneficial because of the close relationship to Gauss-type integration rules [18]. Using orthogonal polynomials allows for the exploitation of a simple transformation from the optimal control problem to the algebraic equations in the nonlinear programming problem. If we assume the node points are chosen such that τ_i represents the i^{th} node where $i = 0, 1...N$ and N is the number of nodes, the approximation of the function $y(\tau)$ is

$$y(\tau) \approx y^N(\tau) = \sum_{i=0}^{N} y_i \phi_i(\tau) \tag{6.2}$$

where $y_i(\tau)$ is the value of y at τ_i and $\phi_i(\tau)$ is the specific choice of interpolating polynomials such as Legendre or Chebyshev [19].

Since we have chosen a global orthogonal polynomial as the interpolating polynomial, it must satisfy the condition that [16, 30],

$$\phi_i(\tau_j) = \begin{cases} 1 & \textbf{if} \quad i = j \\ 0 & \textbf{if} \quad i \neq j \end{cases} \tag{6.3}$$

Using Equation 6.3 we can show that $y^N(\tau)$ in Equation 6.2 is equal to $y(\tau)$ at the node points, τ_i.

$$y(\tau_i) = y^N(\tau_i) \qquad i = 0, 1 \ldots N \tag{6.4}$$

Thus, according to Equation 6.4 the approximation of the function is exact at the nodes [17].

In a pseudospectral method, the derivatives in the differential equations are evaluated by a differentiation matrix. The differentiation matrix is computed from the analytic derivatives of the interpolating polynomials. For the derivative of the function $y(\tau)$ the expression becomes

$$\dot{y}(\tau) \approx \dot{y}^N(\tau) = \sum_{j=0}^{N} y_j \dot{\phi}_j(\tau_i) \tag{6.5}$$

By denoting the differentiation matrix as D, whose elements are $D_{ij} = \dot{\phi}_j(\tau_i)$, the expression for the function derivative is [17]

$$\dot{y}^N = D y^N(\tau) \tag{6.6}$$

Defining the differential equations in this manner produces highly accurate results. Comparing the accuracy of pseudospectral methods to that of the finite difference schemes generally used in collocation methods, the error of a finite difference scheme decreases on the order of N^{-m}, where N is the number of nodes and m is a constant dependent on the smoothness and order of approxi-

mation used in the solution [19]. A pseudospectral method will converge faster for every finite value of m [12].

In traditional collocation schemes the integral in the Bolza cost function is typically converted to a Mayer form [17]. In a pseudospectral method, the integral is approximated by a summation. If we consider the integral of $y(\tau)$ with respect to a weighting function, $\alpha(\tau)$

$$Iy = \int_{-1}^{1} \alpha(\tau)\, y(\tau)\, d\tau$$

we can then substitute the relationship in Equation 6.2 [17].

$$Iy \approx Iy^N = \int_{-1}^{1} \alpha(\tau) \sum_{i=0}^{N} y_i \phi_i(\tau)\, d\tau$$

By defining the discrete weights, w_i, for $i = 0, 1...N$ as

$$w_i = \int_{-1}^{1} \alpha(\tau)\, \phi_i(\tau)\, d\tau$$

where the weights correspond to the choice of orthogonal polynomials used, we can develop the performance measure [17].

$$Iy^N = \sum_{i=0}^{N} w_i y_i \tag{6.7}$$

6.3 Pseudospectral Legendre Method

The Pseudospectral Legendre method is a type of direct method that uses spectral collocation with the Legendre-Gauss-Lobatto (LGL) points as the nodes for the collocation and the globally orthogonal Lagrange polynomials as the interpolating polynomials for the discretization. As stated in the above section, the use of globally orthogonal polynomials and a set of corresponding nodes will yield an exact solution to the state approximation at the nodes. Hence, the approximation occurs only at the intermediate points. The performance index is

discretized using the Gauss-Lobatto quadrature rule.

6.3.1 Legendre-Gauss-Lobatto Points

The choice of nodes for the discretization of the optimal control problem into a nonlinear programming problem is determined by which set of nodes yields the best polynomial approximation, in the least squares sense [17, 19]. The Legendre polynomials of order N, L_N, are orthogonal over the interval [-1 1], with the weighting function, $\alpha(t) = 1$. To determine the node distribution over the interval [-1 1], we define $\tau_0 = -1$ and $\tau_N = 1$. The interior nodes, τ_l, for $l = 1, 2...N-1$ are the roots of $\dot{L}_N$, the derivative of the N^{th} order Legendre polynomial. The values of the nodes must be determined numerically, as there is no closed-form expression [15].

The Legendre polynomials are globally orthogonal over the interval [-1 1]. Hence, to use the LGL nodes, we must transform the problem time ($t \in [t_0 \ t_f]$) of our optimal control problem to the interval [-1 1]. The linear transformation between the problem time, t, and the time at the node point, τ, is

$$t = \frac{(t_f - t_0)\tau + (t_f + t_0)}{2} \tag{6.8}$$

The LGL points are not uniformly spaced. In fact, the LGL points are clustered at both ends of the interval. Figure 6-1 shows the distribution of the node points for different values of N.

6.3.2 Discretization of the State and Control

A Pseudospectral Legendre method uses Lagrange polynomials ($\phi_l(\tau)$) to interpolate the state and control at the LGL points. Lagrange polynomials are related to Legendre polynomials by [17]

$$\phi_l(\tau) = \frac{1}{N(N+1)L_N(\tau_l)} \frac{(\tau^2 - 1)\dot{L}_N(\tau)}{\tau - \tau_l} \tag{6.9}$$

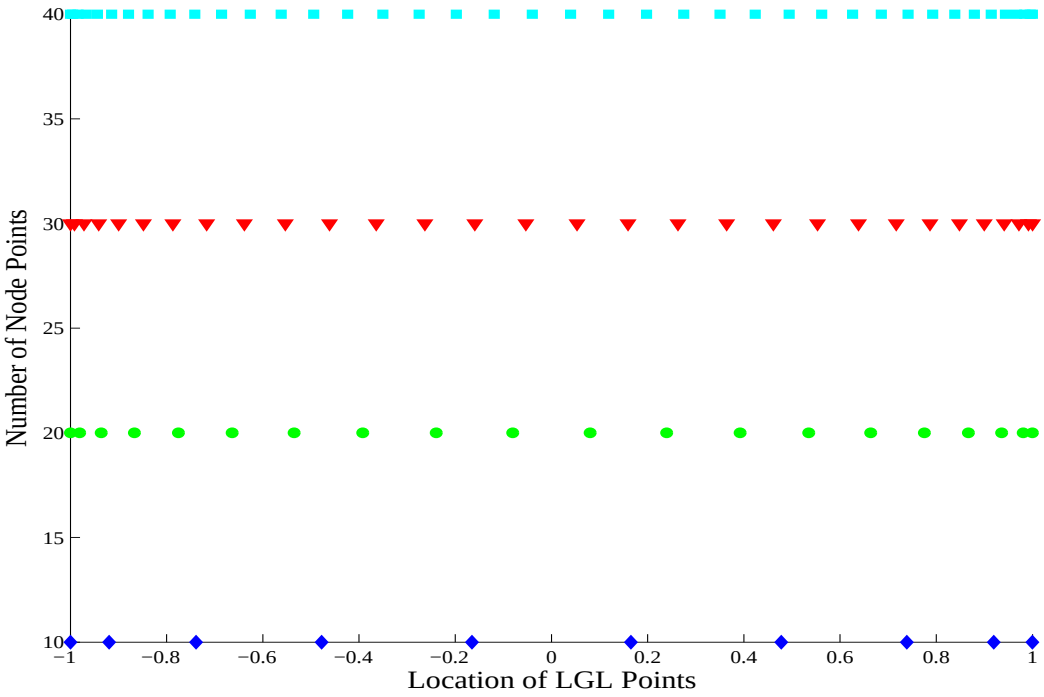

Figure 6-1: Distribution of LGL Points for a Given Number of Nodes

where $\dot{L}_N(\tau)$ is the derivative of the Legendre polynomial. By approximating the continuous state and control as N^{th} degree Lagrange polynomials, we get the following expressions.

$$\begin{aligned} \mathbf{x}(\tau) &\approx \mathbf{x}^N(\tau) = \sum_{l=0}^{N} \mathbf{x}(\tau_l)\,\phi_l(\tau) \\ \mathbf{u}(\tau) &\approx \mathbf{u}^N(\tau) = \sum_{l=0}^{N} \mathbf{u}(\tau_l)\,\phi_l(\tau) \end{aligned} \tag{6.10}$$

Using Equation 6.3, Equation 6.10 becomes

$$\begin{aligned} \mathbf{x}^N(\tau_k) &= \mathbf{x}(\tau_k) \\ \mathbf{u}^N(\tau_k) &= \mathbf{u}(\tau_k) \qquad\qquad k = 0, 1, \ldots N \end{aligned} \tag{6.11}$$

6.3.3 Boundary Conditions and Path Constraints

The transformation of the boundary conditions from $t \in [t_0 \;\; t_f]$ to the LGL interval $\tau \in [-1 \;\; 1]$ is accomplished by simply recognizing that t_0 corresponds to $\tau = -1$ and that t_f corresponds to $\tau = 1$. Therefore, the boundary conditions

on the state simply correspond to

$$\begin{aligned} \mathbf{h}_0\left(\mathbf{x}\left(-1\right), t_0\right) &= 0 \\ \mathbf{h}_f\left(\mathbf{x}\left(1\right), t_f\right) &= 0 \end{aligned} \tag{6.12}$$

for the initial and terminal conditions respectively.

The path constraints that occur over the entire time interval are transformed using Equation 6.8 to transform the time to the interval [-1 1]. Therefore, the expression for the path constraints is

$$\mathbf{g}_{min} \leq \mathbf{g}\left(\mathbf{x}\left(\tau\right), \mathbf{u}\left(\tau\right), \tau, t_0, t_f\right) \leq \mathbf{g}_{max} \tag{6.13}$$

6.3.4 Differential Equations

In the Pseudospectral Legendre method, the differential equations are evaluated at the LGL points by a differentiation matrix. To define the differentiation matrix, the analytic derivative of the state equation is taken and evaluated at the LGL points. Thus, the time derivative of the state in Equation 6.10 is given by a multiplication of the differentiation matrix, D, with the state.

$$\begin{aligned} \dot{\mathbf{x}}\left(\tau_k\right) &= \sum_{l=0}^{N} \mathbf{x}\left(\tau_l\right) \dot{\phi}_l\left(\tau_k\right) \\ \dot{\mathbf{x}}\left(\tau_k\right) &= \sum_{l=0}^{N} D_{kl} \mathbf{x}\left(\tau_l\right) \end{aligned} \tag{6.14}$$

D_{kl} is the $(N+1) \times (N+1)$ differentiation matrix whose elements are defined in Equation 6.15 [10].

$$\mathbf{D} = \left[D_{kl}\right] = \begin{cases} \dfrac{L_N\left(\tau_k\right)}{L_N\left(\tau_l\right)} \dfrac{1}{\tau_k - \tau_l} & k \neq l \\ -\dfrac{N\left(N+1\right)}{4} & k = l = 0 \\ \dfrac{N\left(N+1\right)}{4} & k = l = N \\ 0 & \textbf{otherwise} \end{cases} \tag{6.15}$$

6.3.5 Objective Function

The objective function is evaluated using the Gauss-Lobatto integration rule, which transforms the objective functional into an algebraic expression in terms of the discretized state and control.

$$\begin{aligned} \mathcal{J} \approx \mathcal{J}^N &= \mathcal{M}\left(\mathbf{x}^N(-1), t_0\right) + \mathcal{N}^N\left(\mathbf{x}^N(1), t_f\right) + \frac{t_f - t_0}{2} \int_{-1}^{1} \mathcal{L}\left(\mathbf{x}^N(\tau), \mathbf{u}^N(\tau), \tau\right) d\tau \\ &= \mathcal{M}\left(\mathbf{x}(-1), t_0\right) + \mathcal{N}\left(\mathbf{x}(1), t_f\right) + \frac{t_f - t_0}{2} \sum_{k=0}^{N} \mathcal{L}\left(\mathbf{x}(\tau_k), \mathbf{u}(\tau_k), \tau_k, t_0, t_f\right) w_k \end{aligned} \tag{6.16}$$

The weighting function, $w_k, \quad k = 0, 1, ...N$ is defined as

$$w_k = \frac{2}{N(N+1)} \frac{1}{L_N(\tau_k)^2}$$

when the nodes $\tau_k, \quad k = 0, 1...N$ correspond to the LGL points [10].

6.3.6 Nonlinear Programming Problem

The optimal control problem given in Section 4.2 is transformed into the following nonlinear programming problem via the Pseudospectral Legendre method.

Minimize the cost function

$$\mathcal{J} = \mathcal{M}\left(\mathbf{x}(-1), t_0\right) + \mathcal{N}\left(\mathbf{x}(1), t_f\right) + \frac{t_f - t_0}{2} \sum_{k=0}^{N} \mathcal{L}\left(\mathbf{x}(\tau_k), \mathbf{u}(\tau_k), \tau_k, t_0, t_f\right) w_k \tag{6.17}$$

over the variables

$$\begin{gathered} \mathbf{x}(\tau_k) \in \mathbb{R}, k = 0, 1, \ldots, N \\ \mathbf{u}(\tau_k) \in \mathbb{R}, k = 0, 1, \ldots, N \\ t_0 \in \mathbb{R} \\ t_f \in \mathbb{R} \end{gathered} \tag{6.18}$$

subject to

$$\begin{gathered}\sum_{l=0}^{N} D_{kl}\mathbf{x}(\tau_k) - \left(\frac{t_f - t_0}{2}\right)\mathbf{a}\left(\mathbf{x}(\tau_k), \mathbf{u}(\tau_k), \tau_k, t_0, t_f\right) = 0, \quad k = 0, 1, \ldots, N \\ \mathbf{g}_{min} \leq \mathbf{g}\left(\mathbf{x}(\tau), \mathbf{u}(\tau), \tau, t_0, t_f\right) \leq \mathbf{g}_{max} \quad k = 0, 1, \ldots, N \\ \mathbf{h}_0\left(\mathbf{x}(-1), t_0\right) = 0 \\ \mathbf{h}_f\left(\mathbf{x}(1), t_f\right) = 0\end{gathered} \tag{6.19}$$

6.4 Pseudospectral Legendre Method for Multiple Phase Optimal Control Problems

The optimal control problem presented in this research is modeled as a three phase problem where each phase has the properties of a general optimal control problem. Thus within each phase there is a state, a control, a dynamic model, path constraints, boundary conditions and a performance measure. To ensure that the solution obtained is a solution to the entire problem, linkage constraints are added at the boundaries between adjacent phases, where appropriate.

To discretize the multiple phase optimal control problem into a nonlinear programming problem using the Pseudospectral Legendre method, we must discretize each phase according to the method presented in the previous section. For each phase, i (for $i \in [1, 2, 3]$), we must chose the number of nodes for the phase, $N^{(i)}$. Thus, $\tau_k^{(i)}$, $w_k^{(i)}$, and $D^{(i)}$ are the LGL points, weights and differentiation matrix, respectively, in each phase, i, for $k = 0, 1, \ldots, N^{(i)}$.

The state and control are discretized in each phase such that

$$\begin{aligned}\mathbf{x}^{(i)}\left(\tau^{(i)}\right) &\approx \sum_{l=0}^{N^{(i)}} \mathbf{x}^{(i)}\left(\tau_l^{(i)}\right)\phi_l\left(\tau^{(i)}\right) \\ \mathbf{u}^{(i)}\left(\tau^{(i)}\right) &\approx \sum_{l=0}^{N^{(i)}} \mathbf{u}^{(i)}\left(\tau_l^{(i)}\right)\phi_l\left(\tau^{(i)}\right)\end{aligned} \tag{6.20}$$

The dynamic constraints for each phase, i, are given as

$$\dot{\mathbf{x}}^{(i)}\left(\tau_k^{(i)}\right) = \sum_{l=0}^{N^{(i)}} D_{kl}^{(i)} \mathbf{x}\left(\tau_l^{(i)}\right) \tag{6.21}$$

The boundary conditions for each phase are

$$\begin{aligned} \mathbf{h}_0^{(i)}\left(\mathbf{x}^{(i)}(-1), t_0^{(i)}\right) &= 0 \\ \mathbf{h}_f^{(i)}\left(\mathbf{x}^{(\mathbf{i})}(1), t_f^{(i)}\right) &= 0 \end{aligned} \tag{6.22}$$

The path constraints in each phase are

$$\mathbf{g}_{min}^{(i)} \leq \mathbf{g}^{(i)}\left(\mathbf{x}^{(i)}\left(\tau^{(i)}\right), \mathbf{u}^{(i)}\left(\tau^{(i)}\right), \tau^{(i)}, t_0^{(i)}, t_f^{(i)}\right) \leq \mathbf{g}_{max}^{(i)} \tag{6.23}$$

The performance measure in each phase is given as

$$\begin{aligned} \mathcal{J}^{(i)} &= \mathcal{M}^{(i)}\left(\mathbf{x}^{(i)}(-1), t_0^{(i)}\right) + \mathcal{N}^{(i)}\left(\mathbf{x}^{(i)}(1), t_f^{(i)}\right) \\ &\quad + \frac{t_f^{(i)} - t_0^{(i)}}{2} \sum_{k=0}^{N^{(i)}} \mathcal{L}^{(i)}\left(\mathbf{x}_k^{(i)}, \mathbf{u}_k^{(i)}, \tau_k^{(i)}, t_0^{(i)}, t_f^{(i)}\right) w_k^{(i)} \end{aligned} \tag{6.24}$$

where the following notation is used for convenience.

$$\begin{aligned} \mathbf{x}_k^{(i)} &\equiv \mathbf{x}^{(i)}\left(\tau_k^{(i)}\right) \\ \mathbf{u}_k^{(i)} &\equiv \mathbf{u}^{(i)}\left(\tau_k^{(i)}\right) \end{aligned} \tag{6.25}$$

In addition to the above constraints, we must discretize the linkage constraints between the phases. The linkage constraint for time is

$$t_f^{(i)} - t_0^{(i)} = 0, \quad i = 1, 2 \tag{6.26}$$

If we define a general linkage constraint function, $\mathbf{L}$, that links the appropriate states between phases, then the corresponding discretized linkage constraints are

$$\mathbf{L}\left(\mathbf{x}_{N^{(i)}}^{(i)}, \mathbf{x}_0^{(i+1)}\right) = 0 \quad i = 1, 2 \tag{6.27}$$

Thus, using the Pseudospectral Legendre method, the multiple phase optimal control problem is transformed into the following nonlinear programming problem.

Minimize

$$\mathcal{J} = \sum_{i=1}^{3} \mathcal{J}^{(i)} \tag{6.28}$$

over the variables

$$\begin{aligned} &\mathbf{x}_k^{(i)} \in \mathbb{R}, k = 0, 1, \ldots, N^{(i)} \\ &\mathbf{u}_k^{(i)} \in \mathbb{R}, k = 0, 1, \ldots, N^{(i)} \\ &t_0^{(i)} \in \mathbb{R}, \qquad\qquad i = 1, 2, 3 \\ &t_f^{(i)} \in \mathbb{R} \end{aligned} \tag{6.29}$$

subject to

$$\begin{aligned} &\textstyle\sum_{l=0}^{N^{(i)}} D_{kl}^{(i)} \mathbf{x}_k^{(i)} - \left(\frac{t_f^{(i)} - t_0^{(i)}}{2} \right) \mathbf{a}^{(i)} \left(\mathbf{x}_k^{(i)}, \mathbf{u}_k^{(i)}, \tau_k^{(i)}, t_0^{(i)}, t_f^{(i)} \right) = 0, \quad k = 0, 1, \ldots, N^{(i)} \\ &\mathbf{g}_{min}^{(i)} \leq \mathbf{g}^{(i)} \left(\mathbf{x}^{(i)}(\tau), \mathbf{u}^{(i)}(\tau^{(i)}), \tau^{(i)}, t_0^{(i)}, t_f^{(i)} \right) \leq \mathbf{g}_{max}^{(i)} \quad k = 0, 1, \ldots, N^{(i)} \\ &\mathbf{h}_0^{(i)} \left(\mathbf{x}^{(i)}(-1), t_0^{(i)} \right) = 0, \qquad\qquad i = 1, 2, 3 \\ &\mathbf{h}_f^{(i)} \left(\mathbf{x}^{(i)}(1), t_f^{(i)} \right) = 0 \end{aligned} \tag{6.30}$$

and

$$\begin{aligned} &t_f^{(i)} - t_0^{(i)} = 0 \\ &\mathbf{L} \left(\mathbf{x}_N^{(i)}, \mathbf{x}_0^{(i+1)} \right) = 0 \qquad\qquad i = 1, 2 \end{aligned} \tag{6.31}$$

6.5 Implementation of the Pseudospectral Legendre Method

To apply the Pseudospectral Legendre method to the abort problem presented in this thesis, two implementations of this method have been considered. In Reference 34, Ross and Fahroo have developed an approach for solving non-

smooth optimal control problems and have implemented this method in the software package *Direct Indirect Dynamic Optimization* (DIDO). Although DIDO can be used to solve multiple segment optimal control problems numerically, the version of DIDO that was available at the time this research began did not have the capability to change mathematical models between segments (including changing the dimension of the state or the control between segments). In Reference 30, Rao presents a more general implementation of the Pseudospectral Legendre method. It should be noted that the implementation of Reference 30 allows for the user to conveniently define the first-order analytic derivatives for the problem.

The research presented in this thesis uses the implementation presented in Reference 30. The abort problem, as defined in Section 3.5, uses a different state and control to define the system in each phase, and the implementation presented in Reference 30 allows for this to be accomplished directly. However, the primary benefit of using this implementation is the ability to conveniently input first-order analytic derivatives. The objective functional presented in Section 5.1 contains a term for the sensed acceleration. However, the gradient of the sensed acceleration can become very large. During initial trials, computing the gradient of the sensed acceleration numerically, caused the problem to become infeasible. Although defining the lift and drag accelerations as in Equation 3.2 and minimizing the square of the sensed acceleration as discussed in Section 5.1, increases the accuracy in the numerical derivatives, the problem persists. Thus, to achieve reliable solutions for all cases studied, analytic derivatives are defined for the problem and are given in Appendix B.

6.6 Solving the Nonlinear Programming Problem

The problem that is defined in the previous section is a large scale sparse nonlinear programming problem with both linear and nonlinear equality and inequality constraints. Sequential quadratic programming (SQP) methods are designed

to solve large-scale optimization problems with both linear and nonlinear constraints in an efficient and reliable manner [21]. A general multiple phase optimal control problem is sparse and therefore an efficient approach to solving this problem should take that into account.

Three different NLP solvers that use a SQP method are NPSOL, SNOPT, SPRNLP. NPSOL and SNOPT were written by Gill, Murray, and Saunders [21, 22, 23] and both have a similar structure, but NPSOL is unable to take advantage of the sparsity in the Jacobian. SPRNLP was written at Boeing by Betts and Frank [5]. In Reference 5, a study was performed comparing, among other methods, SPRNLP and SNOPT. The study showed that SPRNLP solves large problems quicker that SNOPT. SPRNLP also computes the full Hessian, which gives it the advantage of using second derivative information. The study also showed SNOPT solves smaller problems faster than SPRNLP and is a reliable method for solving large scale problems. Thus, SNOPT is a reliable method for solving a large scale nonlinear programming problem and is the optimizer chosen in this research.

6.6.1 Description of SNOPT

SNOPT is a sparse nonlinear optimizer that utilizes a sequential quadratic programming method to solve the nonlinear programming problem. A SQP method solves the nonlinear programming problem by iteratively solving a quadratic approximation to the problem (the QP subproblem) through a series of major and minor iterations. The solution to the QP subproblem allows SNOPT to determine the search direction and step length necessary to minimize the performance measure of the original NLP. Although a detailed description is beyond the scope of this thesis, a brief discussion of SNOPT and the SQP method will be presented. The reader is directed to Reference 21 and Reference 23 for a complete explanation.

SNOPT minimizes the performance index of the nonlinear programming problem using a sequential quadratic programming method. First, SNOPT converts

inequality constraints into equality constraint by adding slack variables to the problem. Then, SNOPT begins a major iteration which assigns values to the optimization variables such that all linear constraints are satisfied. To determine a search direction for the next iteration, SNOPT formulates and solves the QP subproblem through a series of minor iterations. The QP subproblem solves a quadratic approximation to the Lagrangian of the NLP subject to a Taylor's series linearization of the nonlinear constraints and the bounds on the variables. A reduced Hessian algorithm is used to solve the QP subproblem, where the Hessian is the matrix of second derivatives. SNOPT uses a BFGS quasi-Newton approximation to the Hessian, instead of other algorithms that utilize the full sparse Hessian, because the computational effort expended to compute the full Hessian is significant and a quasi-Newton method avoids the problem of a non positive definite Hessian [3].

Once a solution to the QP subproblem is obtained, a new iterate of the solution is determined by performing a line search on the augmented Lagrangian merit function. The merit function is used to determine how much progress the algorithm is making. The line search determines the direction that that will produce the largest decrease in the merit function. This process is repeated until the current iterate satisfies the first order conditions for optimality.

6.6.2 Sparsity

SNOPT is a sparse nonlinear optimizer, which has the ability to take advantage of the sparsity of a problem. Although it is not necessary, it is highly advantageous to supply SNOPT with the sparsity matrix for the NLP. The sparsity matrix is composed of a series of zeros and ones that alert SNOPT to a constraint's dependency on a variable. If the constraint is not dependent on a variable, the derivative with respect to that variable is zero. This feature allows SNOPT to automatically set the corresponding elements of the Jacobian, the matrix of first derivatives for the constraints, to zero, without spending the computational ef-

fort to calculate them. If a constraint is dependent on a variable, the sparsity element is one and the corresponding derivative in the Jacobian is computed. Hence, this feature saves a great deal of computational time for sparse problems.

For a multiple phase optimal control problem, this feature is of significant importance, since there are a large number of variables, but only a portion are active in a given phase. Thus, the inherent structure of a multiple phase problem has large blocks of zeros in the sparsity matrix.

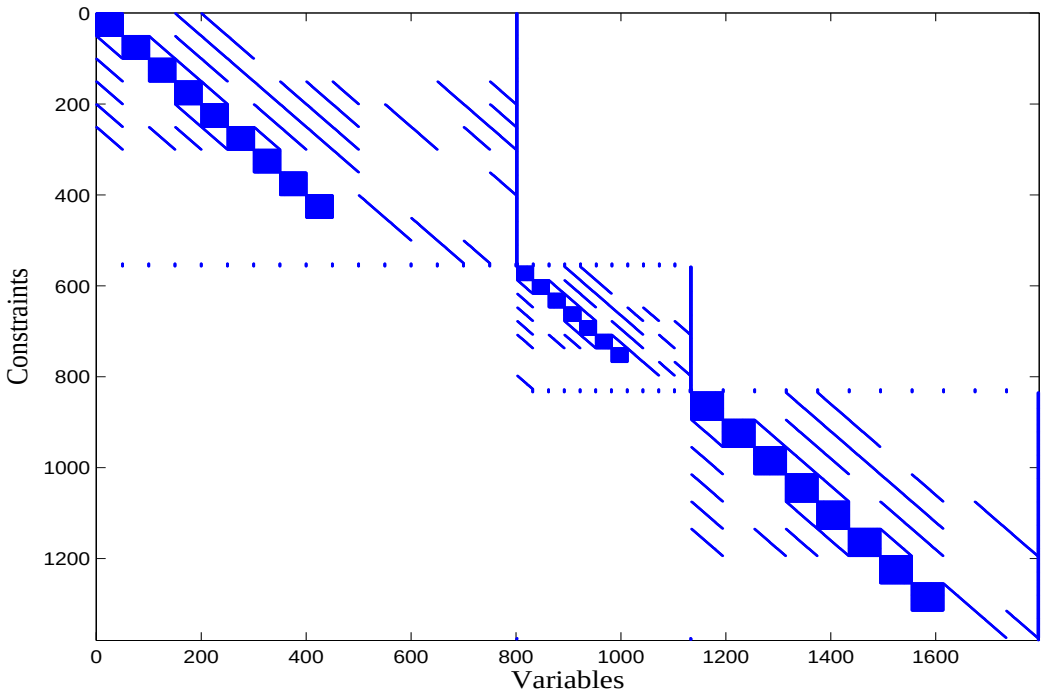

Figure 6-2: Sparsity Pattern for Abort Problem

The sparsity pattern depicted in Figure 6-2 is the matrix of dependencies for the entire nonlinear programming problem. The ordering of the constraints, starting from the top, corresponds to the dynamic constraints for the first phase, followed by the path constraints. The next set of constraints are the linkage constraints between the first two segments. This pattern is repeated for each phase. The last set of constraints correspond to the linear constraints on time. There are three constraints that require time to proceed forward in each phase and two linkage constraints to connect the time between adjacent phases. The

ordering of the variables follows a similar pattern, from left to right, starting with the state, control and time variables for the first phase, followed by the variables for the remaining phases. With the exception of the linkage constraints, the constraints in each phase are decoupled, thus creating a sparse Jacobian.

6.6.3 Scaling

Scaling can be a major issue in the behavior of the optimizer and at the worst case, prohibit the optimizer from finding a solution. Thus, a well-scaled problem is highly desirable, and sometimes necessary. A general guideline for determining scaling factors is to make every state and control the same order of magnitude and close to unity. However, this can become a serious challenge when approaching a multiple phase optimal control problem because the different regimes of flight allow for large variations in the values of the variables.

A canonical scaling is used in this research to preserve the form of the constraints. A canonical scaling allows for certain variables to be scaled independently, but the remaining variables are scaled subject to the chosen scaling. The equations that define a canonical scaling set are

$$\begin{aligned} v &= \frac{l}{t} \\ \rho &= \frac{m}{l^3} \end{aligned} \tag{6.32}$$

where v is speed, l is length, t is time, ρ is density, and m is mass. In this research, the length, speed and mass were set independently based on a series of trials to determine an appropriate scaling set. Thus, the scaling factors chosen

are

$$\begin{aligned} l_{scale} &= 1R_e \\ v_{scale} &= \sqrt{\frac{\mu}{R_e}} \\ t_{scale} &= \frac{l_{scale}}{v_{scale}} \\ m_{scale} &= 1000kg \\ \rho_{scale} &= \frac{m_{scale}}{l_{scale}^3} \end{aligned} \tag{6.33}$$

The scaling for acceleration, force, energy and other quantities can be calculated from the above scaling factors.

Chapter 7

Parameter Optimization Study of a Trans-Atlantic Shuttle Abort

This thesis examines the trans-atlantic abort trajectories initiated by the loss of a single main engine at five different times during a nominal ascent trajectory. In this chapter, the optimized trajectories originating from each initial condition and terminating at either of the two prospective landing sites are examined. For each of these aborts, the weighting factors in the third phase cost functional are varied. Recall that the objective functional for entry (Equation 5.2) minimizes a weighted combination of heating rate, dynamic pressure and sensed acceleration squared. A set of criteria is developed to calculate the cost of each optimized trajectory and evaluate which set of weighting factors produces the best result. Finally, the improvements in cost caused by a model uncertainty will be compared with the improvements from varying the weighting factors to determine if varying the weighting factors produces a significant cost decrease.

7.1 Cost Calculation for the Best Trajectory

The abort trajectories generated are optimal trajectories with respect to a specific choice of weighting factors in the third phase cost functional. However, the goal of this study is to determine the best choice of weighting factors for the

objective functional. Hence, a measure of performance for each case must be designed such that each trajectory from an initial condition can be compared to determine the best trajectory for each abort.

The performance measure selected to determine the best weighting factors for each case is composed of seven terms. Each term assigns a numeric value to important aspects of the trajectory. The set of weighting factors with the lowest combined value is deemed to be the best. The first four terms in this calculation measure the constraint violations in the problem. As previously discussed, instead of employing path constraints for heating rate ($\dot{Q}$), dynamic pressure (q) and sensed acceleration squared (a^2), penalty functions are used to minimize these values. Since violations of the maximum desired values can and do occur, determining the maximum violation of each constraint is of considerable importance. The first term computes the ratio of the maximum value of the squared sensed acceleration in the first phase (a_1^2) to the desired maximum value of sensed acceleration squared (a_{max}^2). The second term computes the ratio of the maximum value of heating rate in the third phase, $\dot{Q}_3$, to the desired maximum heating rate, $\dot{Q}_{max}$. The third term is the ratio of the maximum value of dynamic pressure in the third phase (q_3) to the desired maximum value of dynamic pressure (q_{max}). The fourth term is the ratio of the maximum value of sensed acceleration squared in the third phase (a_3^2) to the maximum desired value of sensed acceleration squared. For better numerical performance the sensed acceleration terms were squared in the cost functionals and remain so in the cost calculation for consistency.

The next three terms measure the accuracy of the control. The equations of motion are integrated using a fourth order variable step size Runga-Kutta integrator and the control is interpolated by a piece-wise cubic spline. The resulting integrated solution is then measured against the optimized solution for accuracy at the TAEM interface. Thus, the remaining three terms represent the accuracy of the integrated dynamics using the interpolated control. The fifth term measures the error in the final energy. The remaining two terms measure the error in lon-

gitude and latitude, respectively. Since the final location may be a distance of 59 miles in either direction around the landing site, the error in the final location is scaled by e_{TAEM}, where e_{TAEM} represents this distance in a degree measurement. To calculate the cost associated with a choice of weighting factors for a specific abort case, the above translates into the following expressions.

$$\begin{aligned}
term_1 &= \frac{max\,(a_1)}{a_{max}} \\
term_2 &= \frac{max\left(\dot{Q}_3\right)}{\dot{Q}_{max}} \\
term_3 &= \frac{max\,(q_3)}{q_{max}} \\
term_4 &= \frac{max\,(a_3)}{a_{max}} \\
term_5 &= 1000\left|\frac{e_{f_{nom}} - e_{f_{int}}}{e_{f_{nom}}}\right| \\
term_6 &= \left|\frac{\theta_{f_{nom}} - \theta_{f_{int}}}{e_{TAEM}}\right| \\
term_7 &= \left|\frac{\phi_{f_{nom}} - \phi_{f_{int}}}{e_{TAEM}}\right|
\end{aligned} \tag{7.1}$$

The subscript nom refers to the value obtained from the optimized solutions. The subscript int refers to the integrated value. The fifth term is multiplied by a factor of one thousand to maintain a consistent order of magnitude between each term. The cost for a trajectory is the sum of the above seven terms.

7.2 Abort Trajectories

The cost calculation described in the previous section creates a means of comparison between all abort trajectories. As stated, an abort occurs at a specific time along a nominal ascent path to orbit after SRB depletion but before the ET is dropped. The times for which an abort occurs are determined by dividing the time interval for a nominal second stage ascent into four equal segments, creat-

ing five times for evaluation. By considering the initial time as the beginning of the second stage of ascent, we can calculate the time at abort as zero percent, twenty-five percent, fifty percent, seventy-five percent and one-hundred percent of the time it takes to complete the nominal second stage ascent mission. For each of these cases, a trajectory is obtained to both of the two potential landing sites, Senegal and Spain. In this section each abort case is examined and the best solution is given along with some description of the trajectory.

7.2.1 Potential Landing Sites

Before delving into the descriptions for each abort, the landing sites must be defined. Two landing sites are chosen for a trans-atlantic abort: Senegal and Spain. Thus, from each abort point, we can compare the trajectory that terminates at either of these landing sites. The TAEM interface dictates the final altitude, speed, and flight path angle.

$$\begin{aligned} h\left(t_f\right) &= 24.3840 \text{ km} \\ v\left(t_f\right) &= 762 \text{ m/s} \\ \gamma\left(t_f\right) &= -5 \text{ deg} \end{aligned} \tag{7.2}$$

In addition to the terminal constraints listed in Equation 7.2, the terminal manifold specifies the distance from a specific landing site. Thus, by assuming a box around the chosen landing site, we create a set of permissible values for longitude and latitude at each landing site. The longitude and latitude coordinates for Dakar, Senegal are $\theta_{sen} = -17.433$ deg and $\phi_{sen} = 14.667$ deg, respectively. Thus, the constraints on the final location are

$$\begin{aligned} \theta_{sen}\left(t_f\right) - e_{TAEM} \leq \theta\left(t_f\right) \leq \theta_{sen} + e_{TAEM} \\ \phi_{sen}\left(t_f\right) - e_{TAEM} \leq \phi\left(t_f\right) \leq \phi_{sen} + e_{TAEM} \end{aligned} \tag{7.3}$$

The longitude and latitude coordinates for Moron, Spain are $\theta_{sp} = -2.4167$ deg and $\phi_{sp} = 41.4167$ deg, respectively. Thus, the constraints on the final location

are

$$\begin{aligned} \theta_{sp}(t_f) - e_{TAEM} \leq \theta(t_f) \leq \theta_{sp} + e_{TAEM} \\ \phi_{sp}(t_f) - e_{TAEM} \leq \phi(t_f) \leq \phi_{sp} + e_{TAEM} \end{aligned} \tag{7.4}$$

7.2.2 Zero Percent Along a Nominal Trajectory

Zero percent along the nominal trajectory refers to the loss of a main engine at the initial point of stage-2 ascent. The initial conditions for this case are the initial conditions for the nominal ascent, namely

$$\begin{array}{lcllcl} t_0 & = & 0 \text{ min} & v(t_0) & = & 1853.1 \text{ m/s} \\ h(t_0) & = & 46.4476 \text{ km} & \gamma(t_0) & = & 26.4090 \text{ deg} \\ \theta(t_0) & = & -80.6146 \text{ deg} & \chi(t_0) & = & 0 \text{ deg} \\ \phi(t_0) & = & 28.3925 \text{ deg} & m(t_0) & = & 6.76 \times 10^5 \text{ kg} \end{array} \tag{7.5}$$

The best trajectory generated for an abort from this point to Senegal is obtained with a weighting factor in the third phase cost functional of $k_1 = 1$, $k_2 = 1$, $k_3 = 3$. These weighting factors are chosen based on the cost calculation given in Equation 7.1.

Examining the values listed for each term in Table 7.1, we can see that only the heating rate constraint and the third phase sensed acceleration constraint are satisfied. In fact, no combination of weighting factors used satisfies all constraints. The dynamic pressure constraint is relatively close to the desired maximum value and may be acceptable, but the sensed acceleration in the first phase is over four times the desired value, which would make this trajectory completely undesirable to fly. The control obtained from the solution is highly unreliable when integrated, as shown by the remaining terms of the cost calculation.

Referring to Figure 7-1, the solution obtained from integrating the control deviates off the path to Senegal and into the Atlantic ocean. The altitude and speed also deviate from the solution. Notice, that the error does not become too large until the third phase. By analyzing the entry bank angle (Figure 7-4), we

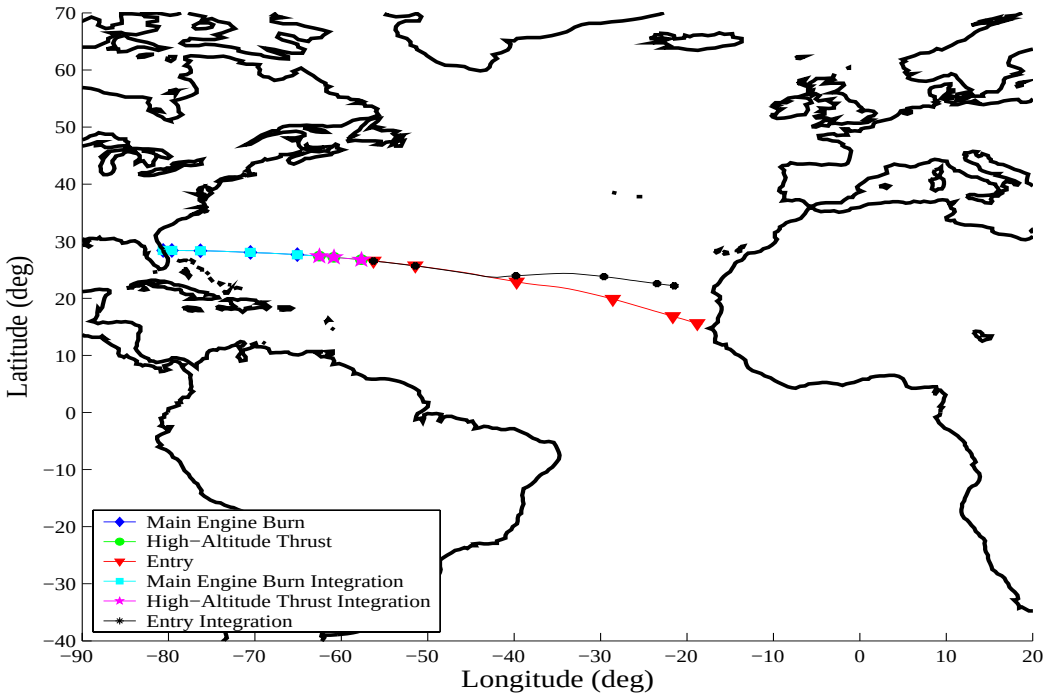

Figure 7-1: Mercator Projection of Zero Percent Abort to Senegal, $k_1 = 1$, $k_2 = 1$, $k_3 = 3$

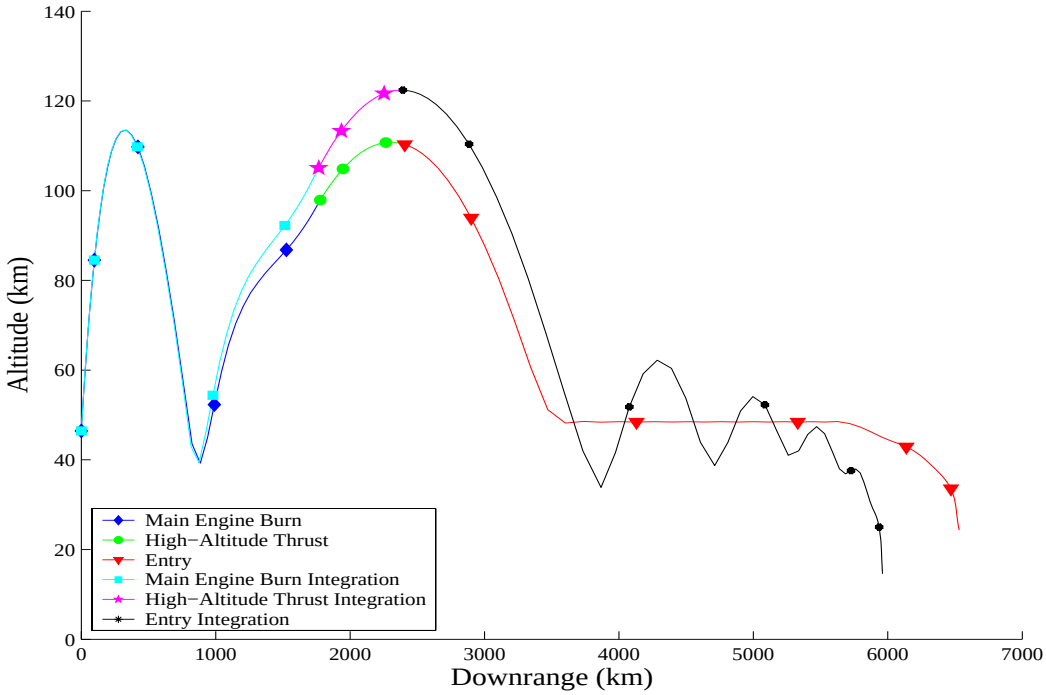

Figure 7-2: Altitude vs. Downrange for a Zero Percent Abort to Senegal, $k_1 = 1$, $k_2 = 1$, $k_3 = 3$

Table 7.1: Cost Calculation for a Zero Percent Abort to Senegal

k_1	k_2	k_3	$term_1$	$term_2$	$term_3$	$term_4$	$term_5$	$term_6$	$term_7$	Cost
1	1	1	4.726	0.841	1.292	1.455	8.085	13.005	14.293	43.700
1.5	1	1	4.739	0.835	1.278	1.590	8.168	13.340	14.621	44.574
2	1	1	4.750	0.837	1.280	1.532	8.183	13.53	14.621	44.741
2.5	1	1	4.782	0.834	1.271	1.618	8.296	14.027	15.037	45.868
3	1	1	4.788	0.836	1.274	1.566	8.279	13.969	14.781	45.495
1	1	1.5	4.819	0.834	1.263	1.530	8.121	13.110	14.224	43.903
1	2	1	4.832	0.835	1.265	1.540	8.120	13.168	14.211	43.973
1	2.5	1	4.957	0.83	1.239	1.584	8.143	13.020	13.689	43.464
1	3	1	4.909	0.832	1.253	1.533	8.210	13.583	14.363	44.686
1	1	1.5	4.704	0.845	1.288	1.178	7.330	9.784	12.471	37.602
1	1	2	4.691	0.844	1.28	1.077	7.063	8.817	12.052	35.833
1	1	2.5	4.646	0.857	1.298	0.981	6.477	7.291	9.360	30.912
1	1	3	4.691	0.847	1.286	0.978	5.219	4.688	9.417	27.129

see that the inaccurate interpolation of the bank angle, due to the assumption of a smooth cubic spline curve fit, causes the error to propagate during the integration of the equations of motion and a significant deviation from the solution arises.

Examining Figure 7-2, two altitude 'increase-decrease' maneuvers are noticed during ME burn. Correlating the downrange distance with that in Figure 7-3, this maneuver is performed to increase the speed to enable the vehicle to travel the large distance to the terminal condition. The maximum value for the flight path angle during entry is zero and referring to Figure 7-5, it can be seen that the flight path angle rides this bound, which corresponds to an equilibrium glide. Without an upper bound on flight path angle, the vehicle would fly at a high altitude to more easily traverse the large distance to the terminal interface. The remaining two main engines and OMS engines operate at full thrust during the entire length of ME burn, as expected.

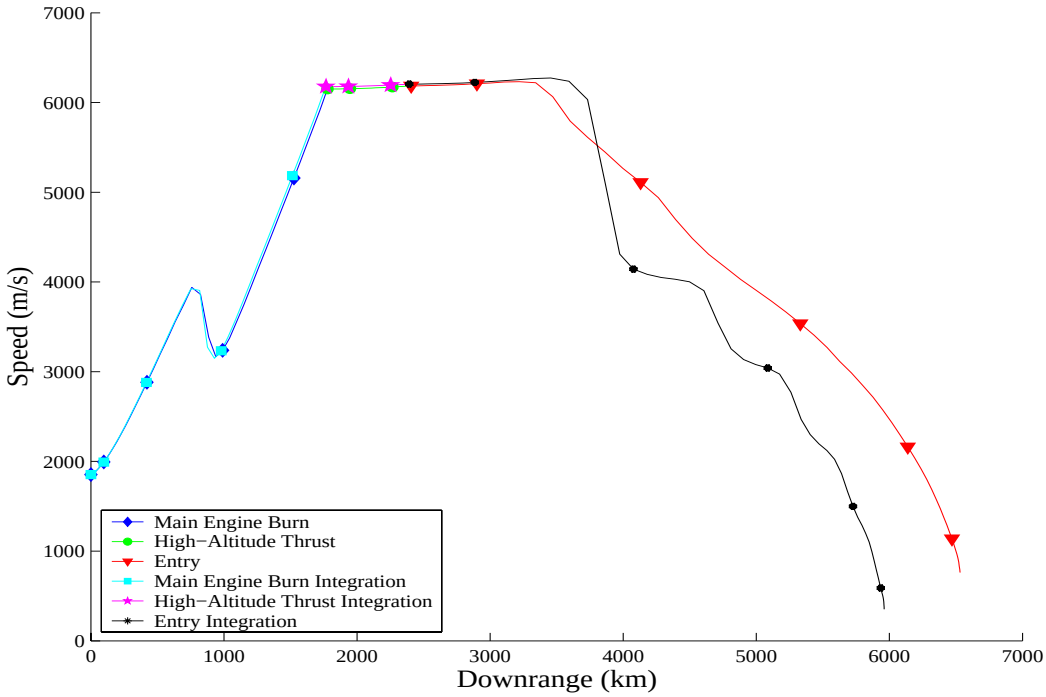

Figure 7-3: Speed vs. Downrange for a Zero Percent Abort to Senegal, $k_1 = 1$, $k_2 = 1$, $k_3 = 3$

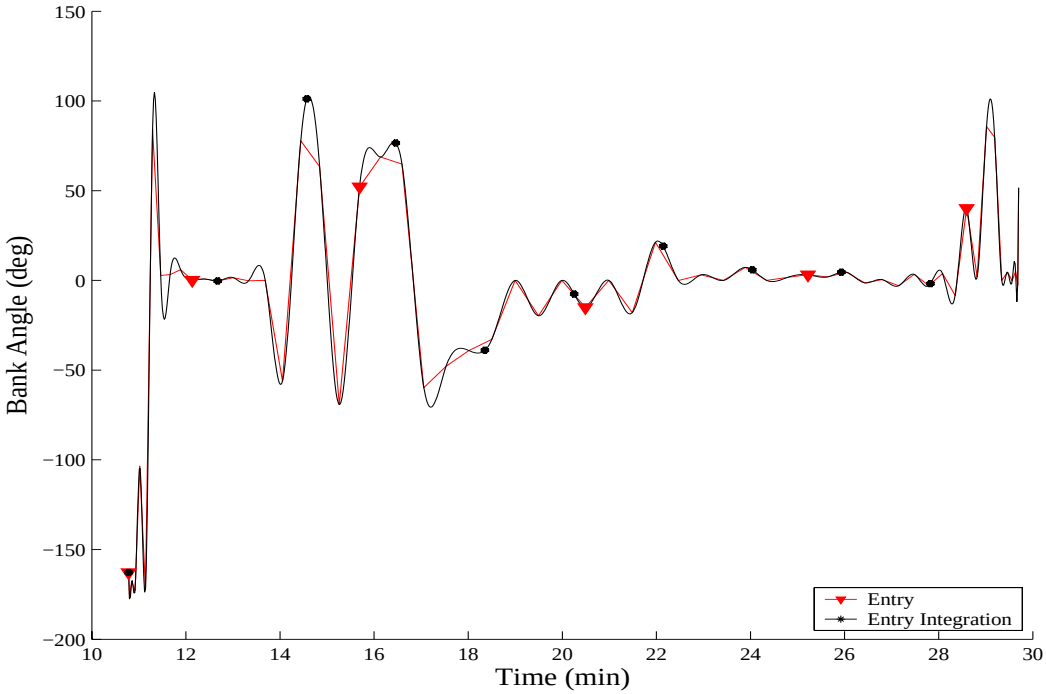

Figure 7-4: Entry Bank Angle vs. Time for Zero Percent Abort to Senegal, $k_1 = 1$, $k_2 = 1$, $k_3 = 3$

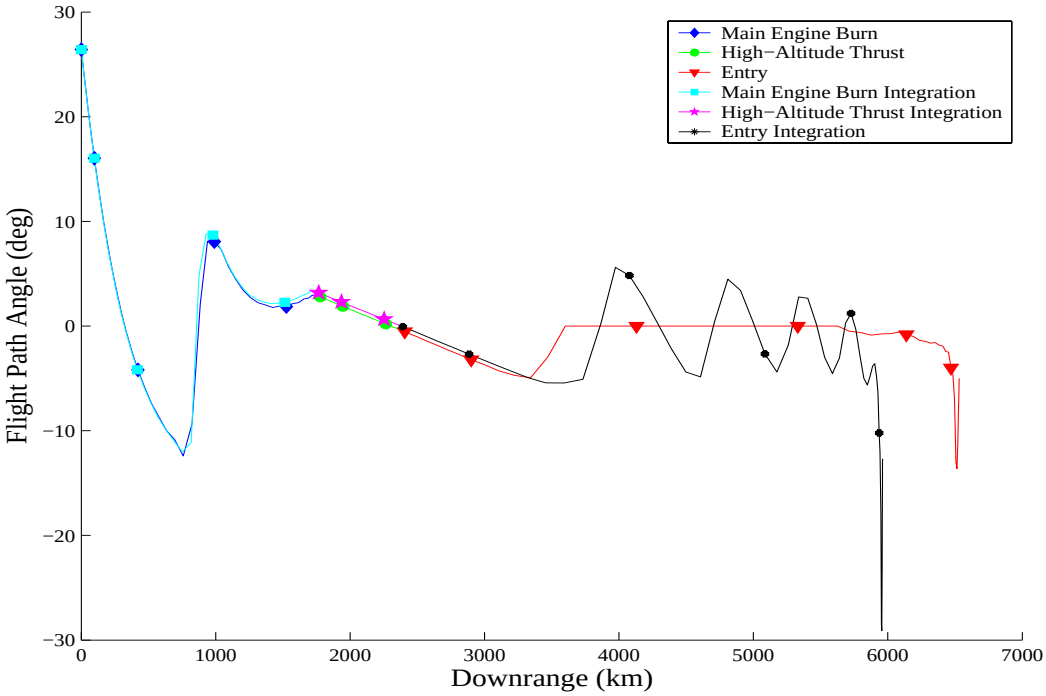

Figure 7-5: Flight Path Angle vs. Downrange for Zero Percent Abort to Senegal, $k_1 = 1$, $k_2 = 1$,$k_3 = 3$

7.2.3 Twenty-five Percent Along a Nominal Trajectory

For this case, the loss of a single ME occurs at twenty-five percent of the time for a nominal ascent. Until this point, the shuttle has been firing with three main engines at full thrust, thus having achieved a significant altitude and speed increase. Equation 7.6 lists the initial conditions.

$$\begin{aligned} t_0 &= 1.6124 \text{ min} & v(t_0) &= 2574.0 \text{ m/s} \\ h(t_0) &= 103.3281 \text{ km} & \gamma(t_0) &= 8.3475 \text{ deg} \\ \theta(t_0) &= -78.5847 \text{ deg} & \chi(t_0) &= -.9547 \text{ deg} \\ \phi(t_0) &= 28.3774 \text{ deg} & m(t_0) &= 5.40 \times 10^5 \text{ kg} \end{aligned} \tag{7.6}$$

The best trajectory generated for an abort from this point to Senegal is obtained with a weighting factor in the third phase cost functional of $k_1 = 1$, $k_2 = 1$, $k_3 = 2.5$. Using Equation 7.1, Table 7.2 gives the breakdown in the cost calculation for this case.

Examining Table 7.2 reveals that the best case for an abort to Senegal vio-

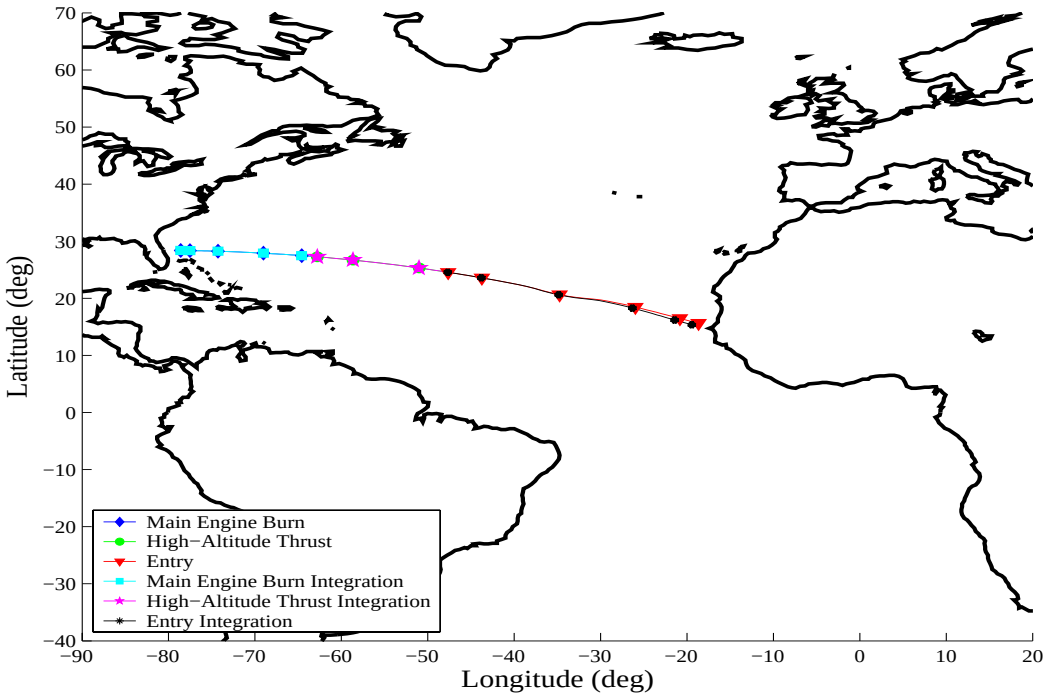

Figure 7-6: Mercator Projection of a Twenty-Five Percent Abort to Senegal, $k_1 = 1$, $k_2 = 1$, $k_3 = 2.5$

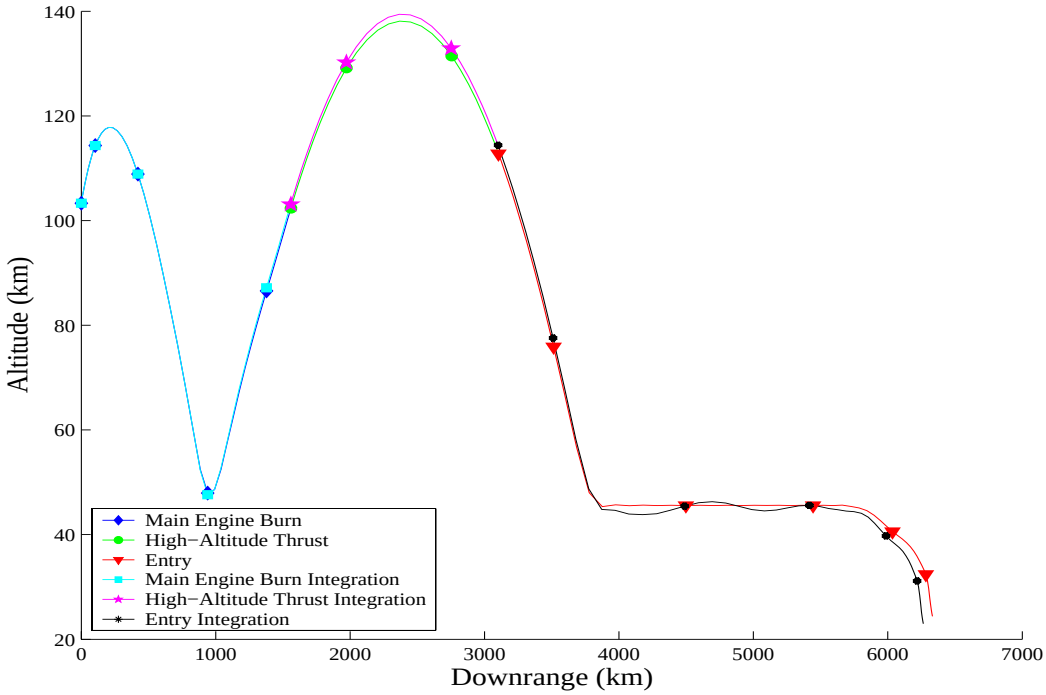

Figure 7-7: Altitude vs. Downrange for Twenty-Five Percent Abort to Senegal, $k_1 = 1$, $k_2 = 1$, $k_3 = 2.5$

Table 7.2: Cost Calculation for a Twenty-five Percent Abort to Senegal

k_1	k_2	k_3	$term_1$	$term_2$	$term_3$	$term_4$	$term_5$	$term_6$	$term_7$	Cost
1	1	1	4.775	0.985	1.845	2.239	3.626	5.639	1.077	20.189
1.5	1	1	4.816	0.981	1.841	2.225	4.067	6.159	0.844	20.935
2	1	1	4.871	0.973	1.829	2.471	4.122	6.306	0.870	21.444
2.5	1	1	4.895	0.969	1.824	2.764	4.108	6.423	1.012	21.997
3	1	1	4.980	0.962	1.809	3.361	4.301	6.673	0.920	23.010
1	1.5	1	5.167	0.973	1.795	2.385	5.848	9.465	1.048	26.683
1	2	1	5.295	0.967	1.784	3.017	6.393	9.306	1.038	27.803
1	2.5	1	5.352	0.971	1.779	2.471	6.163	10.715	1.589	29.043
1	3	1	5.593	0.962	1.739	3.357	6.260	11.595	2.202	31.710
1	1	1.5	4.729	1.001	1.867	2.236	3.154	4.268	0.251	17.510
1	1	2	4.659	1.004	1.870	2.262	2.547	3.802	0.172	16.319
1	1	2.5	4.473	1.009	1.897	2.303	1.128	2.038	0.656	13.507
1	1	3	4.527	1.003	1.883	2.294	1.852	2.800	0.302	14.663

lates the constraints on sensed acceleration, heating rate and dynamic pressure. Although other weighting factor combinations do satisfy the heating rate constraint, other choices yield higher values for other constraints and a less accurate control when integrated. Referring to Figures 7-7 and 7-8, we can see that an altitude 'increase-decrease' maneuver is performed to gain the speed necessary to travel the distance to the terminal conditions at Senegal. Maximum thrust is applied throughout the first two phases to increase the speed.

The best trajectory generated for an abort from this point to Spain is obtained with a weighting factor in the third phase cost functional of $k_1 = 1$, $k_2 = 1$, $k_3 = 3$. Using Equation 7.1, Table 7.3 gives the cost breakdown for this case.

Table 7.3 reveals that even with the best choice of weighting factors, choosing Spain as a landing site yields a higher cost. However, both the heating rate constraint and the third phase sensed acceleration constraint are satisfied for this case. The higher cost is due to the large errors that result from interpolating and integrating the control. The integrated solution banks left into the Atlantic ocean, as shown in Figure 7-9. Referring to Figure 7-10 and Figure 7-11, we can see that the vehicle performs an altitude 'increase-decrease' maneuver

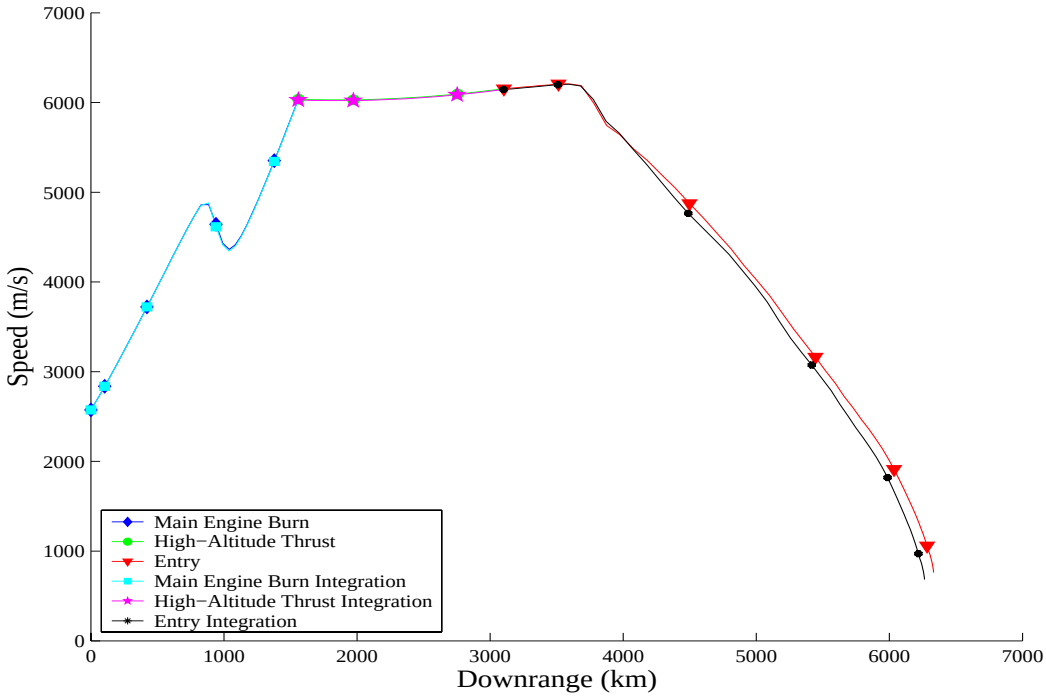

Figure 7-8: Speed vs. Downrange for Twenty-five Percent Abort to Senegal, $k_1 = 1$, $k_2 = 1$, $k_3 = 2.5$

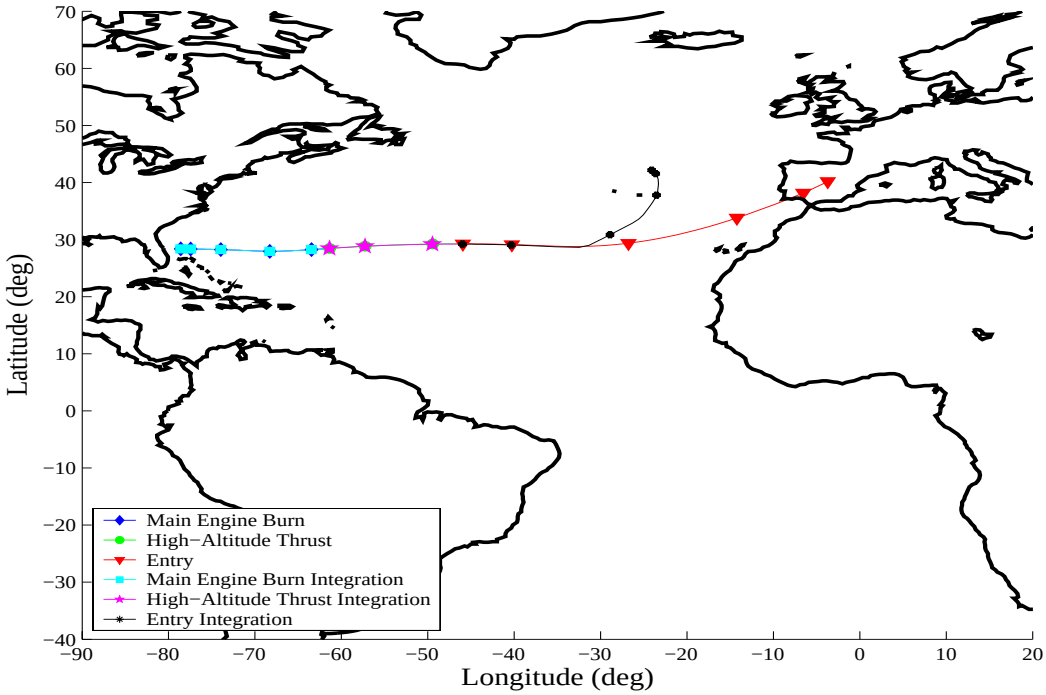

Figure 7-9: Mercator Projection of a Twenty-Five Percent Abort to Spain, $k_1 = 1$, $k_2 = 1$, $k_3 = 3$

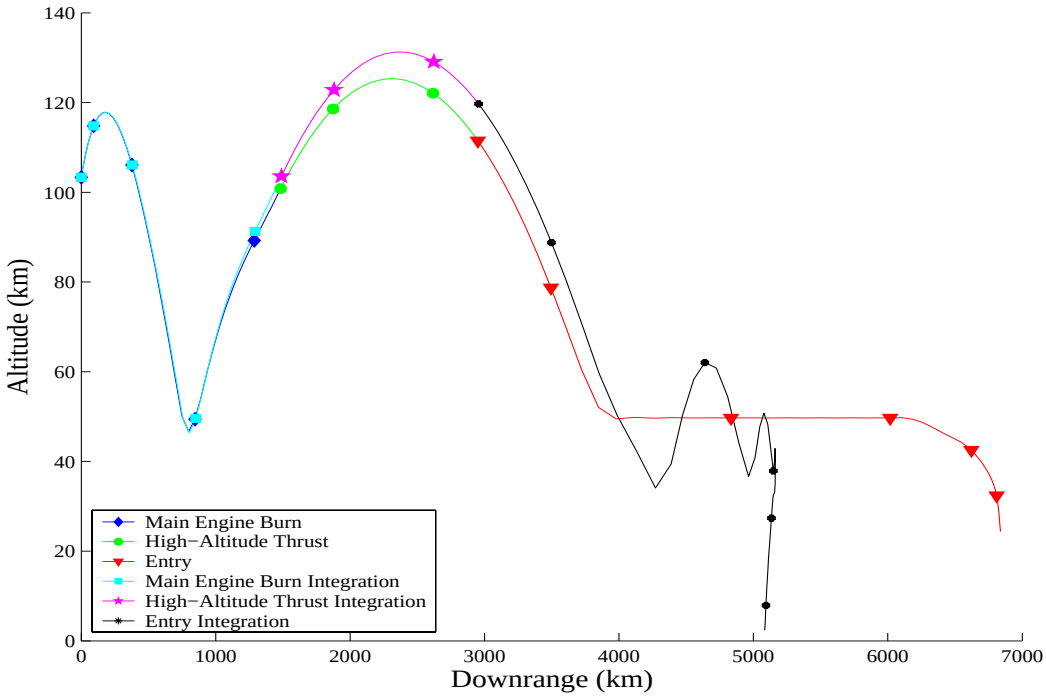

Figure 7-10: Altitude vs. Downrange for a Twenty-Five Percent Abort to Spain, $k_1 = 1$, $k_2 = 1$, $k_3 = 3$

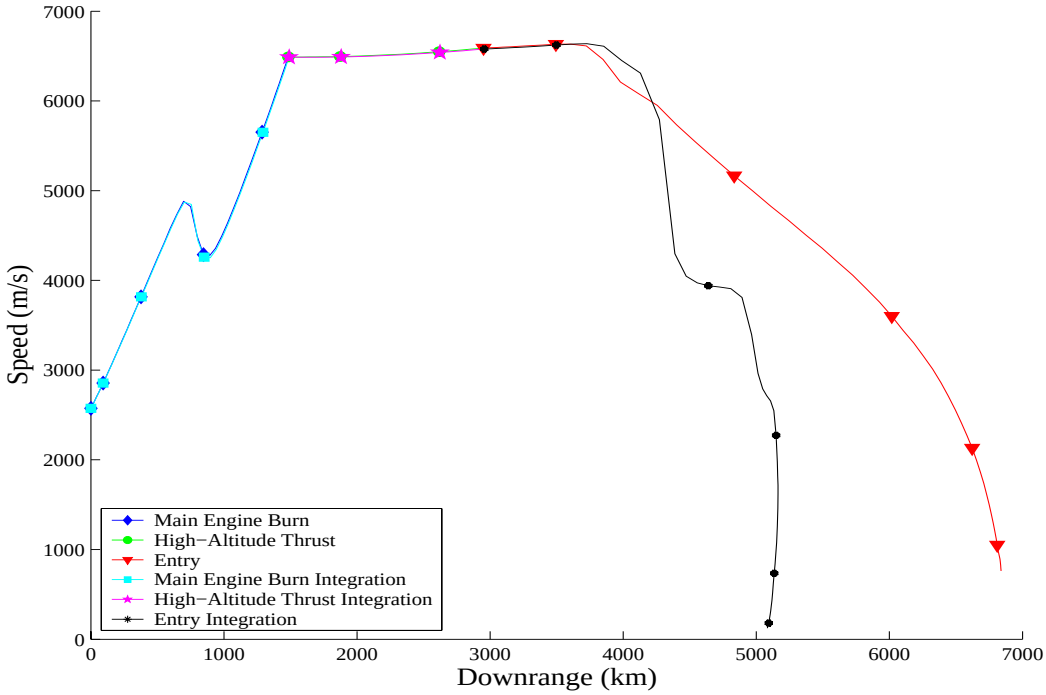

Figure 7-11: Speed vs. Downrange for a Twenty-Five Percent Abort to Spain, $k_1 = 1$, $k_2 = 1$, $k_3 = 3$

Table 7.3: Cost Calculation for a Twenty-five Percent Abort to Spain

k_1	k_2	k_3	$term_1$	$term_2$	$term_3$	$term_4$	$term_5$	$term_6$	$term_7$	Cost
1	1	1	5.309	0.959	1.265	1.084	8.097	27.431	1.097	45.245
1.5	1	1	5.531	0.937	1.207	1.409	8.487	30.466	0.111	48.151
2	1	1	5.606	0.932	1.206	1.586	8.643	31.688	0.270	49.934
2.5	1	1	5.633	0.931	1.217	1.664	8.716	32.367	0.429	50.960
3	1	1	5.747	0.928	1.206	1.679	8.948	34.152	1.407	54.071
1	1.5	1	5.744	0.933	1.176	1.299	8.667	32.069	0.505	50.395
1	2	1	5.971	0.923	1.143	1.358	8.814	33.270	0.967	52.450
1	2.5	1	6.165	0.917	1.130	1.473	8.967	34.467	1.582	54.705
1	3	1	6.316	0.916	1.124	1.458	9.103	35.500	2.276	56.696
1	1	1.5	5.432	0.950	1.215	1.012	8.272	28.878	0.527	46.289
1	1	2	5.4	0.953	1.215	0.984	8.203	28.317	0.643	45.719
1	1	2.5	5.398	0.957	1.219	0.978	8.108	27.624	0.802	45.088
1	1	3	5.371	0.961	1.229	0.981	8.031	27.156	0.963	44.695

to increase speed. Examining the cost values in Tables 7.2 and 7.3, choosing Senegal as the landing site would correspond to the best solution.

7.2.4 Fifty Percent Along a Nominal Trajectory

For this case, the loss of a single ME occurs half-way through the nominal ascent. The shuttle has peaked in altitude and is utilizing all thrusting capability to increase speed. Equation 7.7 lists the initial conditions.

$$\begin{aligned} t_0 &= 3.2249 \text{ min} & v(t_0) &= 3759.9 \text{ m/s} \\ h(t_0) &= 122.0349 \text{ km} & \gamma(t_0) &= .4410 \text{ deg} \\ \theta(t_0) &= -75.5583 \text{ deg} & \chi(t_0) &= -2.4082 \text{ deg} \\ \phi(t_0) &= 28.2990 \text{ deg} & m(t_0) &= 4.04 \times 10^5 \text{ kg} \end{aligned} \tag{7.7}$$

The best trajectory generated for an abort from this point to Senegal is obtained with a weighting factor in the third phase cost functional of $k_1 = 1$, $k_2 = 3$, $k_3 = 1$. Using Equation 7.1, Table 7.4 gives the cost breakdown for this case.

Referring to Table 7.4, it can be seen that only the sensed acceleration constraint in the first phase is satisfied with this weighting factor combination. How-

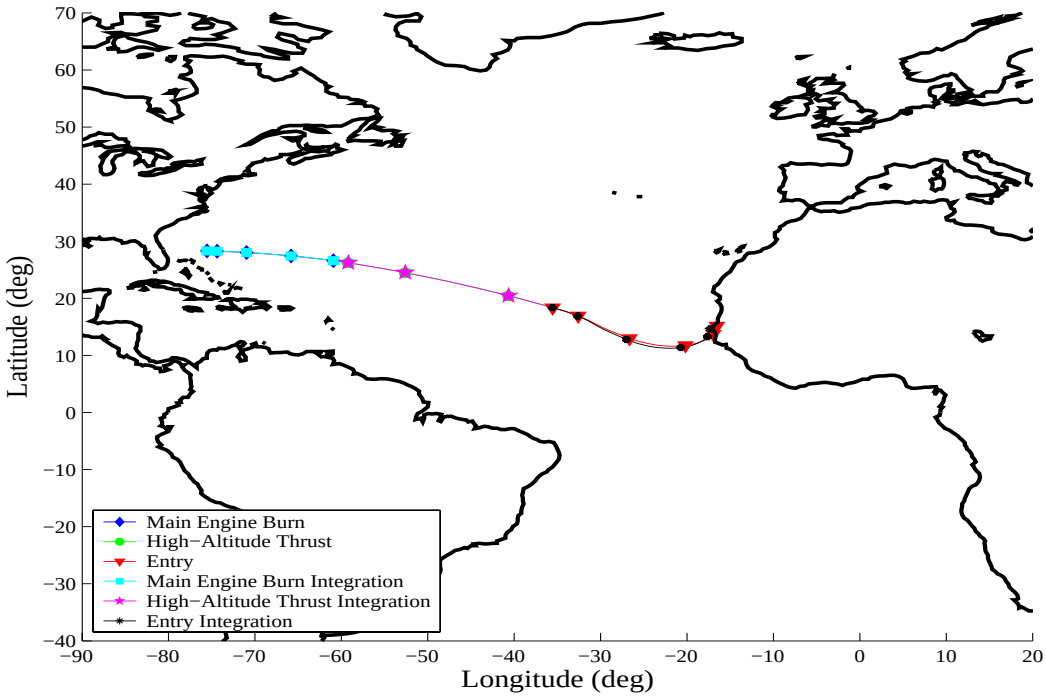

Figure 7-12: Mercator Projection of a Fifty Percent Abort to Senegal, $k_1 = 1$, $k_2 = 3$, $k_3 = 1$

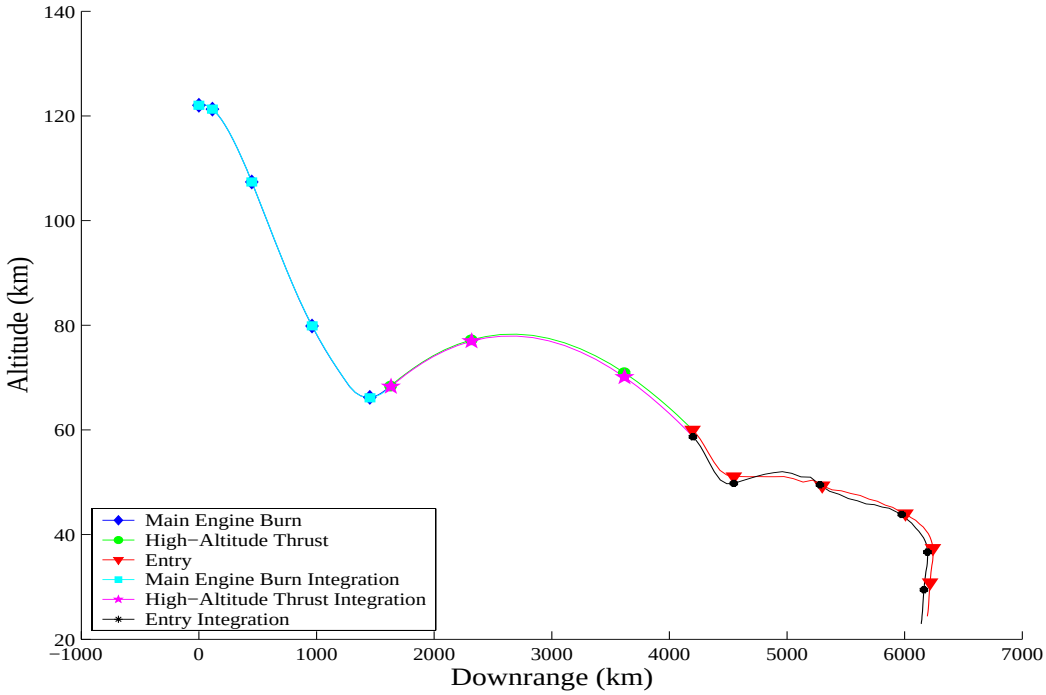

Figure 7-13: Altitude vs. Downrange for a Fifty Percent Abort to Senegal, $k_1 = 1$, $k_2 = 3$, $k_3 = 1$

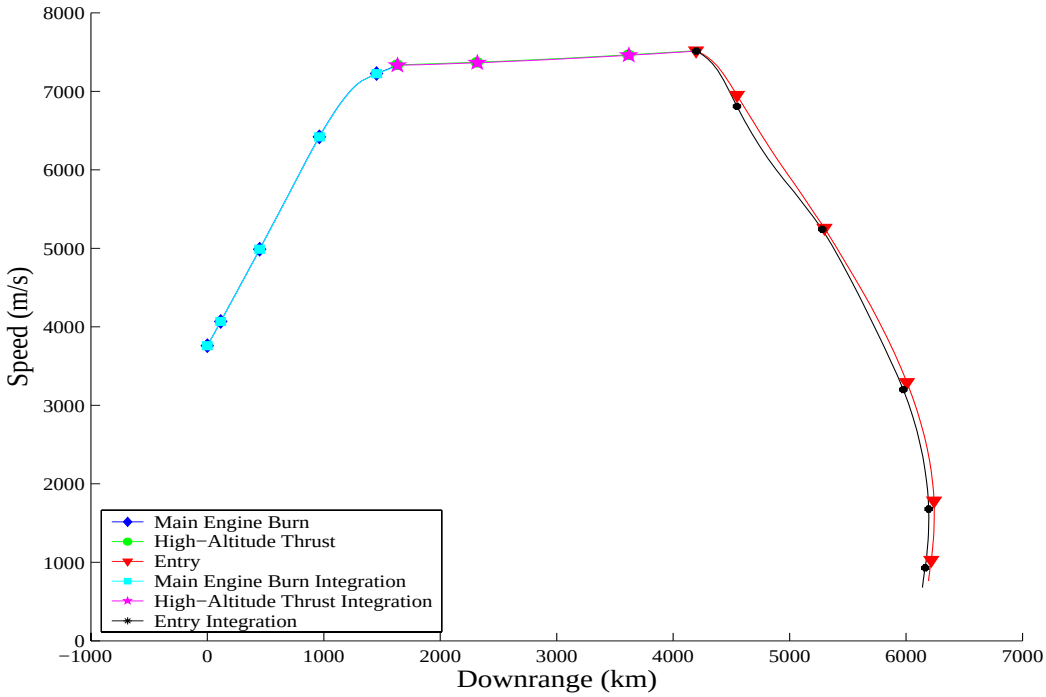

Figure 7-14: Speed vs. Downrange for a Fifty Percent Abort to Senegal, $k_1 = 1$, $k_2 = 3$, $k_3 = 1$

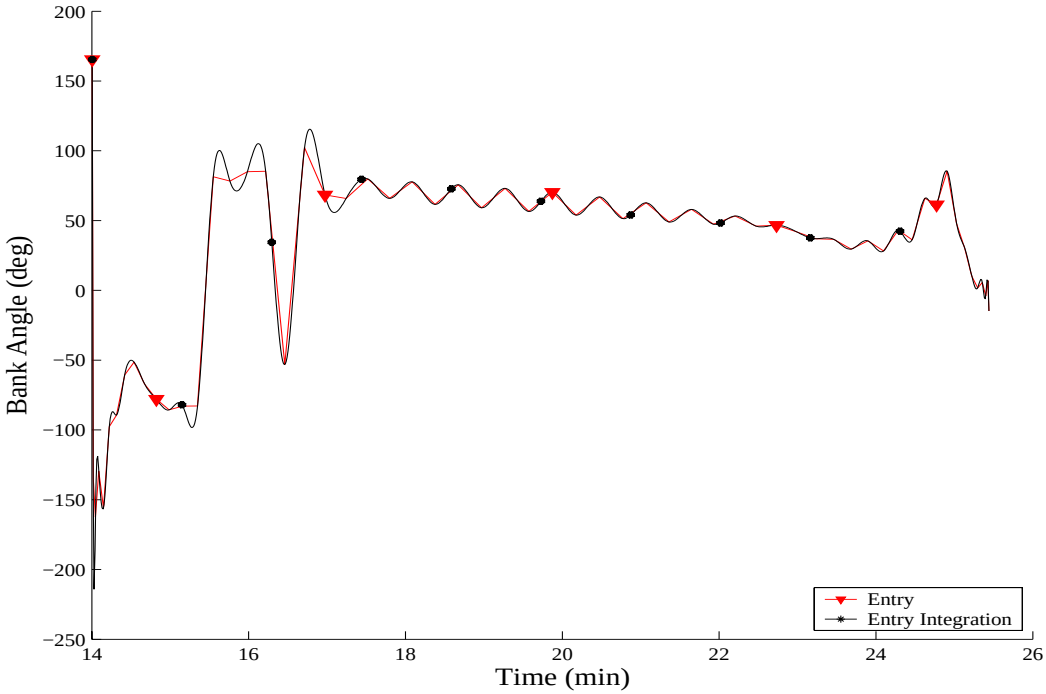

Figure 7-15: Entry Bank Angle vs. Time for a Fifty Percent Abort to Senegal, $k_1 = 1$, $k_2 = 3$, $k_3 = 1$

Table 7.4: Cost Calculation for a Fifty Percent Abort to Senegal

k_1	k_2	k_3	$term_1$	$term_2$	$term_3$	$term_4$	$term_5$	$term_6$	$term_7$	Cost
1	1	1	0.878	1.236	1.464	2.470	5.266	1.697	0.577	13.592
1.5	1	1	0.573	1.459	1.415	2.308	4.406	2.571	1.001	13.735
2	1	1	0.558	1.460	1.525	2.681	4.696	2.916	0.649	14.488
2.5	1	1	0.524	1.471	1.576	2.865	2.347	0.946	0.168	9.900
3	1	1	0.785	1.312	1.444	2.404	18.860	6.575	3.156	34.539
1	1.5	1	0.564	1.346	1.247	1.794	5.942	3.870	0.826	15.592
1	2	1	0.657	1.270	1.239	1.769	4.694	1.985	0.251	11.867
1	2.5	1	0.633	1.221	1.546	2.756	1.279	1.613	0.273	9.323
1	3	1	0.533	1.276	1.223	1.725	1.203	0.005	0.274	6.242
1	1	1.5	0.549	1.203	1.146	1.515	3.312	1.426	0.568	9.721
1	1	2	0.685	1.126	1.004	1.163	0.866	1.414	0.215	6.476
1	1	2.5	0.733	1.009	0.931	0.999	1.008	1.553	0.640	6.876
1	1	3	1.109	0.984	0.95	1.040	3.02	2.743	0.779	10.627

ever, as the bank angle becomes smoother, the interpolation of the control produces a more accurate integration of the dynamics (Figure 7-15). By examining Figure 7-12, we see that the vehicle banks during the third phase and approaches the landing site from behind. Referring to Figure 7-13 and Figure 7-14, we can see that the initial condition corresponds to a maximum altitude, and the vehicle decreases in altitude as it continues to gain speed in the first phase. Figure 7-16 shows that the vehicle is in equilibrium glide over a shorter range than the zero percent abort. An abort from this point has a higher altitude and initial speed. Thus, the vehicle does not maintain the maximum value of flight path angle for as long. In addition, it is no longer necessary for the vehicle to use full thrust capabilities to reach the terminal conditions at Senegal.

For the purposes of this research the lowest cost as calculated by 7.1 is considered to be the best solution for a specific initial condition. However, it is important to note that using the weighting factor $k_1 = 1$, $k_2 = 1$, $k_3 = 2.5$ produces a trajectory with only a slightly higher cost, but one that satisfies the sensed acceleration in both the first and third phases and the dynamic pressure constraint. Also, the heating rate constraint is only slightly higher than the

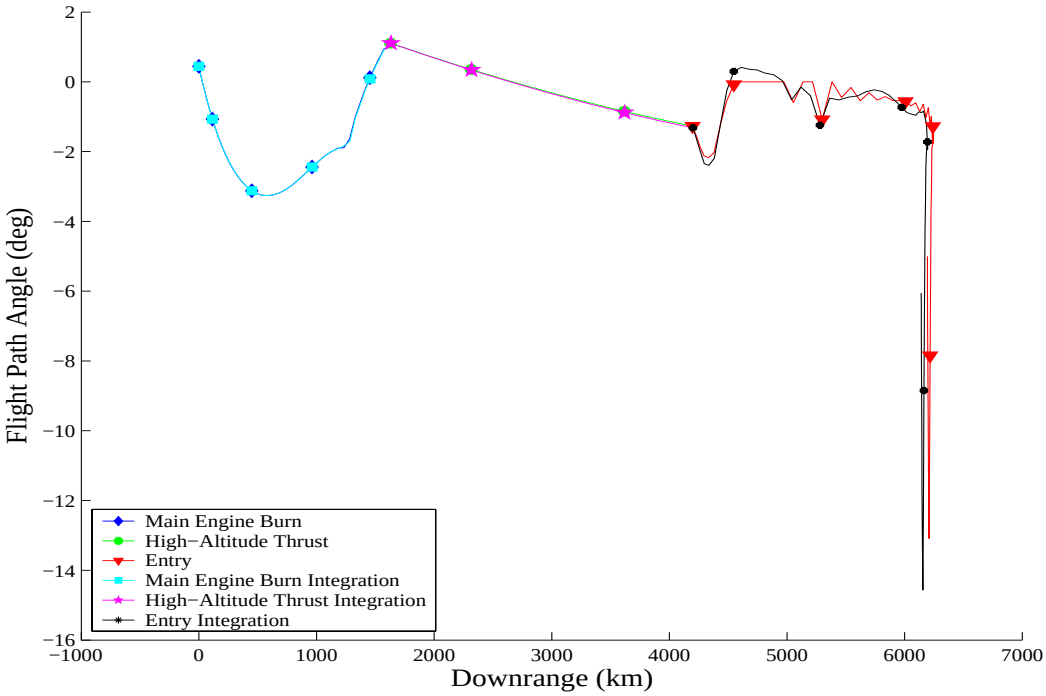

Figure 7-16: Flight Path Angle vs. Downrange for a Fifty Percent Abort to Senegal, $k_1 = 1$, $k_2 = 3$,$k_3 = 1$

maximum desired value for this set of weighting factors.

The best trajectory generated for an abort from this point to Spain is obtained with a weighting factor in the third phase cost functional of $k_1 = 1$, $k_2 = 1$, $k_3 = 3$. Using Equation 7.1, Table 7.5 gives the cost breakdown for this case.

By examining Table 7.5, it is seen that only the dynamic pressure constraint is satisfied when using this set of weighting factors. The sensed acceleration constraint in the third phase is close to the maximum desired value and is probably acceptable. Referring to Figure 7-18 and Figure 7-19, we can see that the initial condition is the maximum altitude and the vehicle decreases altitude as it gains enough speed to meet the terminal conditions at Spain. In fact, the vehicle uses all available main engine fuel to propel itself into a position to reach Spain. Referring to Figure 7-17, we notice that the vehicle does not begin to head towards Spain until the third phase. During the first phase, the ET is attached to the vehicle drastically limiting maneuvering capabilities. Although free of the extra mass in the second phase, the vehicle is at a high-altitude and only has

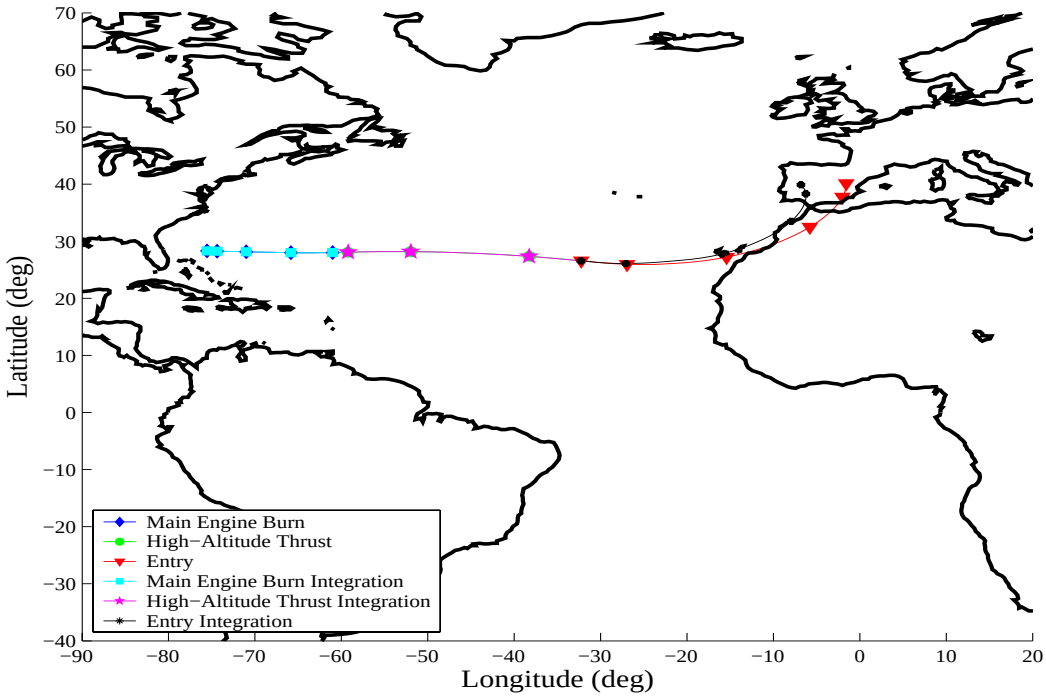

Figure 7-17: Mercator Projection of a Fifty Percent Abort to Spain, $k_1 = 1$, $k_2 = 1$, $k_3 = 3$

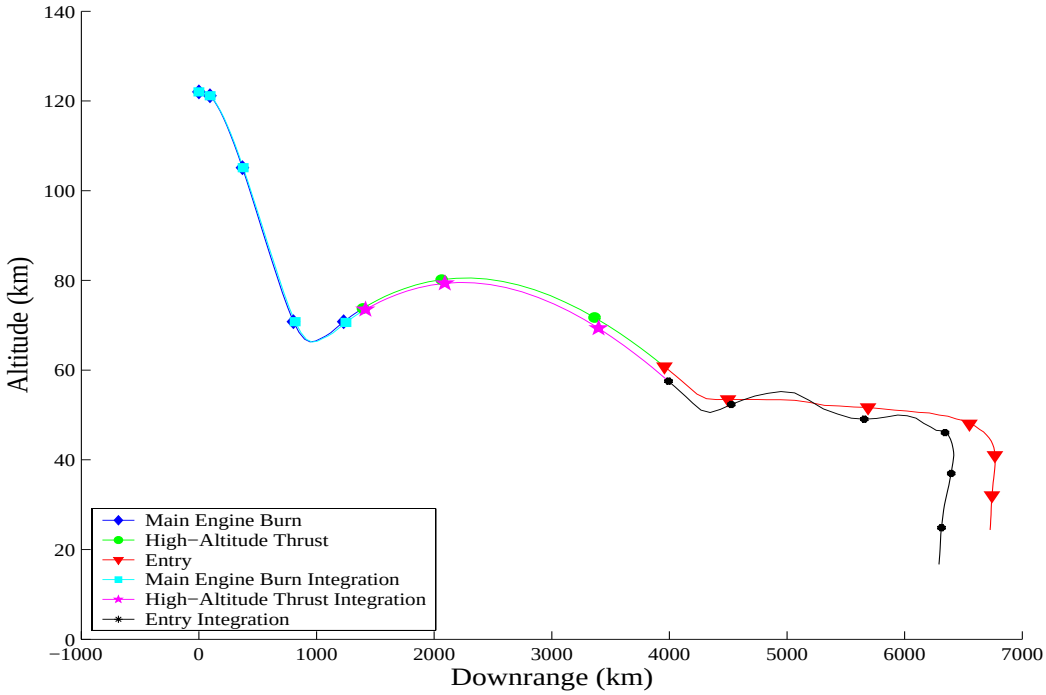

Figure 7-18: Altitude vs. Downrange for a Fifty Percent Abort to Spain, $k_1 = 1$, $k_2 = 1$, $k_3 = 3$

Table 7.5: Cost Calculation for a Fifty Percent Abort to Spain

k_1	k_2	k_3	$term_1$	$term_2$	$term_3$	$term_4$	$term_5$	$term_6$	$term_7$	Cost
1	1	1	1.240	1.379	1.239	1.771	7.719	16.417	4.540	34.308
1.5	1	1	1.445	1.372	1.178	1.600	5.088	7.214	2.054	19.953
2	1	1	1.48	1.396	1.223	1.724	5.461	8.332	2.041	21.663
2.5	1	1	1.071	1.423	1.320	2.009	7.086	15.241	3.027	31.180
3	1	1	1.392	1.434	1.330	2.040	5.392	10.090	1.895	23.576
1	1.5	1	1.432	1.352	1.141	1.502	6.084	9.938	2.634	24.086
1	2	1	1.425	1.349	1.125	1.460	5.894	9.369	2.505	23.130
1	2.5	1	1.476	1.319	1.064	1.305	4.189	5.417	1.610	16.383
1	3	1	1.169	1.261	1.011	1.180	5.745	9.027	1.992	21.388
1	1	1.5	1.206	1.304	1.091	1.372	6.840	12.395	3.223	27.433
1	1	2	1.302	1.249	0.991	1.133	5.962	9.303	2.489	22.432
1	1	2.5	1.203	1.185	0.927	0.991	5.011	6.931	1.725	17.974
1	1	3	1.196	1.219	0.951	1.02	4.507	5.714	1.629	16.239

a small amount of thrust, which limits the vehicle's ability to turn. It is only in the third phase that the vehicle has a significant ability to perform the bank maneuver necessary to meet the terminal conditions at Spain. Comparing Table 7.4 and Table 7.5, we determine that Senegal is the best choice for a landing site.

7.2.5 Seventy-five Percent Along a Nominal Trajectory

For this case, the loss of a single ME occurs seventy-five percent along the nominal ascent. Although the vehicle's altitude has decreased slightly, the vehicle is utilizing full thrusting capability to greatly increase the speed. Equation 7.8 lists the initial conditions.

$$\begin{aligned} t_0 &= 4.8373 \text{ min} & v(t_0) &= 5545.2 \text{ m/s} \\ h(t_0) &= 111.1681 \text{ km} & \gamma(t_0) &= -1.5971 \text{ deg} \\ \theta(t_0) &= -71.1260 \text{ deg} & \chi(t_0) &= -4.5248 \text{ deg} \\ \phi(t_0) &= 28.0623 \text{ deg} & m(t_0) &= 2.681 \times 10^5 \text{ kg} \end{aligned} \tag{7.8}$$

The best trajectory generated for an abort from this point to Senegal is obtained with a weighting factor in the third phase cost functional of $k_1 = 1$, $k_2 = 1$,

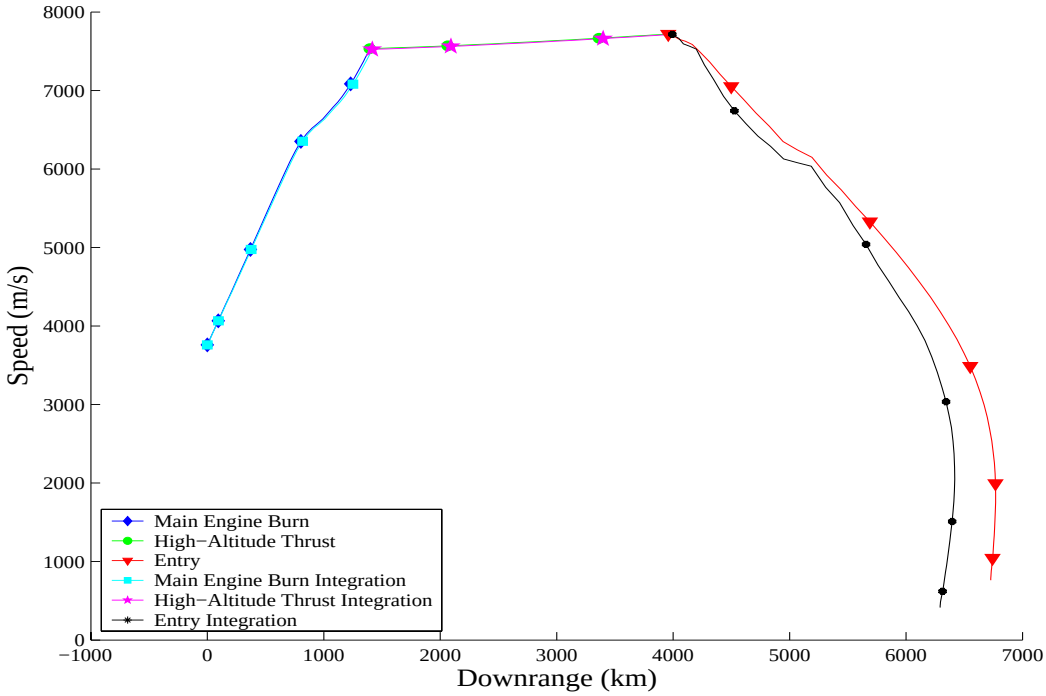

Figure 7-19: Speed vs. Downrange for a Fifty Percent Abort to Spain, $k_1 = 1$, $k_2 = 1$, $k_3 = 3$

$k_3 = 2.5$. Using Equation 7.1, Table 7.6 gives the cost breakdown for this case.

Referring to Table 7.6, we see that for the best case, all of the constraints are satisfied. In addition, the integration produces a final state that is very close to the final state in the solution. By examining Figure 7-23, we see that the smoothness of the bank angle allows for an accurate interpolation with a spline fit, and hence an accurate integration of the dynamics. Examining Figure 7-21 and Figure 7-22, we see that initially, there is a small increase in speed, however, as the altitude begins to increase, the speed decreases slightly. From the initial condition, the vehicle does not have far to travel to reach the terminal conditions and thus can align itself well for entry. Again, notice the bank maneuver during entry as the vehicle turns and reaches the terminal point from slightly behind (Figure 7-20).

The best trajectory generated for an abort from this point to Spain is obtained with a weighting factor in the third phase cost functional of $k_1 = 1$, $k_2 = 1$, $k_3 = 1.5$. Using Equation 7.1, Table 7.7 gives the cost breakdown for this case.

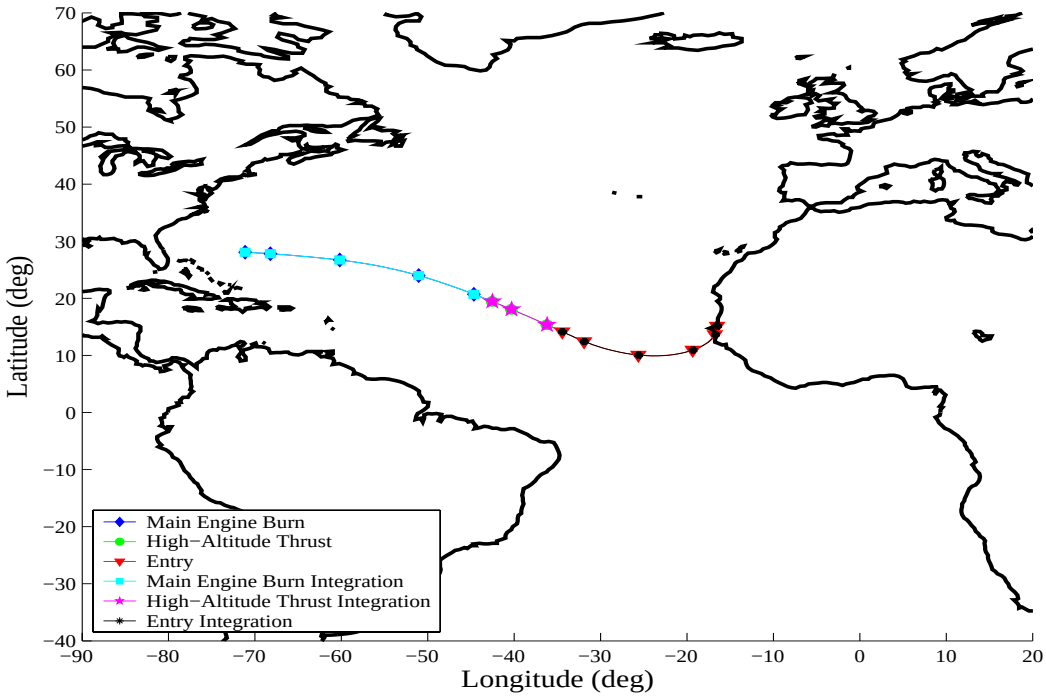

Figure 7-20: Mercator Projection of a Seventy-Five Percent Abort to Senegal, $k_1 = 1$, $k_2 = 1$, $k_3 = 2.5$

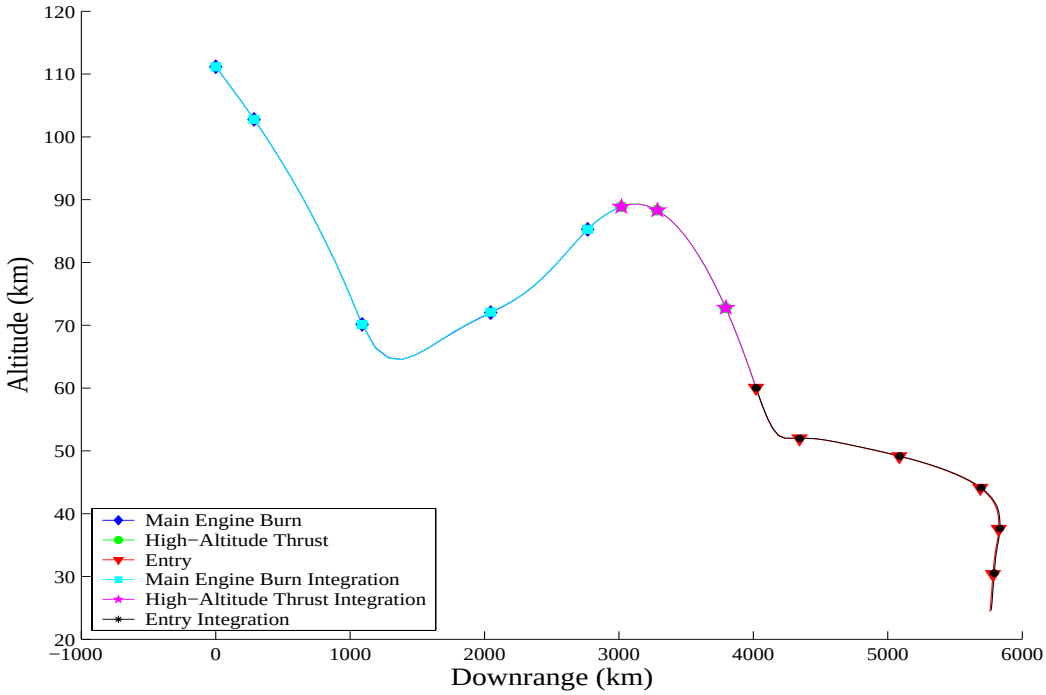

Figure 7-21: Altitude vs. Downrange for a Seventy-Five Percent Abort to Senegal, $k_1 = 1$, $k_2 = 1$, $k_3 = 2.5$

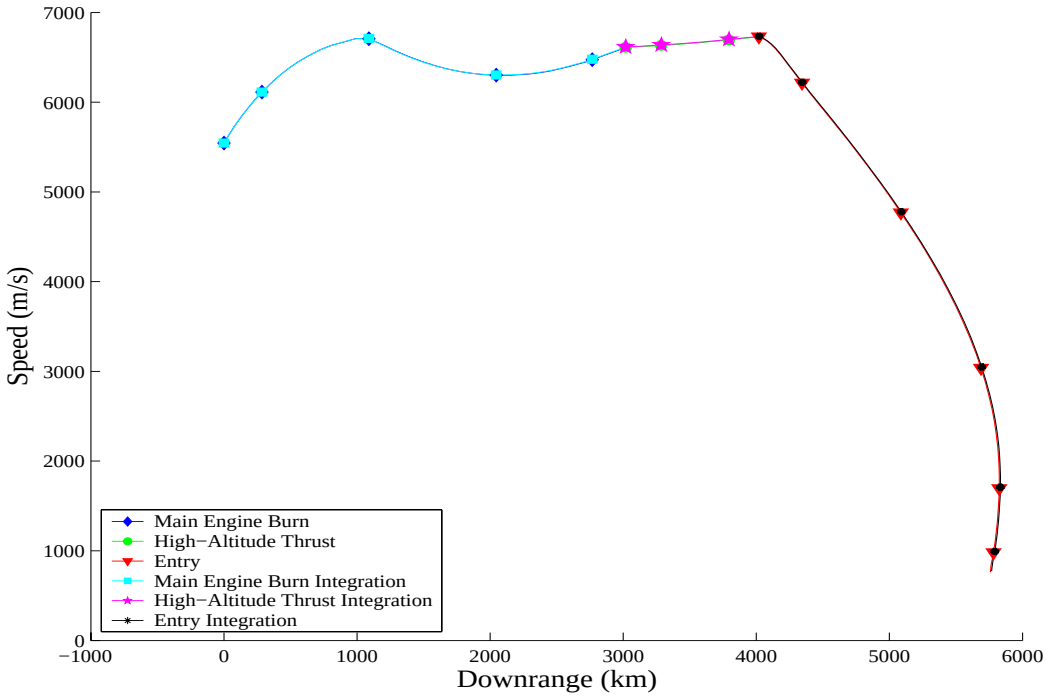

Figure 7-22: Speed vs. Downrange for a Seventy-Five Percent Abort to Senegal, $k_1 = 1$, $k_2 = 1$, $k_3 = 2.5$

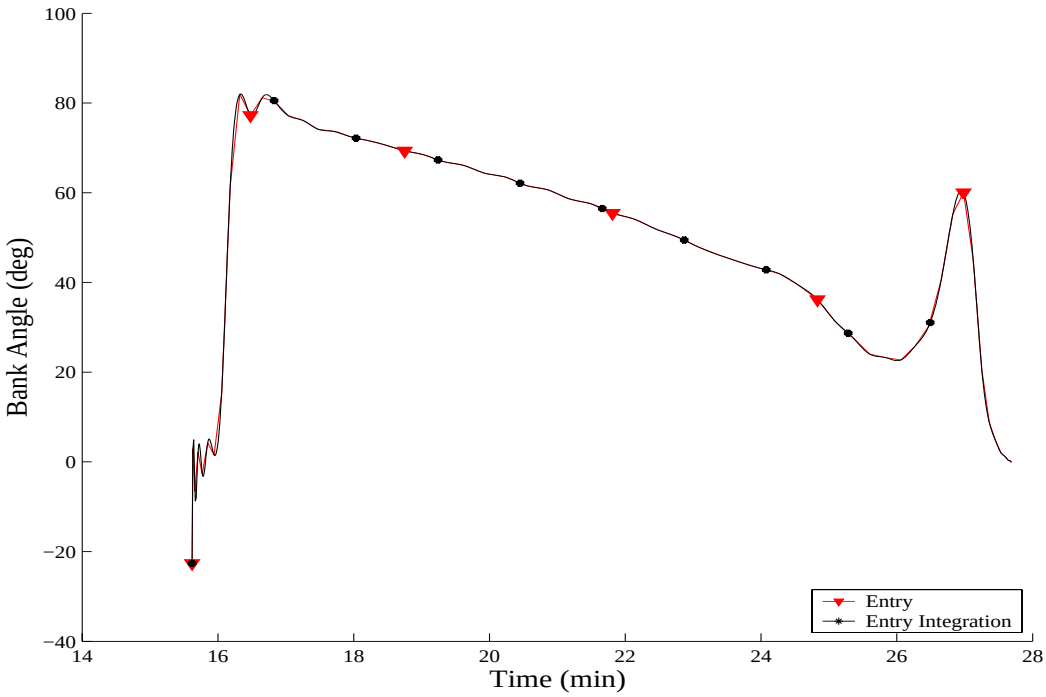

Figure 7-23: Entry Bank Angle vs. Time for a Seventy-Five Percent Abort to Senegal, $k_1 = 1$, $k_2 = 1$, $k_3 = 2.5$

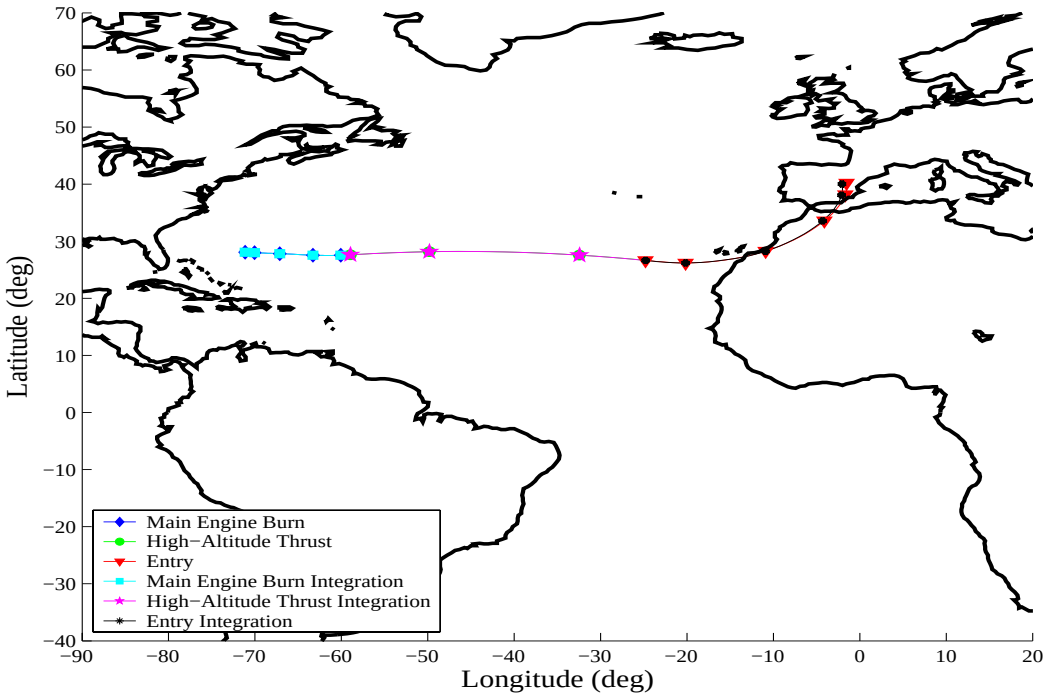

Figure 7-24: Mercator Projection of a Seventy-Five Percent Abort to Spain, $k_1 = 1$, $k_2 = 1$, $k_3 = 1.5$

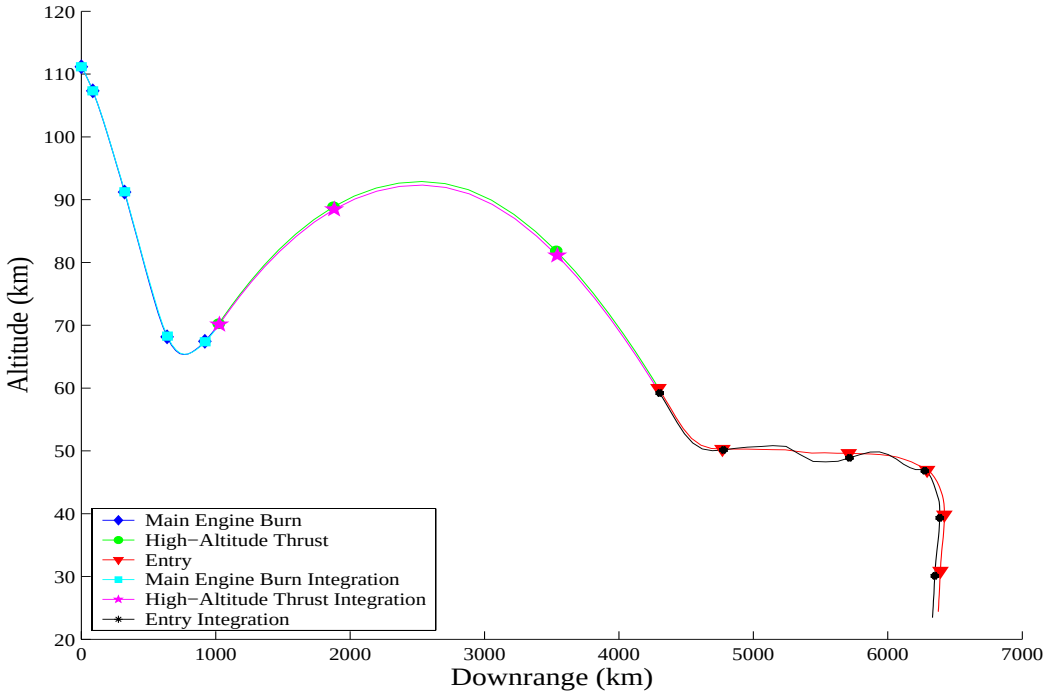

Figure 7-25: Altitude vs. Downrange for a Seventy-five Percent Abort to Spain, $k_1 = 1$, $k_2 = 1$, $k_3 = 1.5$

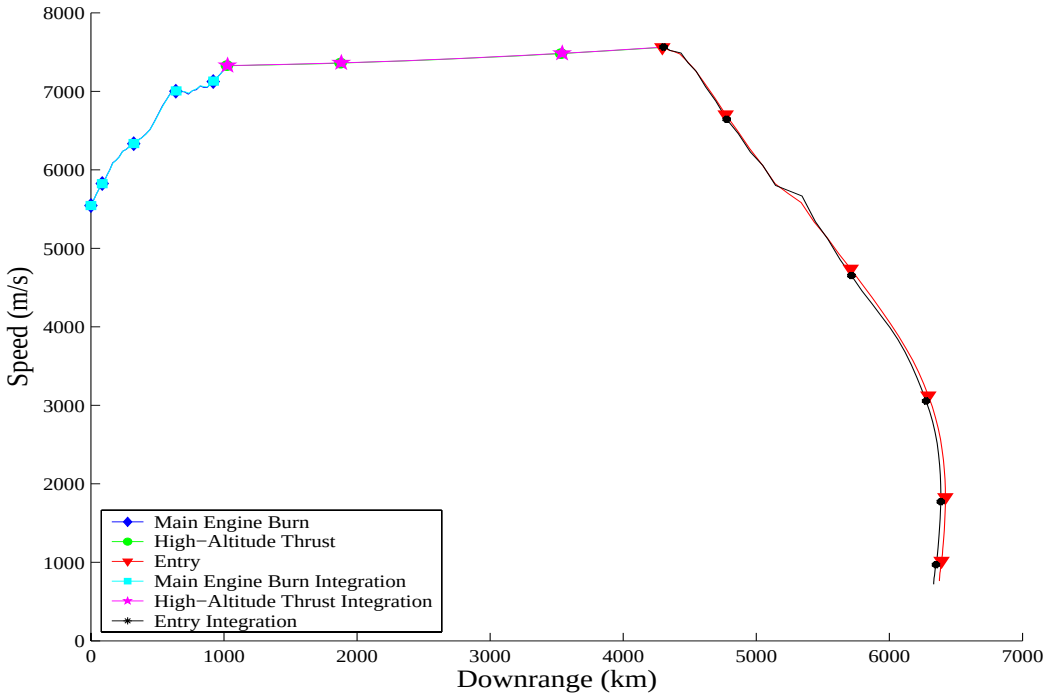

Figure 7-26: Speed vs. Downrange for a Seventy-Five Percent Abort to Spain, $k_1 = 1$, $k_2 = 1$, $k_3 = 1.5$

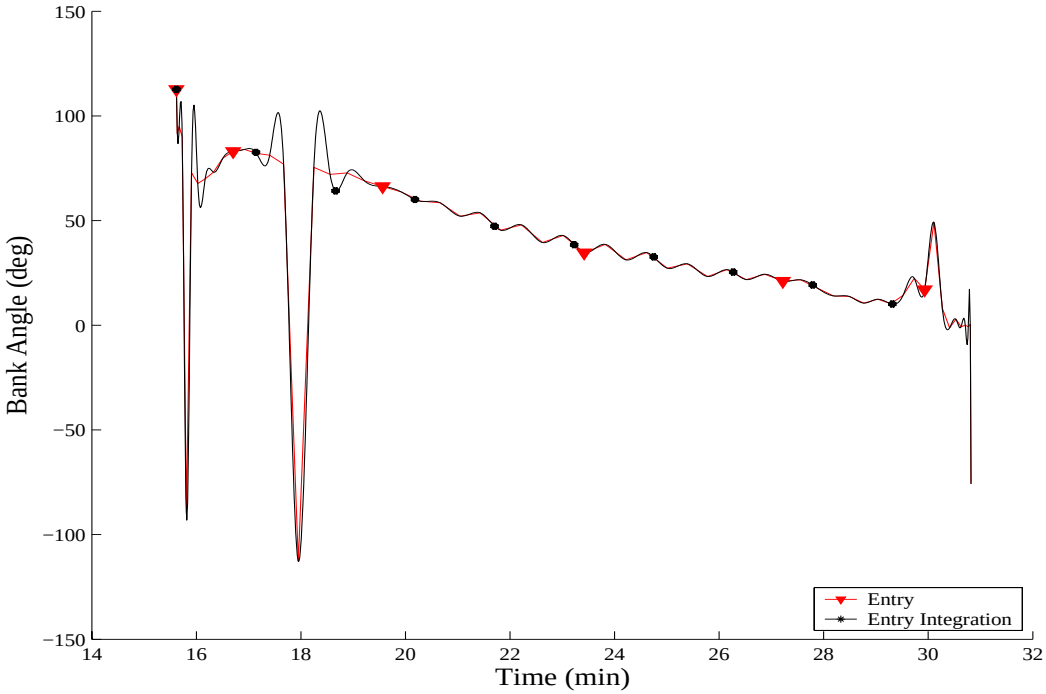

Figure 7-27: Entry Bank Angle vs. Time for a Seventy-Five Percent Abort to Spain, $k_1 = 1$, $k_2 = 1$, $k_3 = 1.5$

Table 7.6: Cost Calculation for a Seventy-five Percent Abort to Senegal

k_1	k_2	k_3	$term_1$	$term_2$	$term_3$	$term_4$	$term_5$	$term_6$	$term_7$	Cost
1	1	1	1.560	1.440	1.356	2.121	0.129	0.930	0.997	8.535
1.5	1	1	1.551	1.454	1.416	2.312	0.041	0.990	0.974	8.742
2	1	1	1.571	1.475	1.448	2.420	0.037	1.034	0.980	8.968
2.5	1	1	0.414	1.467	1.531	2.703	0.158	0.935	0.906	8.11
3	1	1	1.600	1.492	1.493	2.572	0.061	0.976	0.971	9.169
1	1.5	1	1.577	1.422	1.332	2.047	0.032	0.987	0.999	8.399
1	2	1	0.414	1.402	1.306	1.968	0.227	1.140	0.985	7.445
1	2.5	1	1.492	1.360	1.262	1.836	0.490	1.298	0.946	8.686
1	3	1	1.28	1.265	1.168	1.574	0.194	1.120	0.995	7.599
1	1	1.5	1.632	1.466	1.451	2.428	0.127	1.080	1.009	9.196
1	1	2	1.702	1.059	0.987	1.124	1.454	1.898	0.827	9.054
1	1	2.5	0.425	0.908	0.918	0.972	0.158	1.123	0.996	5.504
1	1	3	1.735	1.025	1.115	1.434	1.985	2.229	1.441	10.966

For the case of the best weighting factors, none of the constraints are satisfied. However, the control is considerably smoother, producing accurate results when integrated. Examining Figure 7-24 reveals that the vehicle waits until the third phase to begin the bank maneuver towards Spain. This may explain the higher values of sensed acceleration. The vehicle must have a large value of lift to perform such a maneuver and a large value of lift would increase the sensed acceleration. Referring to Figure 7-25 and Figure 7-26, we still notice an altitude 'increase-decrease' maneuver during the first phase, which is performed to increase the speed so that the vehicle can travel the distance necessary to reach the landing site in Spain. Comparing Table 7.6 and Table 7.7, it is obvious that Senegal is the best landing site choice for an abort from seventy-five percent along the trajectory.

7.2.6 One-hundred Percent Along a Nominal Trajectory

For this case, the loss of a single ME occurs at the end of a nominal ascent. The vehicle has decreased in altitude and increased in speed in order to meet the conditions at the end of ascent. By this point, the vehicle has expended much of

Table 7.7: Cost Calculation for a Seventy-five Percent Abort to Spain

k_1	k_2	k_3	$term_1$	$term_2$	$term_3$	$term_4$	$term_5$	$term_6$	$term_7$	Cost
1	1	1	2.713	1.442	1.623	3.039	1.802	1.145	1.458	13.224
1.5	1	1	2.238	1.466	1.643	3.112	1.387	0.504	1.491	11.844
2	1	1	1.840	1.473	1.642	3.108	1.55	0.724	1.496	11.834
2.5	1	1	1.622	1.429	1.554	2.784	1.342	0.448	1.451	10.632
3	1	1	1.840	1.463	1.62	3.025	1.485	0.645	1.463	11.543
1	1.5	1	2.261	1.455	1.606	2.976	1.087	0.137	1.452	10.977
1	2	1	2.120	1.435	1.561	2.811	1.414	0.608	1.443	11.395
1	2.5	1	1.719	1.392	1.463	2.468	1.441	0.68	1.412	10.577
1	3	1	2.208	1.400	1.484	2.539	1.076	0.204	1.364	10.278
1	1	1.5	1.486	1.328	1.339	2.067	0.644	0.292	1.252	8.410
1	1	2	2.248	1.336	1.340	2.071	1.143	0.270	1.351	9.761
1	1	2.5	1.446	1.174	1.089	1.349	0.671	1.727	1.036	8.49
1	1	3	2.182	1.213	1.161	1.511	1.121	0.282	1.298	8.771

the mass in the ET and is no longer thrusting at full capacity. Equation 7.9 lists the initial conditions for an abort at the end of ascent.

$$\begin{aligned} t_0 &= 6.4498 \text{ min} & v(t_0) &= 7734.0 \text{ m/s} \\ h(t_0) &= 105.5640 \text{ km} & \gamma(t_0) &= .65 \text{ deg} \\ \theta(t_0) &= -64.7004 \text{ deg} & \chi(t_0) &= -7.5176 \text{ deg} \\ \phi(t_0) &= 27.4620 \text{ deg} & m(t_0) &= 1.621 \times 10^5 \text{ kg} \end{aligned} \tag{7.9}$$

The best trajectory generated for an abort from this point to Senegal is obtained with a weighting factor in the third phase cost functional of $k_1 = 1$, $k_2 = 1$, $k_3 = 3$. Using Equation 7.1, Table 7.8 gives the cost breakdown for this case.

By examining Table 7.8, we see that when using the best weighting factors, only the heating rate constraint is satisfied. Referring to Figure 7-29 and Figure 7-30, it can be seen that from the point of abort the vehicle is mainly decreasing in altitude and lowering the large initial speed. The one-hundred percent abort to Senegal is the only case of a significant speed decrease during ME burn. As shown by the initial conditions, there is little ME fuel left to burn and the main engines are barely used. The vehicle makes a sharp turn during entry towards

Table 7.8: Cost Calculation for a One-hundred Percent Abort to Senegal

k_1	k_2	k_3	$term_1$	$term_2$	$term_3$	$term_4$	$term_5$	$term_6$	$term_7$	Cost
1	1	1	1.324	1.023	3.220	11.061	1.326	0.149	1.122	19.229
1.5	1	1	1.313	1.061	2.589	7.729	2.253	0.525	1.528	17.001
2	1	1	1.296	1.050	2.553	7.516	1.839	0.735	1.504	16.496
2.5	1	1	1.253	1.040	2.522	7.334	1.988	0.66	1.527	16.326
3	1	1	1.173	0.960	2.384	6.554	2.160	0.623	1.54	15.398
1	1.5	1	1.270	1.032	2.464	6.999	1.575	0.829	1.489	15.660
1	2	1	1.183	0.947	2.323	6.221	2.080	0.539	1.538	14.833
1	2.5	1	1.159	0.805	2.027	4.735	1.893	0.644	1.451	12.717
1	3	1	1.319	0.809	2.145	5.304	2.416	0.192	1.465	13.652
1	1	1.5	1.302	0.806	2.054	4.864	3.131	0.179	1.557	13.894
1		2	1.486	0.565	1.573	2.852	2.346	0.447	1.353	10.624
1	1	2.5	1.368	0.444	1.356	2.121	3.219	0.280	1.098	9.889
1	1	3	1.125	0.326	1.045	1.261	2.798	0.224	0.966	7.748

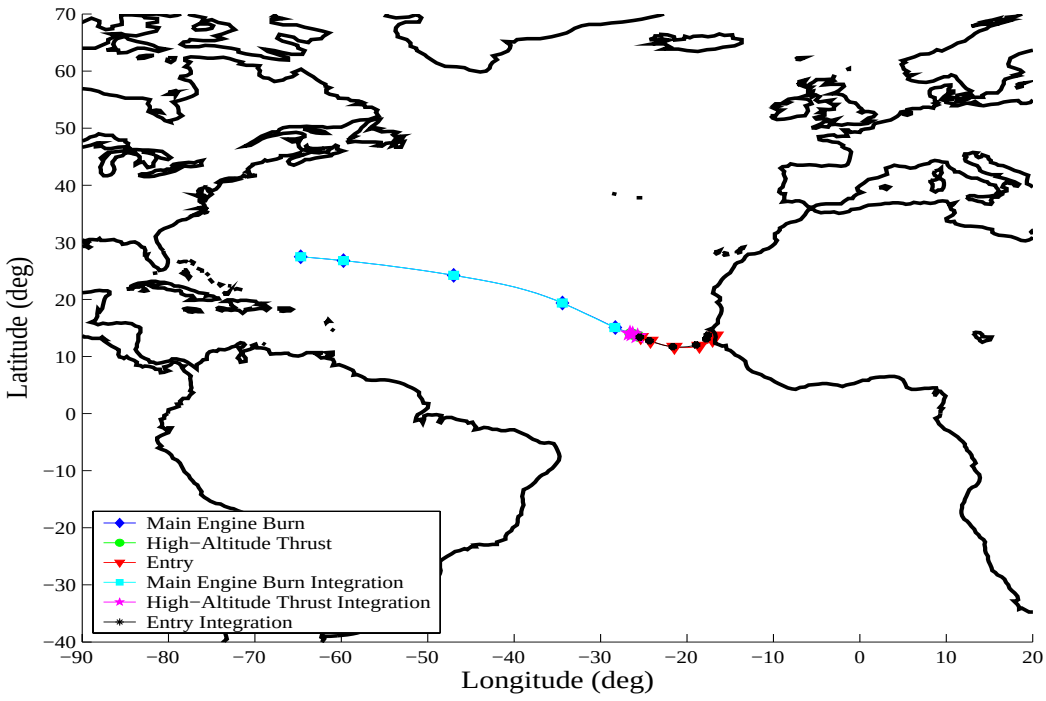

Figure 7-28: Mercator Projection of a One-Hundred Percent Abort to Senegal, $k_1 = 1$, $k_2 = 1$, $k_3 = 3$

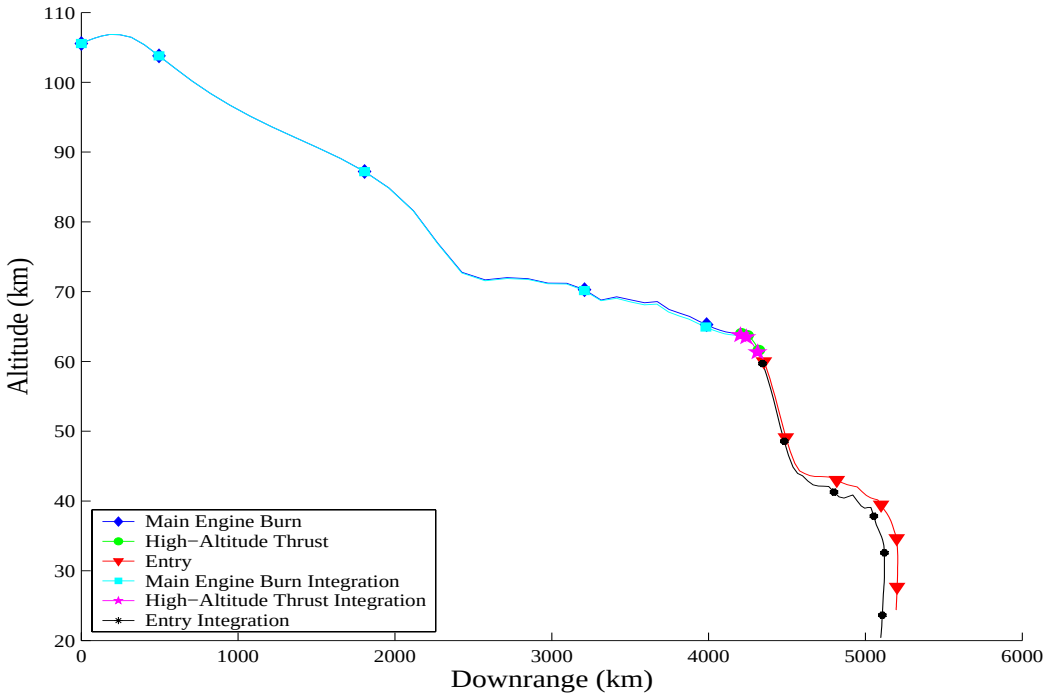

Figure 7-29: Altitude vs. Downrange for a One-Hundred Percent Abort to Senegal, $k_1 = 1$, $k_2 = 1$, $k_3 = 3$

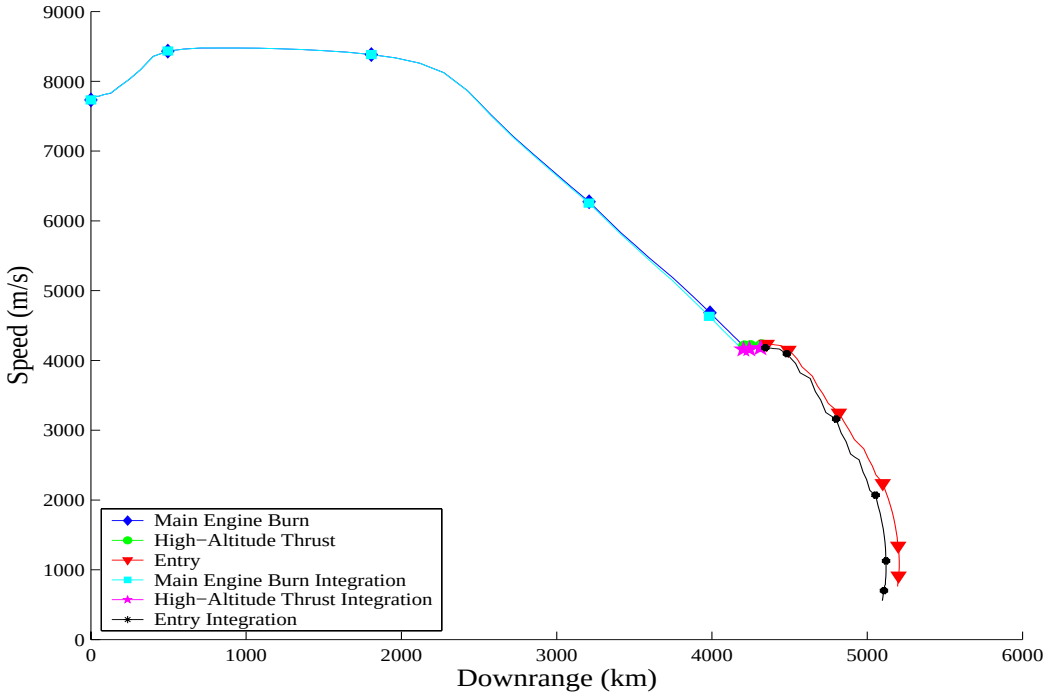

Figure 7-30: Speed vs. Downrange for a One-Hundred Percent Abort to Senegal, $k_1 = 1$, $k_2 = 1$, $k_3 = 3$

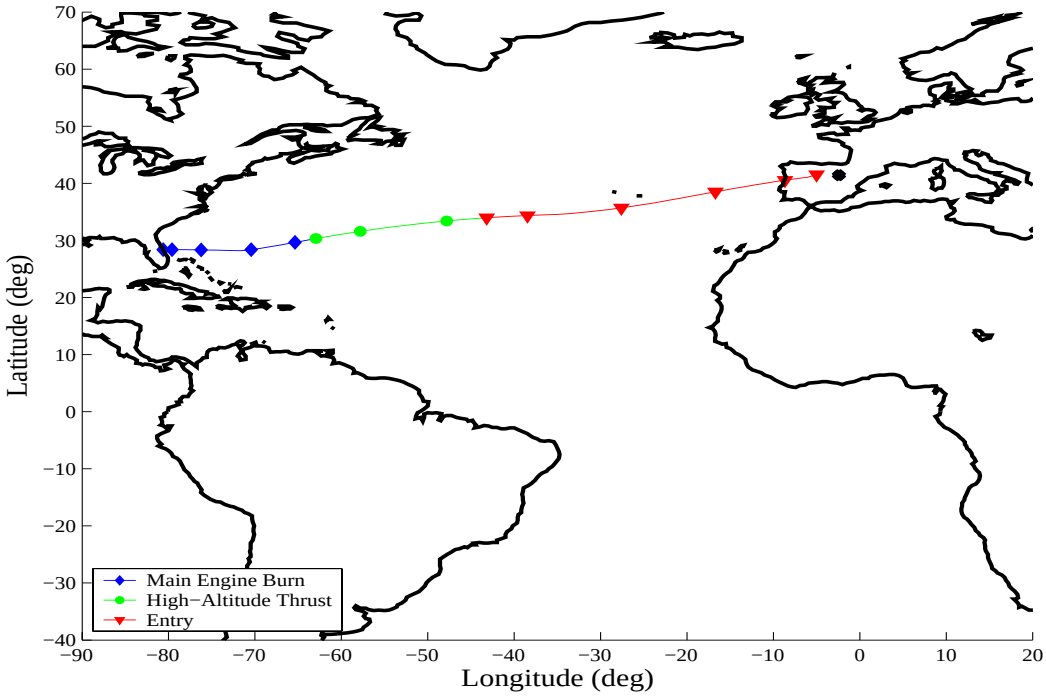

Figure 7-31: Mercator Projection of a Zero Percent Maximum Downrange to Spain

the final conditions (Figure 7-28).

7.3 Infeasible Problems

As the reader may have noticed, two abort cases have been omitted: the zero percent abort to Spain, and the one-hundred percent abort to Spain. This is not an oversight. Each of these cases is an infeasible problem.

7.3.1 A Zero Percent Abort to Spain

The zero percent abort to Spain consists of an abort from the initial point of a nominal ascent and terminates at the Spain landing site. From the initial conditions listed in Equation 7.5, the vehicle must travel a downrange of 7045 km to reach the landing site at Spain. However, if we examine the maximum downrange case (Figure 7-32), we see that from these initial conditions, the maximum down-

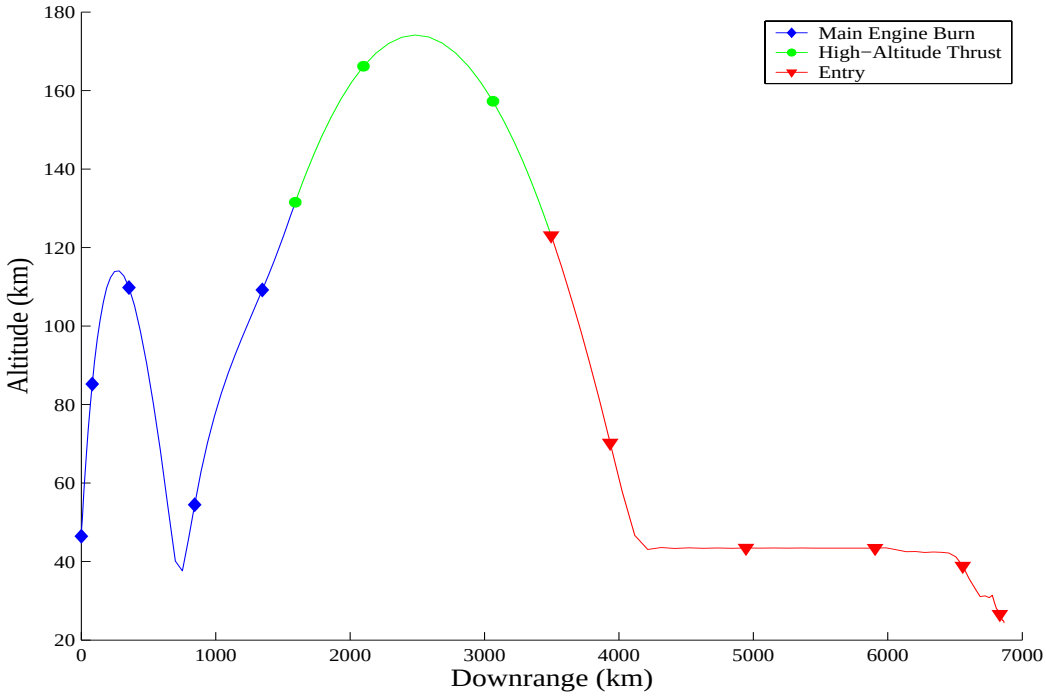

Figure 7-32: Altitude vs. Downrange for a Zero Percent Maximum Downrange to Spain

range, assuming a final crossrange of zero, is 6865 km. Referring to Figure 7-31, we see that this trajectory terminates at a final coordinate of $\theta = -4.5046$ deg and $\phi = 41.8270$ deg and thus is unable to reach Spain.

7.3.2 A One-Hundred Percent Abort to Spain

The one-hundred percent abort to Spain is an abort at the end of nominal ascent which terminates at the final conditions for the Spain landing site. From the initial conditions listed in Equation 7.9, the vehicle must travel a downrange of 5797 km to reach the landing site in Spain. However, if we examine the minimum downrange case (Figure 7-34), we see that from these initial conditions, the minimum downrange, assuming a final crossrange of zero, is 9764 km. Referring to Figure 7-33, we see that this trajectory terminates at a final coordinate of $\theta = 39.5509$ deg and $\phi = 29.8229$ deg and thus is unable to reach Spain.

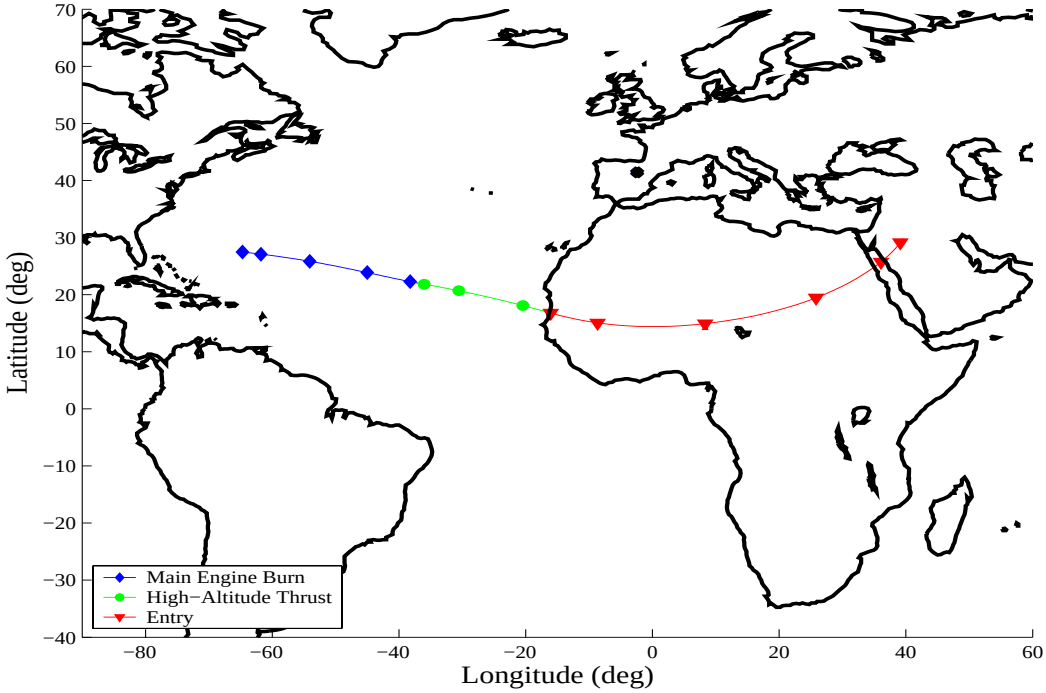

Figure 7-33: Mercator Projection of a One-Hundred Percent Maximum Downrange to Spain

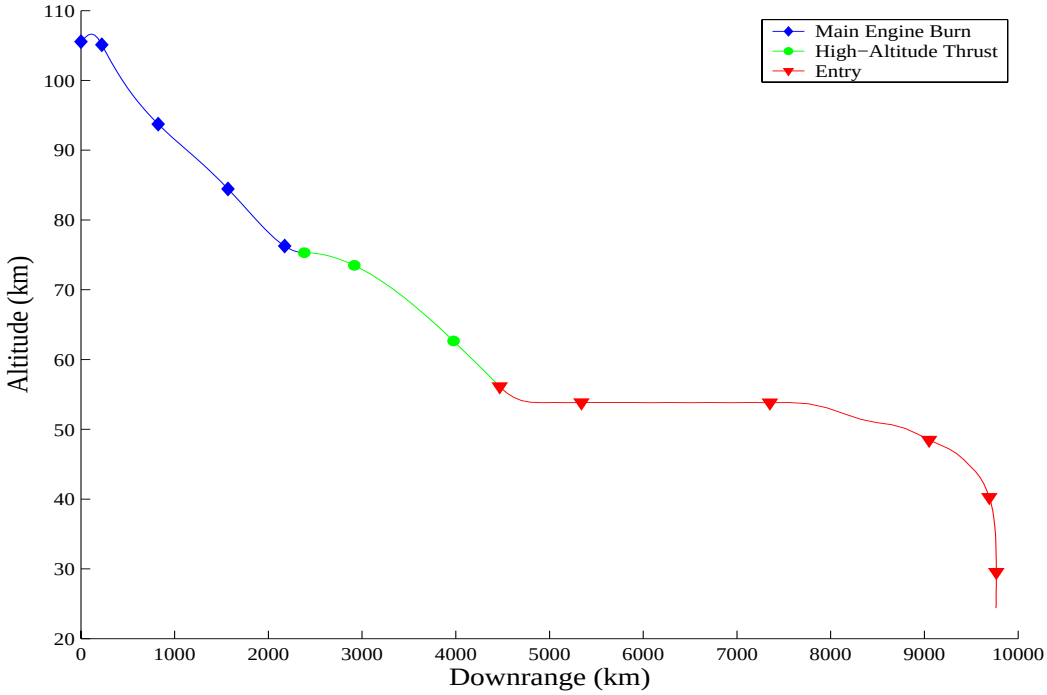

Figure 7-34: Altitude vs. Downrange for a One-Hundred Percent Maximum Downrange to Spain

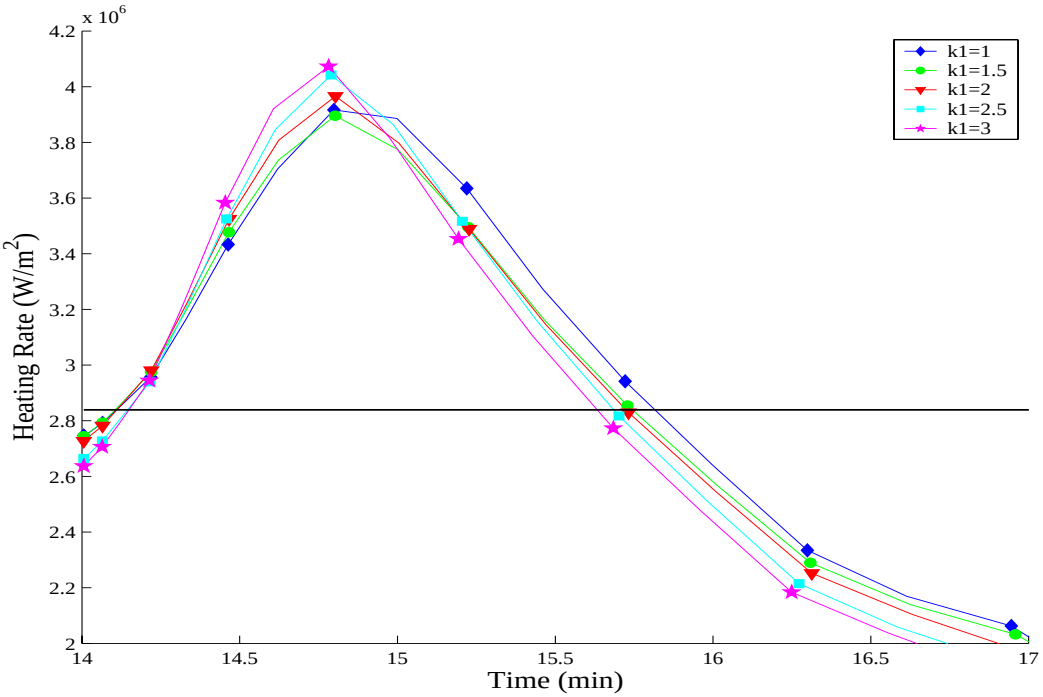

Figure 7-35: Entry Heating Rate vs. Time for a Fifty Percent Abort to Spain

7.4 Penalty Function Weighting

The penalty function for entry consists of three parts: the heating rate constraint, the dynamic pressure constraint, and the square of the sensed acceleration. Each weighting term, k_1, k_2, and k_3 assigns a different value of importance to each of these constraints, respectively. As the value of a weighting factor increases, the violation of the associated constraint increases the cost functional more than an equal violation of the other constraints. Thus, the optimizer will attempt to lower the accumulated violation of the constraint with the largest weighting term to achieve a lower cost. However, by lowering the accumulated violation of the constraint, it is possible to increase the maximum violation of the constraint. Examining Figure 7-35, we see that as the weighting factor k_1 is increased, the accumulated violation of heating rate decreases, but the maximum value increases. Since the cost calculation in Equation 7.1 penalizes the maximum violation of the constraints, the cost for this abort increases as the weighting factor increases.

Table 7.9: Inclinations for Each Abort to Senegal and Spain

Abort Time	Senegal	Spain
0	28.4089 deg	43.7045 deg
25	28.3774 deg	43.3826 deg
50	28.3281 deg	42.9304 deg
75	28.2486 deg	42.3405 deg
100	28.1142 deg	41.6933 deg

7.5 Selection of a Weighting Factor Combination

Examining Tables 7.1 through 7.8, we notice two trends. First, as has been stated for each abort, the best choice for the landing site is always Senegal. The inclination for the nominal ascent orbit is $i = 28.4$ deg. If we calculate the inclination of an abort originating at each initial condition and terminating at each landing site (Table 7.9), we can see that for every abort, the original inclination is much closer to the inclination of Senegal than the inclination of Spain. Thus, the choice of a landing site should coincide with the current orbit inclination. This result agrees with the current NASA protocol for performing a trans-atlantic abort.

The second important trend is the selection of weighting factors that lowers the cost as defined in Equation 7.1. Although there is not one set of weighting factors that satisfies each constraint for each abort, the trend for the best weighting factor combination is $k_1 = 1$ $k_2 = 1$ $k_3 = 3$. Although this is not the best choice for every case, this combination of weighting factors often yields lower values for the constraints, at the possible expense of inaccuracies in the final point of integration. This weighting factor combination selects the sensed acceleration as the most important constraint to be minimized and yields reliable solutions.

7.6 Evaluation of Optimization Study

The results presented thus far in this chapter focus on the effect of varying a set of weighting factors in the entry cost functional to determine the best trajectory for an abort from a specific set of initial conditions. The choice of a particular set of weighting factors depends on the cost assigned by Equation 7.1. In this section, we will evaluate how meaningful varying the weighting factors is in finding the best trajectory.

The solutions obtained from the optimizer are accurate with respect to the modeling information given. However, inaccuracies in the model often occur as simplifying assumptions are made. The entry aerodynamic model is a polynomic fit to a table of data and therefore may be slightly inaccurate. In this section, the entry aerodynamic coefficients for lift and drag, C_L and C_D, respectively are perturbed by assuming an uncertainty in the values for each. The four cases considered have a $\pm 5\%$ and $\pm 10\%$ uncertainty in both of the aerodynamic coefficients. When the control from the solution is integrated, the entry dynamics will have one of these perturbations in the aerodynamic model. The error in the integration due to this uncertainty will be measured by finding the cost for the trajectory using Equation 7.1. This new cost will be compared to the cost for the same trajectory without a perturbation to determine how much of an effect a model perturbation has on the cost. By comparing this difference to the difference in cost for the best choice of weighting factors, we can determine if the results given in this chapter have significance.

Table 7.10: Cost Calculation for Perturbations in a Zero Percent Abort to Senegal, $k_1 = 1$,$k_2 = 1$, $k_3 = 1$

Perturbation	$term_1$	$term_2$	$term_3$	$term_4$	$term_5$	$term_6$	$term_7$	Cost
-10%	4.726	0.841	1.292	1.455	8.209	13.026	14.339	43.889
-5%	4.726	0.841	1.292	1.455	8.146	13.020	14.320	43.802
$+5\%$	4.726	0.841	1.292	1.455	8.026	12.983	14.259	43.584
$+10\%$	4.726	0.841	1.292	1.455	7.968	12.955	14.219	43.457

Table 7.11: Cost Calculation for Perturbations in a Twenty-Five Percent Abort to Senegal, $k_1 = 1$,$k_2 = 1$, $k_3 = 1$

Perturbation	$term_1$	$term_2$	$term_3$	$term_4$	$term_5$	$term_6$	$term_7$	Cost
−10%	4.775	0.985	1.845	2.239	4.472	6.949	1.547	22.815
−5%	4.775	0.985	1.845	2.239	4.050	6.270	1.306	21.473
+5%	4.775	0.985	1.845	2.239	3.198	5.053	0.863	18.961
+10%	4.775	0.985	1.845	2.239	2.768	4.506	0.664	17.786

Table 7.12: Cost Calculation for Perturbations in a Twenty-Five Percent Abort to Spain, $k_1 = 1$,$k_2 = 1$, $k_3 = 1$

Perturbation	$term_1$	$term_2$	$term_3$	$term_4$	$term_5$	$term_6$	$term_7$	Cost
−10%	5.309	0.959	1.265	1.084	8.378	28.821	0.733	46.551
−5%	5.309	0.959	1.265	1.084	8.237	28.125	0.923	45.904
+5%	5.309	0.959	1.265	1.084	7.960	26.740	1.254	44.573
+10%	5.309	0.959	1.265	1.084	7.823	26.055	1.396	43.892

Tables 7.10 through 7.17 show the cost calculation for each abort with each uncertainty in the entry aerodynamic model. The optimized solution used in the calculation will be referred to as the baseline solution and corresponds to an abort using the weighting factors $k_1 = 1$, $k_2 = 1$, and $k_3 = 1$. Hence, the first four terms in each table are the same for each perturbation since these terms evaluate the constraint violations for the optimized solution.

Figure 7-36 plots the relative cost, with respect to the baseline, for each weighting factor combination and each entry aerodynamic perturbation, for each abort. Examining Figure 7-36 from left to right, we notice that only a twenty-five percent abort to Spain shows more improvement from a perturbation than from using the best choice in weighting factors (i.e. the cost due to a perturbation was lower than that of any weighting factor combination). For all other aborts, using the best choice of weighting factors gives an improvement over the baseline solution that is at least twice as large as the largest improvement due to an uncertainty. Tables 7.18 through 7.25 list the improvements in cost due to the best choice of weighting factors and the perturbations with the lowest cost for each abort. Thus, varying the weighting factors significantly lowers the cost for

Table 7.13: Cost Calculation for Perturbations in a Fifty Percent Abort to Senegal, $k_1 = 1$,$k_2 = 1$, $k_3 = 1$

Perturbation	$term_1$	$term_2$	$term_3$	$term_4$	$term_5$	$term_6$	$term_7$	Cost
−10%	0.878	1.236	1.464	2.470	5.541	1.775	0.491	13.858
−5%	0.878	1.236	1.464	2.470	5.523	1.812	0.512	13.898
+5%	0.878	1.236	1.464	2.470	4.717	1.411	0.698	12.878
+10%	0.878	1.236	1.464	2.470	2.768	4.506	0.664	13.990

Table 7.14: Cost Calculation for Perturbations in a Fifty Percent Abort to Spain, $k_1 = 1$,$k_2 = 1$, $k_3 = 1$

Perturbation	$term_1$	$term_2$	$term_3$	$term_4$	$term_5$	$term_6$	$term_7$	Cost
−10%	1.240	1.379	1.239	1.771	7.103	13.255	3.356	29.346
−5%	1.240	1.379	1.239	1.771	7.448	14.945	3.939	31.964
+5%	1.240	1.379	1.239	1.771	7.937	17.695	5.141	36.404
+10%	1.240	1.379	1.239	1.771	8.118	18.800	5.723	38.272

almost all of the aborts.

Table 7.15: Cost Calculation for Perturbations in a Seventy-Five Percent Abort to Senegal, $k_1 = 1$,$k_2 = 1$, $k_3 = 1$

Perturbation	$term_1$	$term_2$	$term_3$	$term_4$	$term_5$	$term_6$	$term_7$	Cost
−10%	1.560	1.440	1.356	2.121	0.153	0.955	0.983	8.570
−5%	1.560	1.440	1.356	2.121	0.190	0.914	0.986	8.570
+5%	1.560	1.440	1.356	2.121	0.023	0.999	1.012	8.513
+10%	1.560	1.440	1.356	2.121	3.776	0.921	0.881	12.057

Table 7.16: Cost Calculation for Perturbations in a Seventy-Five Percent Abort to Spain, $k_1 = 1$,$k_2 = 1$, $k_3 = 1$

Perturbation	$term_1$	$term_2$	$term_3$	$term_4$	$term_5$	$term_6$	$term_7$	Cost
−10%	2.713	1.442	1.623	3.039	1.390	0.369	1.463	12.041
−5%	2.713	1.442	1.623	3.039	1.605	0.766	1.459	12.649
+5%	2.713	1.442	1.623	3.039	1.980	1.504	1.459	13.762
+10%	2.713	1.442	1.623	3.039	2.150	1.853	1.464	14.287

Table 7.17: Cost Calculation for Perturbations in a One-Hundred Percent Abort to Senegal, $k_1 = 1$,$k_2 = 1$, $k_3 = 1$

Perturbation	$term_1$	$term_2$	$term_3$	$term_4$	$term_5$	$term_6$	$term_7$	Cost
−10%	1.324	1.023	3.220	11.061	1.709	0.062	1.175	19.576
−5%	1.324	1.023	3.220	11.061	1.513	0.107	1.148	19.398
+5%	1.324	1.023	3.220	11.061	1.146	0.191	1.099	19.066
+10%	1.324	1.023	3.220	11.061	0.265	1.118	1.032	19.046

Table 7.18: Cost Comparison for a Zero Percent Abort to Senegal

	Cost	Cost Decrease	Percent Decrease
$k_1 = 1$, $k_2 = 1$,$k_3 = 3$	27.129	-16.571	-37.919
+10% Uncertainty	43.457	-0.242	-0.555

Table 7.19: Cost Comparison for a Twenty-five Percent Abort to Senegal

	Cost	Cost Decrease	Percent Decrease
$k_1 = 1$, $k_2 = 1$,$k_3 = 2.5$	13.507	-6.681	-33.094
+10% Uncertainty	17.786	-2.403	-11.903

Table 7.20: Cost Comparison for a Twenty-Five Percent Abort to Spain

	Cost	Cost Decrease	Percent Decrease
$k_1 = 1$, $k_2 = 1$,$k_3 = 3$	44.695	-0.549	-1.215
+10% Uncertainty	43.892	-1.352	-2.989

Table 7.21: Cost Comparison for a Fifty Percent Abort to Senegal

	Cost	Cost Decrease	Percent Decrease
$k_1 = 1$, $k_2 = 3$,$k_3 = 1$	6.242	-7.349	-54.073
+5% Uncertainty	12.878	-0.714	-5.255

Table 7.22: Cost Comparison for a Fifty Percent Abort to Spain

	Cost	Cost Decrease	Percent Decrease
$k_1 = 1$, $k_2 = 1$,$k_3 = 3$	16.239	-18.069	-52.666
−10% Uncertainty	29.346	-4.962	-14.463

Table 7.23: Cost Comparison for a Seventy-Five Percent Abort to Senegal

	Cost	Cost Decrease	Percent Decrease
$k_1 = 1$, $k_2 = 1$,$k_3 = 2.5$	5.504	-3.031	-35.510
+5% Uncertainty	8.513	-0.021	-0.254

Table 7.24: Cost Comparison for a Seventy-Five Percent Abort to Spain

	Cost	Cost Decrease	Percent Decrease
$k_1 = 1$, $k_2 = 1$,$k_3 = 1.5$	8.410	-4.813	-36.401
−10% Uncertainty	12.041	-1.183	-8.945

Table 7.25: Cost Comparison for a One-Hundred Percent Abort to Senegal

	Cost	Cost Decrease	Percent Decrease
$k_1 = 1$, $k_2 = 1$,$k_3 = 3$	7.748	-11.480	-59.702
+10% Uncertainty	19.046	-0.182	-0.949

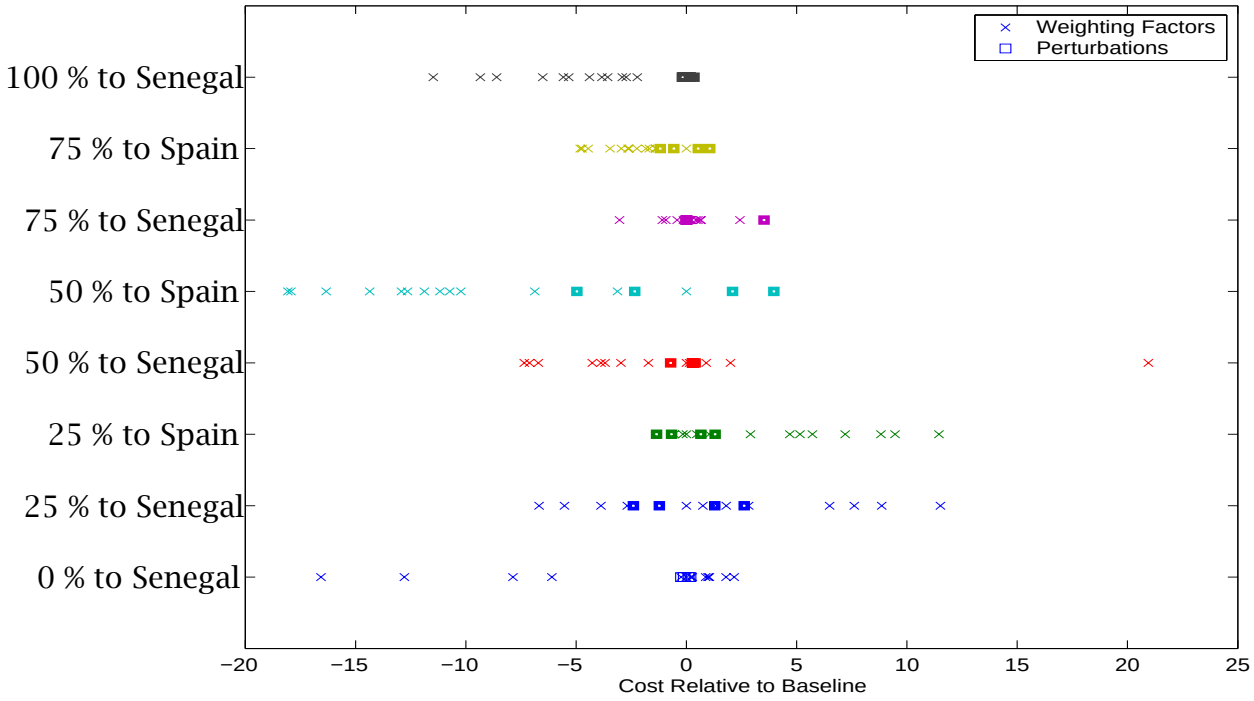

Figure 7-36: Relative Cost to Baseline for Each Abort and Each Perturbation

Chapter 8

Conclusions

8.1 Summary

The current shuttle capabilities are limited by the technologies used to generate and fly both the nominal mission and abort trajectories. NASA is investigating the design of a new space transportation vehicle, which among other improvements, has the ability to generate optimal abort trajectories. In this thesis, the abort trajectories generated initiate from the current state at the time of a single main engine failure and terminate at the TAEM interface for a landing site. The abort trajectory consisted of three regimes or phases of flight and each phase had a different dynamic model governing the motion of the vehicle.

To successfully perform an abort for a manned RLV, certain additional constraints must be met to ensure survival of the crew and vehicle. Since the primary desire was to obtain a solution, regardless of whether or not the solution was desirable, instead of imposing hard constraints, soft constraints were imposed as penalties in the cost functions. The important soft constraints were different for different phases of flight, hence different penalty functions were defined. In the first phase of abort, the ratio of the sensed acceleration squared to the desired maximum value was minimized. In addition, the specific final energy was minimized with respect to the specific final energy at the end of a nominal ascent to orbit. The third phase cost functional minimized a weighted

combination of heating rate, dynamic pressure and squared sensed acceleration with respect to the associated desired maximum values.

The abort problem described in this thesis was a multiple phase optimal control problem. A multiple phase optimal control problem has the same form as a single phase optimal control problem, except that at unknown times, the dynamic model and constraints governing the vehicle switch to a different set of constraints. The solution to the multiple phase optimal control problem was obtained by using a direct Pseudospectral Legendre method.

The Pseudospectral Legendre method discretized the optimal control problem at the Legendre-Gauss-Lobatto (LGL) points to form a nonlinear programming problem. Applying the Pseudospectral Legendre method to the multiple phase optimal control problem allowed for a natural discretization of the dynamics and constraints in each phase. To ensure that the minimization of the NLP yielded a optimal control for the entire abort problem, linkage constraints were added to connect adjacent phases. By reviewing Bellman's principle of optimality, we concluded that the additional constraints do not violate this principle because they are inherent in the original problem formulation.

The solution to the NLP was obtained using SNOPT, a sparse nonlinear optimization program and a brief discussion on the computational approach of SNOPT was given. The advantage of using SNOPT is that it allows the user to define a sparsity matrix. Due to the inherent sparsity of a multiple phase problem, having provided SNOPT with a description of the dependencies for each constraint on each variable saved a great deal of computational effort.

At five points along the nominal ascent trajectory, an abort due to a single main engine failure was optimized to one of two potential landing sites. The first study investigated the effects on the trajectory due to varying the relative weighting for each term in the third phase cost functional. A cost calculation was devised to evaluate the trajectory for each set of weighting factors and the trajectory with the lowest cost from a given initial condition was deemed to be the best. To determine if varying the weighting factors produced a significant

decrease in cost, as compared to the cost for a trajectory with equal weighting factors, the decrease was compared to the decrease in cost due to an entry aerodynamic model perturbation.

8.2 Conclusions

The Pseudospectral Legendre method is capable of solving a multiple phase nonlinear optimal control problem. The abort trajectories obtained were optimal with respect to the total cost functional for the problem. By examining the cost calculations for the various third phase cost functional weighting factors, the best trajectory for each initial condition and the corresponding set of weighting factors was determined. Although no set of weighting factors produced the lowest cost for a trajectory in each case considered, the weighting factors $k_1 = 1, k_2 = 1, k_3 = 3$ consistently produce great results. This weighting factor combination corresponds to an increased emphasis on lowering the violation of the sensed acceleration constraint. From each initial condition, the best landing site for each abort was Senegal. The inclination for an abort to Senegal was closer to the nominal mission inclination than the inclination for an abort to Spain. This result is in agreement with the current NASA procedure for choosing a trans-atlantic abort landing site.

Two infeasible trajectories arose during the investigation of abort trajectories. For the zero percent abort to Spain, the maximum downrange from the initial condition fell short of the downrange necessary to reach the terminal conditions at Spain. For the one-hundred percent abort to Spain, the opposite occurred. The minimum downrange case produced a trajectory that had a longer downrange than the downrange necessary to reach Spain. Hence, for the zero percent abort and the one-hundred percent abort, Senegal was the only choice for a trans-atlantic landing site.

The third phase cost functional was constructed to minimize the violations of the combined constraints over the duration of entry. In the cost calculation

presented the maximum value of the violation was considered. Generally, the optimizer minimized the value of a constraint by lowering the value of the constraint throughout the duration of entry. However, in some cases the optimizer choose to minimize the violation over the phase by decreasing the integral of the constraint, but raising the maximum value of the violation.

The entry aerodynamic model is a polynomic approximation to a table of data and subject to modeling error. Knowing that there existed a possibility of model uncertainty, a perturbation in the model was included during the integration of the solution with equal weighting factors. The cost calculation for each perturbation was compared to the cost calculation for the same case without a perturbation to determine the decrease in cost due to an uncertainty. By comparing the decrease in cost due to an uncertainty with the decrease in cost from choosing the best set of weighting factors, we determined that in every case except one, the decrease in the cost due to the selection of the best weighting factors was significantly greater.

8.3 Future Work

The abort problem is extremely complicated and this thesis is only a first step in examining the problem. The optimization criteria for the problem was selected to minimize the constraints without strictly imposing them, with the desire that a weighting factor combination would be determined for each abort, such that no constraints were violated. However, implementing a greater increase on the relative value for the weighting factor on sensed acceleration might yet produce the solution desired. When evaluating the effect on the weighting factors, certain cases increased the maximum value of the constraint but lowered the accumulated value. A possible alternate cost functional would actually penalize the maximum value of each constraint. However, the discontinuity of the associated cost functional may cause numerical problems. Another option is to eliminate the second phase of the problem. By incorporating the the second phase into the

third phase, the vehicle could choose whether to fly at a high altitude to utilize the limited thrust capability or enter at a low altitude and possibly avoid high values for the third phase penalty function. However, the constraints and objective functional for the third phase would have to apply over the entire interval to ensure that the solution is reasonable.

[This page intentionally left blank.]

Appendix A

Aerodynamic Coefficients

Lift Coefficients for ME burn

$$\begin{aligned} C_{L_1} &= 10.27573018 \\ C_{L_2} &= -2.510577161 \\ C_{L_3} &= .2693040532 \\ C_{L_4} &= 3.40756328 \\ C_{L_5} &= .2358657940 \\ C_{L_6} &= .04273683824 \\ C_{L_7} &= -10.66992871 \\ C_{L_8} &= 2.562677918 \\ C_{L_9} &= -.2777210471 \end{aligned} \tag{A.1}$$

Drag Coefficients for ME burn

$$
\begin{aligned}
C_{D_1} &= 5.843066454 \\
C_{D_2} &= 2.712861119 \\
C_{D_3} &= -.06602454483 \\
C_{D_4} &= -.2431101587 \\
C_{D_5} &= .1959055632 \\
C_{D_6} &= -.012459511135 \\
C_{D_7} &= -5.740226972 \\
C_{D_8} &= -2.593918270 \\
C_{D_9} &= .07108121429
\end{aligned}
\tag{A.2}
$$

Lift Coefficients for Entry

$$
\begin{aligned}
C_{L_0} &= -.2070 \\
C_{L_1} &= 1.6756
\end{aligned}
\tag{A.3}
$$

Drag Coefficients for Entry

$$
\begin{aligned}
C_{D_0} &= .0785 \\
C_{D_1} &= -.3529 \\
C_{D_2} &= 2.0400
\end{aligned}
\tag{A.4}
$$

Appendix B

Partial Derivatives

The partial derivatives in the Jacobian are computed analytically for better performance. In addition, the gradients for the cost functions were derived. The constraint derivatives and the cost function gradients are listed in this appendix.

B.1 Partial Derivatives for the Kinematics

Partial Derivatives for $\dot{r}$

$$\dot{r} = v \sin\gamma \tag{B.1}$$

$$\begin{aligned}
\frac{\partial \dot{r}}{\partial r} &= 0 & \frac{\partial \dot{r}}{\partial \theta} &= 0 & \frac{\partial \dot{r}}{\partial \phi} &= 0 \\
\frac{\partial \dot{r}}{\partial v} &= \sin\gamma & \frac{\partial \dot{r}}{\partial \gamma} &= v\cos\gamma & \frac{\partial \dot{r}}{\partial \chi} &= 0 \\
\frac{\partial \dot{r}}{\partial m_1} &= 0 & \frac{\partial \dot{r}}{\partial m_2} &= 0 & \frac{\partial \dot{r}}{\partial \alpha} &= 0 \\
\frac{\partial \dot{r}}{\partial T_1} &= 0 & \frac{\partial \dot{r}}{\partial w_1} &= 0 & \frac{\partial \dot{r}}{\partial u_1} &= 0 \\
\frac{\partial \dot{r}}{\partial u_2} &= 0 & \frac{\partial \dot{r}}{\partial u_3} &= 0 & \frac{\partial \dot{r}}{\partial u_4} &= 0 \\
\frac{\partial \dot{r}}{\partial T_2} &= 0 & \frac{\partial \dot{r}}{\partial t} &= 0
\end{aligned} \tag{B.2}$$

Partial Derivatives for $\dot{\theta}$

$$\dot{\theta} = \frac{v \cos\gamma \cos\chi}{r \cos\phi} \tag{B.3}$$

$$\begin{aligned}
\frac{\partial\dot{\theta}}{\partial r} &= \frac{-v\cos\gamma\cos\chi}{r^2\cos\phi} & \frac{\partial\dot{\theta}}{\partial\theta} &= 0 & \frac{\partial\dot{\theta}}{\partial\phi} &= \frac{v\cos\gamma\cos\chi\tan\phi}{r\cos\phi} \\
\frac{\partial\dot{\theta}}{\partial v} &= \frac{\cos\gamma\cos\chi}{r\cos\phi} & \frac{\partial\dot{\theta}}{\partial\gamma} &= \frac{-v\sin\gamma\cos\chi}{r\cos\phi} & \frac{\partial\dot{\theta}}{\partial\chi} &= \frac{-v\cos\gamma\sin\chi}{r\cos\phi} \\
\frac{\partial\dot{\theta}}{\partial m_1} &= 0 & \frac{\partial\dot{\theta}}{\partial m_2} &= 0 & \frac{\partial\dot{\theta}}{\partial\alpha} &= 0 \\
\frac{\partial\dot{\theta}}{\partial T_1} &= 0 & \frac{\partial\dot{\theta}}{\partial w_1} &= 0 & \frac{\partial\dot{\theta}}{\partial u_1} &= 0 \\
\frac{\partial\dot{\theta}}{\partial u_2} &= 0 & \frac{\partial\dot{\theta}}{\partial u_3} &= 0 & \frac{\partial\dot{\theta}}{\partial u_4} &= 0 \\
\frac{\partial\dot{\theta}}{\partial T_2} &= 0 & \frac{\partial\dot{\theta}}{\partial t} &= 0
\end{aligned} \tag{B.4}$$

Partial Derivatives for $\dot{\phi}$

$$\dot{\phi} = \frac{v \cos\gamma \sin\chi}{r} \tag{B.5}$$

$$\begin{aligned}
\frac{\partial\dot{\phi}}{\partial r} &= \frac{-v\cos\gamma\sin\chi}{r^2} & \frac{\partial\dot{\phi}}{\partial\theta} &= 0 & \frac{\partial\dot{\phi}}{\partial\phi} &= 0 \\
\frac{\partial\dot{\phi}}{\partial v} &= \frac{\cos\gamma\sin\chi}{r} & \frac{\partial\dot{\phi}}{\partial\gamma} &= \frac{-v\sin\gamma\sin\chi}{r} & \frac{\partial\dot{\phi}}{\partial\chi} &= \frac{v\cos\gamma\cos\chi}{r} \\
\frac{\partial\dot{\phi}}{\partial m_1} &= 0 & \frac{\partial\dot{\phi}}{\partial m_2} &= 0 & \frac{\partial\dot{\phi}}{\partial\alpha} &= 0 \\
\frac{\partial\dot{\phi}}{\partial T_1} &= 0 & \frac{\partial\dot{\phi}}{\partial w_1} &= 0 & \frac{\partial\dot{\phi}}{\partial u_1} &= 0 \\
\frac{\partial\dot{\phi}}{\partial u_2} &= 0 & \frac{\partial\dot{\phi}}{\partial u_3} &= 0 & \frac{\partial\dot{\phi}}{\partial u_4} &= 0 \\
\frac{\partial\dot{\phi}}{\partial T_2} &= 0 & \frac{\partial\dot{\phi}}{\partial t} &= 0
\end{aligned} \tag{B.6}$$

B.2 Partial Derivatives for Main Engine Burn

Partial Derivatives for $\dot{v}$

$$\dot{v} = -D + \frac{Tu_3}{m} - g\sin\gamma \tag{B.7}$$

$$\begin{aligned}
\frac{\partial \dot{v}}{\partial r} &= -\frac{\partial D}{\partial r} - \frac{\partial g}{\partial r}\sin\gamma & \frac{\partial \dot{v}}{\partial \theta} &= 0 \\
\frac{\partial \dot{v}}{\partial \phi} &= 0 & \frac{\partial \dot{v}}{\partial v} &= -\frac{\partial D}{\partial v} \\
\frac{\partial \dot{v}}{\partial \gamma} &= -g\cos\gamma & \frac{\partial \dot{v}}{\partial \chi} &= 0 \\
\frac{\partial \dot{v}}{\partial m_1} &= -\frac{\partial D}{\partial m}\frac{\partial m}{\partial m_1} - \frac{Tu_3}{m^2}\frac{\partial m}{\partial m_1} & \frac{\partial \dot{v}}{\partial m_2} &= -\frac{\partial D}{\partial m}\frac{\partial m}{\partial m_2} - \frac{Tu_3}{m^2}\frac{\partial m}{\partial m_2} \\
\frac{\partial \dot{v}}{\partial \alpha} &= -\frac{\partial D}{\partial \alpha} & \frac{\partial \dot{v}}{\partial T_1} &= \frac{u_3}{m}\frac{\partial T}{\partial T_1} \\
\frac{\partial \dot{v}}{\partial w_1} &= 0 & \frac{\partial \dot{v}}{\partial u_1} &= 0 \\
\frac{\partial \dot{v}}{\partial u_2} &= 0 & \frac{\partial \dot{v}}{\partial u_3} &= \frac{T}{m} \\
\frac{\partial \dot{v}}{\partial u_4} &= 0 & \frac{\partial \dot{v}}{\partial T_2} &= \frac{u_3}{m}\frac{\partial T}{\partial T_2} \\
\frac{\partial \dot{v}}{\partial t} &= 0
\end{aligned} \tag{B.8}$$

Partial Derivatives for $\dot{\gamma}$

$$\dot{\gamma} = \frac{Lu_1}{v} + \frac{Tu_1u_4}{mv} - \left(\frac{g}{v} - \frac{v}{r}\right)\cos\gamma \tag{B.9}$$

$$
\begin{aligned}
\frac{\partial \dot{\gamma}}{\partial r} &= \frac{\partial L}{\partial r}\frac{u_1}{v} - \left(\frac{\partial g}{\partial r}\frac{1}{v} + \frac{v}{r^2}\right)\cos\gamma & \frac{\partial \dot{\gamma}}{\partial \theta} &= 0 \\
\frac{\partial \dot{\gamma}}{\partial \phi} &= 0 & & \\
\frac{\partial \dot{\gamma}}{\partial v} &= \frac{\partial L}{\partial v}\frac{u_1}{v} - \frac{Lu_1}{v^2} - \frac{Tu_1u_4}{mv^2} - \left(\frac{-g}{v^2} - \frac{1}{r}\right)\cos\gamma & & \\
\frac{\partial \dot{\gamma}}{\partial \gamma} &= \left(\frac{g}{v} - \frac{v}{r}\right)\sin\gamma & \frac{\partial \dot{\gamma}}{\partial \chi} &= 0 \\
\frac{\partial \dot{\gamma}}{\partial m_1} &= \frac{\partial L}{\partial m}\frac{\partial m}{\partial m_1}\frac{u_1}{v} - \frac{Tu_1u_4}{m^2v}\frac{\partial m}{\partial m_1} & \frac{\partial \dot{\gamma}}{\partial \alpha} &= 0 \\
\frac{\partial \dot{\gamma}}{\partial T_1} &= \frac{u_1u_4}{mv}\frac{\partial T}{\partial T_1} & \frac{\partial \dot{\gamma}}{\partial w_1} &= 0 \\
\frac{\partial \dot{\gamma}}{\partial u_1} &= \frac{L}{v} + \frac{Tu_4}{mv} & \frac{\partial \dot{\gamma}}{\partial u_2} &= 0 \\
\frac{\partial \dot{\gamma}}{\partial u_3} &= 0 & \frac{\partial \dot{\gamma}}{\partial u_4} &= \frac{Tu_1}{mv} \\
\frac{\partial \dot{\gamma}}{\partial t} &= 0 & &
\end{aligned}
\tag{B.10}
$$

Partial Derivatives for $\dot{\chi}$

$$
\dot{\chi} = \frac{Lu_2}{v\cos\gamma} + \frac{Tu_2u_4}{mv\cos\gamma} - \frac{v}{r}\cos\gamma\cos\chi\tan\phi \tag{B.11}
$$

$$
\begin{aligned}
\frac{\partial \dot{\chi}}{\partial r} &= \frac{u_2}{v \cos\gamma} \frac{\partial L}{\partial r} \\
\frac{\partial \dot{\chi}}{\partial \theta} &= 0 \\
\frac{\partial \dot{\chi}}{\partial \phi} &= -\frac{v}{r} \cos\gamma \cos\chi \sec^2\phi \\
\frac{\partial \dot{\chi}}{\partial v} &= \frac{u_2}{v \cos\gamma} \frac{\partial L}{\partial v} - \frac{L u_2}{v^2 \cos\gamma} - \frac{T u_2 u_4}{m v^2 \cos\gamma} - \frac{\cos\gamma \cos\chi \tan\phi}{r} \\
\frac{\partial \dot{\chi}}{\partial \gamma} &= \frac{L u_2 \tan\gamma}{v \cos\gamma} + \frac{T u_2 u_4 \tan\gamma}{m v \cos\gamma} + \frac{v \sin\gamma \cos\chi \tan\phi}{r} \\
\frac{\partial \dot{\chi}}{\partial \chi} &= \frac{v \cos\gamma \sin\chi \tan\phi}{r} \\
\frac{\partial \dot{\chi}}{\partial m_1} &= \frac{u_2}{v \cos\gamma} \frac{\partial L}{\partial m} \frac{\partial m}{\partial m_1} - \frac{T u_2 u_4}{m^2 v \cos\gamma} \frac{\partial m}{\partial m_1} \\
\frac{\partial \dot{\chi}}{\partial m_2} &= \frac{u_2}{v \cos\gamma} \frac{\partial L}{\partial m} \frac{\partial m}{\partial m_2} - \frac{T u_2 u_4}{m^2 v \cos\gamma} \frac{\partial m}{\partial m_2} \\
\frac{\partial \dot{\chi}}{\partial \alpha} &= \frac{u_2}{v \cos\gamma} \frac{\partial L}{\partial \alpha} \\
\frac{\partial \dot{\chi}}{\partial T_1} &= \frac{u_2 u_4}{m v \cos\gamma} \frac{\partial T}{\partial T_1} \\
\frac{\partial \dot{\chi}}{\partial w_1} &= 0 \\
\frac{\partial \dot{\chi}}{\partial u_1} &= 0 \\
\frac{\partial \dot{\chi}}{\partial u_2} &= \frac{T u_4}{m v \cos\gamma} \\
\frac{\partial \dot{\chi}}{\partial u_3} &= 0 \\
\frac{\partial \dot{\chi}}{\partial u_4} &= \frac{T u_2}{m v \cos\gamma} \\
\frac{\partial \dot{\chi}}{\partial T_2} &= \frac{u_2 u_4}{m v \cos\gamma} \frac{\partial T}{\partial T_2} \\
\frac{\partial \dot{\chi}}{\partial t} &= 0
\end{aligned}
\tag{B.12}
$$

Partial Derivatives for $\dot{m}_1$

$$\dot{m}_1 = -\frac{T_1}{I_{sp_1} g_0} \tag{B.13}$$

$$\begin{array}{lllllll}
\frac{\partial \dot{m}_1}{\partial r} & = & 0 & \frac{\partial \dot{m}_1}{\partial \theta} & = & 0 & \frac{\partial \dot{m}_1}{\partial \phi} = 0 \\
\frac{\partial \dot{m}_1}{\partial v} & = & 0 & \frac{\partial \dot{m}_1}{\partial \gamma} & = & 0 & \frac{\partial \dot{m}_1}{\partial \chi} = 0 \\
\frac{\partial \dot{m}_1}{\partial m_1} & = & 0 & \frac{\partial \dot{m}_1}{\partial m_2} & = & 0 & \frac{\partial \dot{m}_1}{\partial \alpha} = 0 \\
\frac{\partial \dot{m}_1}{\partial T_1} & = & -\frac{1}{I_{sp_1} g_0} & \frac{\partial \dot{m}_1}{\partial w_1} & = & 0 & \frac{\partial \dot{m}_1}{\partial u_1} = 0 \\
\frac{\partial \dot{m}_1}{\partial u_2} & = & 0 & \frac{\partial \dot{m}_1}{\partial u_3} & = & 0 & \frac{\partial \dot{m}_1}{\partial u_4} = 0 \\
\frac{\partial \dot{m}_1}{\partial T_2} & = & 0 & \frac{\partial \dot{m}_1}{\partial t} & = & 0 &
\end{array} \tag{B.14}$$

Partial Derivatives for $\dot{m}_2$

$$\dot{m}_1 = -\frac{T_2}{I_{sp_2} g_0} \tag{B.15}$$

$$\begin{array}{lllllll}
\frac{\partial \dot{m}_1}{\partial r} & = & 0 & \frac{\partial \dot{m}_1}{\partial \theta} & = & 0 & \frac{\partial \dot{m}_1}{\partial \phi} = 0 \\
\frac{\partial \dot{m}_1}{\partial v} & = & 0 & \frac{\partial \dot{m}_1}{\partial \gamma} & = & 0 & \frac{\partial \dot{m}_1}{\partial \chi} = 0 \\
\frac{\partial \dot{m}_1}{\partial m_1} & = & 0 & \frac{\partial \dot{m}_1}{\partial m_2} & = & 0 & \frac{\partial \dot{m}_1}{\partial \alpha} = 0 \\
\frac{\partial \dot{m}_1}{\partial T_1} & = & 0 & \frac{\partial \dot{m}_1}{\partial w_1} & = & 0 & \frac{\partial \dot{m}_1}{\partial u_1} = 0 \\
\frac{\partial \dot{m}_1}{\partial u_2} & = & 0 & \frac{\partial \dot{m}_1}{\partial u_3} & = & 0 & \frac{\partial \dot{m}_1}{\partial u_4} = 0 \\
\frac{\partial \dot{m}_1}{\partial T_2} & = & -\frac{1}{I_{sp_2} g_0} & \frac{\partial \dot{m}_1}{\partial t} & = & 0 &
\end{array} \tag{B.16}$$

Partial Derivatives for $\dot{\alpha}$

$$\dot{\alpha} = w_1 \tag{B.17}$$

$$
\begin{array}{llllll}
\frac{\partial \dot{\alpha}}{\partial r} & = 0 & \frac{\partial \dot{\alpha}}{\partial \theta} & = 0 & \frac{\partial \dot{\alpha}}{\partial \phi} & = 0 \\
\frac{\partial \dot{\alpha}}{\partial v} & = 0 & \frac{\partial \dot{\alpha}}{\partial \gamma} & = 0 & \frac{\partial \dot{\alpha}}{\partial \chi} & = 0 \\
\frac{\partial \dot{\alpha}}{\partial m_1} & = 0 & \frac{\partial \dot{\alpha}}{\partial m_2} & = 0 & \frac{\partial \dot{\alpha}}{\partial \alpha} & = 0 \\
\frac{\partial \dot{\alpha}}{\partial T_1} & = 0 & \frac{\partial \dot{\alpha}}{\partial w_1} & = 1 & \frac{\partial \dot{\alpha}}{\partial u_1} & = 0 \\
\frac{\partial \dot{\alpha}}{\partial u_2} & = 0 & \frac{\partial \dot{\alpha}}{\partial u_3} & = 0 & \frac{\partial \dot{\alpha}}{\partial u_4} & = 0 \\
\frac{\partial \dot{\alpha}}{\partial T_2} & = 0 & \frac{\partial \dot{\alpha}}{\partial t} & = 0 & &
\end{array}
\tag{B.18}
$$

Partial Derivatives for g

$$
g = \frac{\mu}{r^2} \tag{B.19}
$$

$$
\begin{array}{llllll}
\frac{\partial g}{\partial r} & = -\frac{2g}{r} & \frac{\partial g}{\partial \theta} & = 0 & \frac{\partial g}{\partial \phi} & = 0 \\
\frac{\partial g}{\partial v} & = 0 & \frac{\partial g}{\partial \gamma} & = 0 & \frac{\partial g}{\partial \chi} & = 0 \\
\frac{\partial g}{\partial m_1} & = 0 & \frac{\partial g}{\partial m_2} & = 0 & \frac{\partial g}{\partial \alpha} & = 0 \\
\frac{\partial g}{\partial T_1} & = 0 & \frac{\partial g}{\partial w_1} & = 0 & \frac{\partial g}{\partial u_1} & = 0 \\
\frac{\partial g}{\partial u_2} & = 0 & \frac{\partial g}{\partial u_3} & = 0 & \frac{\partial g}{\partial u_4} & = 0 \\
\frac{\partial g}{\partial T_2} & = 0 & \frac{\partial g}{\partial t} & = 0 & &
\end{array}
\tag{B.20}
$$

Partial Derivatives for D

$$
D = \frac{\rho v^2 S C_D}{2m} \tag{B.21}
$$

$$
\begin{array}{lcllcl}
\frac{\partial D}{\partial r} & = & \frac{v^2 S C_D}{2m}\frac{\partial \rho}{\partial r} & \frac{\partial D}{\partial \theta} & = & 0 \\
\frac{\partial D}{\partial \phi} & = & 0 & \frac{\partial D}{\partial v} & = & \frac{\rho v S C_D}{m} + \frac{\rho v^2 S}{2m}\frac{\partial C_D}{\partial v} \\
\frac{\partial D}{\partial \gamma} & = & 0 & \frac{\partial D}{\partial \chi} & = & 0 \\
\frac{\partial D}{\partial m_1} & = & -\frac{\rho v^2 S C_D}{2m^2}\frac{\partial m}{\partial m_1} & \frac{\partial D}{\partial m_2} & = & -\frac{\rho v^2 S C_D}{2m^2}\frac{\partial m}{\partial m_2} \\
\frac{\partial D}{\partial \alpha} & = & \frac{\rho v^2 S}{2m}\frac{\partial C_D}{\partial \alpha} & \frac{\partial D}{\partial T_1} & = & 0 \\
\frac{\partial D}{\partial w_1} & = & 0 & \frac{\partial D}{\partial u_1} & = & 0 \\
\frac{\partial D}{\partial u_2} & = & 0 & \frac{\partial D}{\partial u_3} & = & 0 \\
\frac{\partial D}{\partial u_4} & = & 0 & \frac{\partial D}{\partial T_2} & = & 0 \\
\frac{\partial D}{\partial t} & = & 0 & & &
\end{array}
\tag{B.22}
$$

Partial Derivatives for L

$$
L = \frac{\rho v^2 S C_L}{2m} \tag{B.23}
$$

$$
\begin{array}{llll}
\frac{\partial L}{\partial r} & = & \frac{v^2 S C_L}{2m}\frac{\partial \rho}{\partial r} & \frac{\partial L}{\partial \theta} = 0 \\
\frac{\partial L}{\partial \phi} & = & 0 & \frac{\partial L}{\partial v} = \frac{\rho v S C_L}{m} + \frac{\rho v^2 S}{2m}\frac{\partial C_L}{\partial v} \\
\frac{\partial L}{\partial \gamma} & = & 0 & \frac{\partial L}{\partial \chi} = 0 \\
\frac{\partial L}{\partial m_1} & = & -\frac{\rho v^2 S C_L}{2m^2}\frac{\partial m}{\partial m_1} & \frac{\partial L}{\partial m_2} = -\frac{\rho v^2 S C_L}{2m^2}\frac{\partial m}{\partial m_2} \\
\frac{\partial L}{\partial \alpha} & = & \frac{\rho v^2 S}{2m}\frac{\partial C_L}{\partial \alpha} & \frac{\partial L}{\partial T_1} = 0 \\
\frac{\partial L}{\partial w_1} & = & 0 & \frac{\partial L}{\partial u_1} = 0 \\
\frac{\partial L}{\partial u_2} & = & 0 & \frac{\partial L}{\partial u_3} = 0 \\
\frac{\partial L}{\partial u_4} & = & 0 & \frac{\partial L}{\partial T_2} = 0 \\
\frac{\partial L}{\partial t} & = & 0 &
\end{array}
\tag{B.24}
$$

Partial Derivatives for ρ

$$
\rho = \rho_0 \exp(-(r - R_e)/H) \tag{B.25}
$$

$$
\begin{array}{lllllll}
\frac{\partial \rho}{\partial r} & = & -\frac{\rho}{H} & \frac{\partial \rho}{\partial \theta} & = & 0 \\
\frac{\partial \rho}{\partial \phi} & = & 0 & \frac{\partial \rho}{\partial v} & = & 0 \\
\frac{\partial \rho}{\partial \gamma} & = & 0 & \frac{\partial \rho}{\partial \chi} & = & 0 \\
\frac{\partial \rho}{\partial m_1} & = & 0 & \frac{\partial \rho}{\partial m_2} & = & 0 \\
\frac{\partial \rho}{\partial \alpha} & = & 0 & \frac{\partial \rho}{\partial T_1} & = & 0 \\
\frac{\partial \rho}{\partial w_1} & = & 0 & \frac{\partial \rho}{\partial u_1} & = & 0 \\
\frac{\partial \rho}{\partial u_2} & = & 0 & \frac{\partial \rho}{\partial u_3} & = & 0 \\
\frac{\partial \rho}{\partial u_4} & = & 0 & \frac{\partial \rho}{\partial T_2} & = & 0 \\
\frac{\partial \rho}{\partial t} & = & 0 & & &
\end{array}
\tag{B.26}
$$

Partial Derivatives for C_D

$$
\begin{aligned}
C_D &= (C_{D_1} + C_{D_2} M + C_{D_3} M^2) + (C_{D_4} + C_{D_5} M + C_{D_6} M^2) \sin\alpha \\
&\quad + (C_{D_7} + C_{D_8} M + C_{D_9} M^2) \cos\alpha
\end{aligned}
\tag{B.27}
$$

$$
\begin{aligned}
\frac{\partial C_D}{\partial r} &= 0 \\
\frac{\partial C_D}{\partial \theta} &= 0 \\
\frac{\partial C_D}{\partial \phi} &= 0 \\
\frac{\partial C_D}{\partial v} &= \left[(C_{D_2} + 2C_{D_3}) + (C_{D_5} + 2C_{D_6}) \sin\alpha \, (C_{D_8} + 2C_{D_9}) \cos\alpha \right] \frac{1}{v_{sos}} \\
\frac{\partial C_D}{\partial \gamma} &= 0 \\
\frac{\partial C_D}{\partial \chi} &= 0 \\
\frac{\partial C_D}{\partial m_1} &= 0 \\
\frac{\partial C_D}{\partial m_2} &= 0 \\
\frac{\partial C_D}{\partial \alpha} &= (C_{D_4} + C_{D_5} M + C_{D_6} M^2) \cos\alpha - (C_{D_7} + C_{D_8} M + C_{D_9} M^2) \sin\alpha \\
\frac{\partial C_D}{\partial T_1} &= 0 \\
\frac{\partial C_D}{\partial w_1} &= 0 \\
\frac{\partial C_D}{\partial u_1} &= 0 \\
\frac{\partial C_D}{\partial u_2} &= 0 \\
\frac{\partial C_D}{\partial u_3} &= 0 \\
\frac{\partial C_D}{\partial u_4} &= 0 \\
\frac{\partial C_D}{\partial T_2} &= 0 \\
\frac{\partial C_D}{\partial t} &= 0
\end{aligned}
\tag{B.28}
$$

Partial Derivatives for C_L

$$C_L = (C_{L_1} + C_{L_2}M + C_{L_3}M^2) + (C_{L_4} + C_{L_5}M + C_{L_6}M^2)\sin\alpha + (C_{L_7} + C_{L_8}M + C_{L_9}M^2)\cos\alpha \quad \text{(B.29)}$$

$$
\begin{aligned}
\frac{\partial C_L}{\partial r} &= 0 \\
\frac{\partial C_L}{\partial \theta} &= 0 \\
\frac{\partial C_L}{\partial \phi} &= 0 \\
\frac{\partial C_L}{\partial v} &= \left[(C_{L_2} + 2C_{L_3}) + (C_{L_5} + 2C_{L_6}) \sin\alpha \, (C_{L_8} + 2C_{L_9}) \cos\alpha \right] \frac{1}{v_{sos}} \\
\frac{\partial C_L}{\partial \gamma} &= 0 \\
\frac{\partial C_L}{\partial \chi} &= 0 \\
\frac{\partial C_L}{\partial m_1} &= 0 \\
\frac{\partial C_L}{\partial m_2} &= 0 \\
\frac{\partial C_L}{\partial \alpha} &= (C_{L_4} + C_{L_5} M + C_{L_6} M^2) \cos\alpha - (C_{L_7} + C_{L_8} M + C_{L_9} M^2) \sin\alpha \\
\frac{\partial C_L}{\partial T_1} &= 0 \\
\frac{\partial C_L}{\partial w_1} &= 0 \\
\frac{\partial C_L}{\partial u_1} &= 0 \\
\frac{\partial C_L}{\partial u_2} &= 0 \\
\frac{\partial C_L}{\partial u_3} &= 0 \\
\frac{\partial C_L}{\partial u_4} &= 0 \\
\frac{\partial C_L}{\partial T_2} &= 0 \\
\frac{\partial C_L}{\partial t} &= 0
\end{aligned}
\tag{B.30}
$$

Partial Derivatives for m

$$
m = m_1 + m_2 \tag{B.31}
$$

$$
\begin{aligned}
\frac{\partial m}{\partial r} &= 0 \quad \frac{\partial m}{\partial \theta} = 0 \\
\frac{\partial m}{\partial \phi} &= 0 \quad \frac{\partial m}{\partial v} = 0 \\
\frac{\partial m}{\partial \gamma} &= 0 \quad \frac{\partial m}{\partial \chi} = 0 \\
\frac{\partial m}{\partial m_1} &= 1 \quad \frac{\partial m}{\partial m_2} = 1 \\
\frac{\partial m}{\partial \alpha} &= 0 \quad \frac{\partial m}{\partial T_1} = 0 \\
\frac{\partial m}{\partial w_1} &= 0 \quad \frac{\partial m}{\partial u_1} = 0 \\
\frac{\partial m}{\partial u_2} &= 0 \quad \frac{\partial m}{\partial u_3} = 0 \\
\frac{\partial m}{\partial u_4} &= 0 \quad \frac{\partial m}{\partial T_2} = 0 \\
\frac{\partial m}{\partial t} &= 0
\end{aligned}
\tag{B.32}
$$

Partial Derivatives for T

$$
T = T_1 + T_2 \tag{B.33}
$$

$$
\begin{aligned}
\frac{\partial T}{\partial r} &= 0 \quad \frac{\partial T}{\partial \theta} = 0 \\
\frac{\partial T}{\partial \phi} &= 0 \quad \frac{\partial T}{\partial v} = 0 \\
\frac{\partial T}{\partial \gamma} &= 0 \quad \frac{\partial T}{\partial \chi} = 0 \\
\frac{\partial T}{\partial m_1} &= 0 \quad \frac{\partial T}{\partial m_2} = 0 \\
\frac{\partial T}{\partial \alpha} &= 0 \quad \frac{\partial T}{\partial T_1} = 1 \\
\frac{\partial T}{\partial w_1} &= 0 \quad \frac{\partial T}{\partial u_1} = 0 \\
\frac{\partial T}{\partial u_2} &= 0 \quad \frac{\partial T}{\partial u_3} = 0 \\
\frac{\partial T}{\partial u_4} &= 0 \quad \frac{\partial T}{\partial T_2} = 1 \\
\frac{\partial T}{\partial t} &= 0
\end{aligned}
\tag{B.34}
$$

Partial Derivatives for a^2

$$
a^2 = ||\mathbf{L} + \mathbf{D} + \mathbf{T}/m||^2 \tag{B.35}
$$

$$
\begin{aligned}
\frac{\partial a^2}{\partial r} &= 2\left(\mathbf{L}+\mathbf{D}+\mathbf{T}/m\right)\cdot\left(\frac{\partial \mathbf{L}}{\partial r}+\frac{\partial \mathbf{D}}{\partial r}+\frac{\partial \mathbf{T}/m}{\partial r}\right)\\
\frac{\partial a^2}{\partial \theta} &= 0\\
\frac{\partial a^2}{\partial \phi} &= 0\\
\frac{\partial a^2}{\partial v} &= 2\left(\mathbf{L}+\mathbf{D}+\mathbf{T}/m\right)\cdot\left(\frac{\partial \mathbf{L}}{\partial v}+\frac{\partial \mathbf{D}}{\partial v}+\frac{\partial \mathbf{T}/m}{\partial v}\right)\\
\frac{\partial a^2}{\partial \gamma} &= 0\\
\frac{\partial a^2}{\partial \chi} &= 0\\
\frac{\partial a^2}{\partial m_1} &= 2\left(\mathbf{L}+\mathbf{D}+\mathbf{T}/m\right)\cdot\left(\frac{\partial \mathbf{L}}{\partial m}\frac{\partial m}{\partial m_1}+\frac{\partial \mathbf{D}}{\partial m}\frac{\partial m}{\partial m_1}+\frac{\partial \mathbf{T}/m}{\partial m}\frac{\partial m}{\partial m_1}\right)\\
\frac{\partial a^2}{\partial m_2} &= 2\left(\mathbf{L}+\mathbf{D}+\mathbf{T}/m\right)\cdot\left(\frac{\partial \mathbf{L}}{\partial m}\frac{\partial m}{\partial m_2}+\frac{\partial \mathbf{D}}{\partial m}\frac{\partial m}{\partial m_1}+\frac{\partial \mathbf{T}/m}{\partial m}\frac{\partial m}{\partial m_1}\right)\\
\frac{\partial a^2}{\partial \alpha} &= 2\left(\mathbf{L}+\mathbf{D}+\mathbf{T}/m\right)\cdot\left(\frac{\partial \mathbf{L}}{\partial \alpha}+\frac{\partial \mathbf{D}}{\partial \alpha}+\frac{\partial \mathbf{T}/m}{\partial \alpha}\right) \qquad \text{(B.36)}\\
\frac{\partial a^2}{\partial T_1} &= 2\left(\mathbf{L}+\mathbf{D}+\mathbf{T}/m\right)\cdot\left(\frac{\partial \mathbf{L}}{\partial T}\frac{\partial T}{\partial T_1}+\frac{\partial \mathbf{D}}{\partial T}\frac{\partial T}{\partial T_1}+\frac{\partial \mathbf{T}/m}{\partial T}\frac{\partial T}{\partial T_1}\right)\\
\frac{\partial a^2}{\partial w_1} &= 0\\
\frac{\partial a^2}{\partial u_1} &= 2\left(\mathbf{L}+\mathbf{D}+\mathbf{T}/m\right)\cdot\left(\frac{\partial \mathbf{L}}{\partial u_1}+\frac{\partial \mathbf{D}}{\partial u_1}+\frac{\partial \mathbf{T}/m}{\partial u_1}\right)\\
\frac{\partial a^2}{\partial u_1} &= 2\left(\mathbf{L}+\mathbf{D}+\mathbf{T}/m\right)\cdot\left(\frac{\partial \mathbf{L}}{\partial u_1}+\frac{\partial \mathbf{D}}{\partial u_1}+\frac{\partial \mathbf{T}/m}{\partial u_2}\right)\\
\frac{\partial a^2}{\partial u_1} &= 2\left(\mathbf{L}+\mathbf{D}+\mathbf{T}/m\right)\cdot\left(\frac{\partial \mathbf{L}}{\partial u_1}+\frac{\partial \mathbf{D}}{\partial u_1}+\frac{\partial \mathbf{T}/m}{\partial u_3}\right)\\
\frac{\partial a^2}{\partial u_1} &= 2\left(\mathbf{L}+\mathbf{D}+\mathbf{T}/m\right)\cdot\left(\frac{\partial \mathbf{L}}{\partial u_1}+\frac{\partial \mathbf{D}}{\partial u_1}+\frac{\partial \mathbf{T}/m}{\partial u_4}\right)\\
\frac{\partial a^2}{\partial T_2} &= 2\left(\mathbf{L}+\mathbf{D}+\mathbf{T}/m\right)\cdot\left(\frac{\partial \mathbf{L}}{\partial T}\frac{\partial T}{\partial T_2}+\frac{\partial \mathbf{D}}{\partial T}\frac{\partial T}{\partial T_2}+\frac{\partial \mathbf{T}/m}{\partial T}\frac{\partial T}{\partial T_2}\right)\\
\frac{\partial a^2}{\partial t} &= 0
\end{aligned}
$$

Partial Derivatives for $\mathbf{T}/m$

$$\mathbf{T}/m = \begin{bmatrix} \frac{Tu_3}{m} \\ \frac{Tu_2u_4}{m} \\ \frac{Tu_1u_4}{m} \end{bmatrix} \tag{B.37}$$

$$\frac{\partial \mathbf{T}}{\partial r} = \begin{bmatrix} 0 \\ 0 \\ 0 \end{bmatrix} \quad \frac{\partial \mathbf{T}/m}{\partial \theta} = \begin{bmatrix} 0 \\ 0 \\ 0 \end{bmatrix} \quad \frac{\partial \mathbf{T}/m}{\partial \phi} = \begin{bmatrix} 0 \\ 0 \\ 0 \end{bmatrix}$$

$$\frac{\partial \mathbf{T}/m}{\partial v} = \begin{bmatrix} 0 \\ 0 \\ 0 \end{bmatrix} \quad \frac{\partial \mathbf{T}/m}{\partial \gamma} = \begin{bmatrix} 0 \\ 0 \\ 0 \end{bmatrix} \quad \frac{\partial \mathbf{T}/m}{\partial \chi} = \begin{bmatrix} 0 \\ 0 \\ 0 \end{bmatrix}$$

$$\frac{\partial \mathbf{T}/m}{\partial m_1} = \begin{bmatrix} -\frac{Tu_3}{m^2}\frac{\partial m}{\partial m_1} \\ -\frac{Tu_2u_4}{m^2}\frac{\partial m}{\partial m_1} \\ -\frac{Tu_1u_4}{m^2}\frac{\partial m}{\partial m_1} \end{bmatrix} \quad \frac{\partial \mathbf{T}/m}{\partial m_2} = \begin{bmatrix} -\frac{Tu_3}{m^2}\frac{\partial m}{\partial m_2} \\ -\frac{Tu_2u_4}{m^2}\frac{\partial m}{\partial m_2} \\ -\frac{Tu_1u_4}{m^2}\frac{\partial m}{\partial m_2} \end{bmatrix} \quad \frac{\partial \mathbf{T}/m}{\partial \alpha} = \begin{bmatrix} 0 \\ 0 \\ 0 \end{bmatrix}$$

$$\frac{\partial \mathbf{T}/m}{\partial T_1} = \begin{bmatrix} \frac{u_3}{m}\frac{\partial T}{\partial T_1} \\ \frac{u_2u_4}{m}\frac{\partial T}{\partial T_1} \\ \frac{u_1u_4}{m}\frac{\partial T}{\partial T_1} \end{bmatrix} \quad \frac{\partial \mathbf{T}/m}{\partial w_1} = \begin{bmatrix} 0 \\ 0 \\ 0 \end{bmatrix} \quad \frac{\partial \mathbf{T}/m}{\partial u_1} = \begin{bmatrix} 0 \\ 0 \\ \frac{Tu_4}{m} \end{bmatrix}$$

$$\frac{\partial \mathbf{T}/m}{\partial u_2} = \begin{bmatrix} 0 \\ \frac{Tu_4}{m} \\ 0 \end{bmatrix} \quad \frac{\partial \mathbf{T}/m}{\partial u_3} = \begin{bmatrix} \frac{T}{m} \\ 0 \\ 0 \end{bmatrix} \quad \frac{\partial \mathbf{T}/m}{\partial u_4} = \begin{bmatrix} 0 \\ \frac{Tu_2}{m} \\ \frac{Tu_1}{m} \end{bmatrix}$$

$$\frac{\partial \mathbf{T}/m}{\partial T_2} = \begin{bmatrix} \frac{u_3}{m}\frac{\partial T}{\partial T_2} \\ \frac{u_2u_4}{m}\frac{\partial T}{\partial T_2} \\ \frac{u_1u_4}{m}\frac{\partial T}{\partial T_2} \end{bmatrix} \quad \frac{\partial \mathbf{T}/m}{\partial t} = \begin{bmatrix} 0 \\ 0 \\ 0 \end{bmatrix} \tag{B.38}$$

Partial Derivatives for **L**

$$\mathbf{L} = \begin{bmatrix} 0 \\ Lu_2 \\ Lu_1 \end{bmatrix} \tag{B.39}$$

$$\frac{\partial \mathbf{L}}{\partial r} = \begin{bmatrix} 0 \\ \frac{\partial L}{\partial r}u_2 \\ \frac{\partial L}{\partial r}u_1 \end{bmatrix} \quad \frac{\partial \mathbf{L}}{\partial \theta} = \begin{bmatrix} 0 \\ 0 \\ 0 \end{bmatrix} \quad \frac{\partial \mathbf{L}}{\partial \phi} = \begin{bmatrix} 0 \\ 0 \\ 0 \end{bmatrix}$$

$$\frac{\partial \mathbf{L}}{\partial v} = \begin{bmatrix} 0 \\ \frac{\partial L}{\partial v}u_2 \\ \frac{\partial L}{\partial v}u_1 \end{bmatrix} \quad \frac{\partial \mathbf{L}}{\partial \gamma} = \begin{bmatrix} 0 \\ 0 \\ 0 \end{bmatrix} \quad \frac{\partial \mathbf{L}}{\partial \chi} = \begin{bmatrix} 0 \\ 0 \\ 0 \end{bmatrix}$$

$$\frac{\partial \mathbf{L}}{\partial m_1} = \begin{bmatrix} 0 \\ \frac{\partial L}{\partial m}\frac{\partial m}{\partial m_1}u_2 \\ \frac{\partial L}{\partial m}\frac{\partial m}{\partial m_1}u_1 \end{bmatrix} \quad \frac{\partial \mathbf{L}}{\partial m_2} = \begin{bmatrix} 0 \\ \frac{\partial L}{\partial m}\frac{\partial m}{\partial m_2}u_2 \\ \frac{\partial L}{\partial m}\frac{\partial m}{\partial m_2}u_1 \end{bmatrix} \quad \frac{\partial \mathbf{L}}{\partial \alpha} = \begin{bmatrix} 0 \\ \frac{\partial L}{\partial \alpha}u_2 \\ \frac{\partial L}{\partial \alpha}u_1 \end{bmatrix}$$

$$\frac{\partial \mathbf{L}}{\partial T_1} = \begin{bmatrix} 0 \\ 0 \\ 0 \end{bmatrix} \quad \frac{\partial \mathbf{L}}{\partial w_1} = \begin{bmatrix} 0 \\ 0 \\ 0 \end{bmatrix} \quad \frac{\partial \mathbf{L}}{\partial u_1} = \begin{bmatrix} 0 \\ 0 \\ L \end{bmatrix}$$

$$\frac{\partial \mathbf{L}}{\partial u_2} = \begin{bmatrix} 0 \\ L \\ 0 \end{bmatrix} \quad \frac{\partial \mathbf{L}}{\partial u_3} = \begin{bmatrix} 0 \\ 0 \\ 0 \end{bmatrix} \quad \frac{\partial \mathbf{L}}{\partial u_4} = \begin{bmatrix} 0 \\ 0 \\ 0 \end{bmatrix}$$

$$\frac{\partial \mathbf{L}}{\partial T_2} = \begin{bmatrix} 0 \\ 0 \\ 0 \end{bmatrix} \quad \frac{\partial \mathbf{L}}{\partial t} = \begin{bmatrix} 0 \\ 0 \\ 0 \end{bmatrix} \tag{B.40}$$

Partial Derivatives for **D**

$$\mathbf{D} = \begin{bmatrix} -D \\ 0 \\ 0 \end{bmatrix} \tag{B.41}$$

$$\begin{aligned}
\frac{\partial \mathbf{D}}{\partial r} &= \begin{bmatrix} -\frac{\partial D}{\partial r} \\ 0 \\ 0 \end{bmatrix} & \frac{\partial \mathbf{D}}{\partial \theta} &= \begin{bmatrix} 0 \\ 0 \\ 0 \end{bmatrix} & \frac{\partial \mathbf{D}}{\partial \phi} &= \begin{bmatrix} 0 \\ 0 \\ 0 \end{bmatrix} \\
\frac{\partial \mathbf{D}}{\partial v} &= \begin{bmatrix} -pdv \\ 0 \\ 0 \end{bmatrix} & \frac{\partial \mathbf{D}}{\partial \gamma} &= \begin{bmatrix} 0 \\ 0 \\ 0 \end{bmatrix} & \frac{\partial \mathbf{D}}{\partial \chi} &= \begin{bmatrix} 0 \\ 0 \\ 0 \end{bmatrix} \\
\frac{\partial \mathbf{D}}{\partial m_1} &= \begin{bmatrix} -\frac{\partial D}{\partial m}\frac{\partial m}{\partial m_1} \\ 0 \\ 0 \end{bmatrix} & \frac{\partial \mathbf{D}}{\partial m_2} &= \begin{bmatrix} -\frac{\partial D}{\partial m}\frac{\partial m}{\partial m_2} \\ 0 \\ 0 \end{bmatrix} & \frac{\partial \mathbf{D}}{\partial \alpha} &= \begin{bmatrix} -\frac{\partial D}{\partial \alpha} \\ 0 \\ 0 \end{bmatrix} \\
\frac{\partial \mathbf{D}}{\partial T_1} &= \begin{bmatrix} 0 \\ 0 \\ 0 \end{bmatrix} & \frac{\partial \mathbf{D}}{\partial w_1} &= \begin{bmatrix} 0 \\ 0 \\ 0 \end{bmatrix} & \frac{\partial \mathbf{D}}{\partial u_1} &= \begin{bmatrix} 0 \\ 0 \\ 0 \end{bmatrix} \\
\frac{\partial \mathbf{D}}{\partial u_2} &= \begin{bmatrix} 0 \\ 0 \\ 0 \end{bmatrix} & \frac{\partial \mathbf{D}}{\partial u_3} &= \begin{bmatrix} 0 \\ 0 \\ 0 \end{bmatrix} & \frac{\partial \mathbf{D}}{\partial u_4} &= \begin{bmatrix} 0 \\ 0 \\ 0 \end{bmatrix} \\
\frac{\partial \mathbf{D}}{\partial T_2} &= \begin{bmatrix} 0 \\ 0 \\ 0 \end{bmatrix} & \frac{\partial \mathbf{D}}{\partial t} &= \begin{bmatrix} 0 \\ 0 \\ 0 \end{bmatrix}
\end{aligned} \tag{B.42}$$

Partial Derivatives for the Final Energy

$$e = \frac{v^2}{2} - \frac{\mu}{r} \tag{B.43}$$

$$
\begin{array}{llll}
\frac{\partial e}{\partial r} & = & -\frac{\mu}{r^2} & \frac{\partial e}{\partial \theta} = 0 \\
\frac{\partial e}{\partial \phi} & = & 0 & \frac{\partial e}{\partial v} = v \\
\frac{\partial e}{\partial \gamma} & = & 0 & \frac{\partial e}{\partial \chi} = 0 \\
\frac{\partial e}{\partial m_1} & = & 0 & \frac{\partial e}{\partial m_2} = 0 \\
\frac{\partial e}{\partial \alpha} & = & 0 & \frac{\partial e}{\partial T_1} = 0 \\
\frac{\partial e}{\partial w_1} & = & 0 & \frac{\partial e}{\partial u_1} = 0 \\
\frac{\partial e}{\partial u_2} & = & 0 & \frac{\partial e}{\partial u_3} = 0 \\
\frac{\partial e}{\partial u_4} & = & 0 & \frac{\partial e}{\partial T_2} = 0 \\
\frac{\partial e}{\partial t} & = & 0 &
\end{array}
\tag{B.44}
$$

Partial Derivatives for the Path Constraint on Bank Angle

$$
p_1 = u_1^2 + u_2^2 \tag{B.45}
$$

$$
\begin{aligned}
\frac{\partial p_1}{\partial r} &= 0 & \frac{\partial p_1}{\partial \theta} &= 0 \\
\frac{\partial p_1}{\partial \phi} &= 0 & \frac{\partial p_1}{\partial v} &= 0 \\
\frac{\partial p_1}{\partial \gamma} &= 0 & \frac{\partial p_1}{\partial \chi} &= 0 \\
\frac{\partial p_1}{\partial m_1} &= 0 & \frac{\partial p_1}{\partial m_2} &= 0 \\
\frac{\partial p_1}{\partial \alpha} &= 0 & \frac{\partial p_1}{\partial T_1} &= 0 \\
\frac{\partial p_1}{\partial w_1} &= 0 & \frac{\partial p_1}{\partial u_1} &= 2u_1 \\
\frac{\partial p_1}{\partial u_2} &= 2u_2 & \frac{\partial p_1}{\partial u_3} &= 0 \\
\frac{\partial p_1}{\partial u_4} &= 0 & \frac{\partial p_1}{\partial T_2} &= 0 \\
\frac{\partial p_1}{\partial t} &= 0
\end{aligned}
\tag{B.46}
$$

Partial Derivatives for the Path Constraint on Thrust Angle of Attack

$$
p_2 = u_3^2 + u_4^2 \tag{B.47}
$$

$$
\begin{aligned}
\frac{\partial p_2}{\partial r} &= 0 & \frac{\partial p_2}{\partial \theta} &= 0 \\
\frac{\partial p_2}{\partial \phi} &= 0 & \frac{\partial p_2}{\partial v} &= 0 \\
\frac{\partial p_2}{\partial \gamma} &= 0 & \frac{\partial p_2}{\partial \chi} &= 0 \\
\frac{\partial p_2}{\partial m_1} &= 0 & \frac{\partial p_2}{\partial m_2} &= 0 \\
\frac{\partial p_2}{\partial \alpha} &= 0 & \frac{\partial p_2}{\partial T_1} &= 0 \\
\frac{\partial p_2}{\partial w_1} &= 0 & \frac{\partial p_2}{\partial u_1} &= 0 \\
\frac{\partial p_2}{\partial u_2} &= 0 & \frac{\partial p_2}{\partial u_3} &= 2u_3 \\
\frac{\partial p_2}{\partial u_4} &= 2u_4 & \frac{\partial p_2}{\partial T_2} &= 0 \\
\frac{\partial p_2}{\partial t} &= 0
\end{aligned}
\tag{B.48}
$$

B.3 Partial Derivatives for High-Altitude Thrust

Partial Derivatives for $\dot{v}$

$$
\dot{v} = \frac{T_2 u_5}{m} - g \sin \gamma \tag{B.49}
$$

$$
\begin{array}{llll}
\frac{\partial \dot{v}}{\partial r} & = & -\frac{\partial g}{\partial r}\sin\gamma & \frac{\partial \dot{v}}{\partial \theta} = 0 \\
\frac{\partial \dot{v}}{\partial \phi} & = & 0 & \frac{\partial \dot{v}}{\partial v} = 0 \\
\frac{\partial \dot{v}}{\partial \gamma} & = & -g\cos\gamma & \frac{\partial \dot{v}}{\partial \chi} = 0 \\
\frac{\partial \dot{v}}{\partial m} & = & -\frac{T_2 u_5}{m^2} & \frac{\partial \dot{v}}{\partial T_2} = \frac{u_5}{m} \\
\frac{\partial \dot{v}}{\partial u_5} & = & \frac{T_2}{m} & \frac{\partial \dot{v}}{\partial u_6} = 0 \\
\frac{\partial \dot{v}}{\partial u_7} & = & 0 & \frac{\partial \dot{v}}{\partial t} = 0
\end{array}
\tag{B.50}
$$

Partial Derivatives for $\dot{\gamma}$

$$
\dot{\gamma} = \frac{T_2 u_7}{m} - \left(\frac{g}{v} - \frac{v}{r}\right)\cos\gamma \tag{B.51}
$$

$$
\begin{array}{llll}
\frac{\partial \dot{\gamma}}{\partial r} & = & -\left(\frac{1}{v}\frac{\partial g}{\partial r} + \frac{v^2}{r}\right)\cos\gamma & \frac{\partial \dot{\gamma}}{\partial \theta} = 0 \\
\frac{\partial \dot{\gamma}}{\partial \phi} & = & 0 & \frac{\partial \dot{\gamma}}{\partial v} = -\frac{T_2 u_7}{m v^2} - \left(-\frac{g}{v^2} - \frac{1}{r}\right)\cos\gamma \\
\frac{\partial \dot{\gamma}}{\partial \gamma} & = & g\sin\gamma & \frac{\partial \dot{\gamma}}{\partial \chi} = 0 \\
\frac{\partial \dot{\gamma}}{\partial m} & = & -\frac{T_2 u_7}{m^2 v} & \frac{\partial \dot{\gamma}}{\partial T_2} = \frac{u_7}{m v} \\
\frac{\partial \dot{\gamma}}{\partial u_5} & = & 0 & \frac{\partial \dot{\gamma}}{\partial u_6} = 0 \\
\frac{\partial \dot{\gamma}}{\partial u_7} & = & \frac{T_2}{m v} & \frac{\partial \dot{\gamma}}{\partial t} = 0
\end{array}
\tag{B.52}
$$

Partial Derivatives for $\dot{\chi}$

$$
\dot{\chi} = \frac{T_2 u_6}{m v \cos\gamma} - \frac{v}{r}\cos\gamma\cos\chi\tan\phi \tag{B.53}
$$

$$
\begin{aligned}
\frac{\partial \dot{\chi}}{\partial r} &= -\tfrac{v}{r^2}\cos\gamma\cos\chi\tan\phi & \frac{\partial \dot{\chi}}{\partial \theta} &= 0\\
\frac{\partial \dot{\chi}}{\partial \phi} &= -\tfrac{v}{r}\cos\gamma\cos\chi\sec^2\phi & \frac{\partial \dot{\chi}}{\partial v} &= -\tfrac{T_2 u_6}{mv^2\cos\gamma} - \tfrac{\cos\gamma\cos\chi\tan\phi}{r}\\
\frac{\partial \dot{\chi}}{\partial \gamma} &= \tfrac{T_2 u_6\tan\gamma}{mv\cos\gamma} + \tfrac{v}{r}\sin\gamma\cos\chi\tan\phi & \frac{\partial \dot{\chi}}{\partial \chi} &= \tfrac{v}{r}\cos\gamma\sin\chi\tan\phi\\
\frac{\partial \dot{\chi}}{\partial m} &= -\tfrac{T_2 u_6}{m^2 v\cos\gamma} & \frac{\partial \dot{\chi}}{\partial T_2} &= \tfrac{u_6}{mv\cos\gamma}\\
\frac{\partial \dot{\chi}}{\partial u_5} &= 0 & \frac{\partial \dot{\chi}}{\partial u_6} &= \tfrac{T_2}{mv\cos\gamma}\\
\frac{\partial \dot{\chi}}{\partial u_7} &= 0 & \frac{\partial \dot{\chi}}{\partial t} &= 0
\end{aligned}
\tag{B.54}
$$

Partial Derivatives for $\dot{m}$

$$
\dot{m} = -\frac{T_2}{I_{sp_2} g_0} \tag{B.55}
$$

$$
\begin{aligned}
\frac{\partial \dot{m}}{\partial r} &= 0 & \frac{\partial \dot{m}}{\partial \theta} &= 0\\
\frac{\partial \dot{m}}{\partial \phi} &= 0 & \frac{\partial \dot{m}}{\partial v} &= 0\\
\frac{\partial \dot{m}}{\partial \gamma} &= 0 & \frac{\partial \dot{m}}{\partial \chi} &= 0\\
\frac{\partial \dot{m}}{\partial m} &= 0 & \frac{\partial \dot{m}}{\partial T_2} &= -\tfrac{1}{I_{sp_2} g_0}\\
\frac{\partial \dot{m}}{\partial u_5} &= 0 & \frac{\partial \dot{m}}{\partial u_6} &= 0\\
\frac{\partial \dot{m}}{\partial u_7} &= 0 & \frac{\partial \dot{m}}{\partial t} &= 0
\end{aligned}
\tag{B.56}
$$

Partial Derivatives for g

$$
g = \frac{\mu}{r^2} \tag{B.57}
$$

$$\begin{array}{lllll}
\frac{\partial g}{\partial r} & = & -\frac{2g}{r} & \frac{\partial g}{\partial \theta} & = 0 \\
\frac{\partial g}{\partial \phi} & = & 0 & \frac{\partial g}{\partial v} & = 0 \\
\frac{\partial g}{\partial \gamma} & = & 0 & \frac{\partial g}{\partial \chi} & = 0 \\
\frac{\partial g}{\partial m} & = & 0 & \frac{\partial g}{\partial T_2} & = 0 \\
\frac{\partial g}{\partial u_5} & = & 0 & \frac{\partial g}{\partial u_6} & = 0 \\
\frac{\partial g}{\partial u_7} & = & 0 & \frac{\partial g}{\partial t} & = 0
\end{array} \tag{B.58}$$

Partial Derivative for the Path Constraint on Altitude

$$p_3 = r - R_e \tag{B.59}$$

$$\begin{array}{lllll}
\frac{\partial p_3}{\partial r} & = & 1 & \frac{\partial p_3}{\partial \theta} & = 0 \\
\frac{\partial p_3}{\partial \phi} & = & 0 & \frac{\partial p_3}{\partial v} & = 0 \\
\frac{\partial p_3}{\partial \gamma} & = & 0 & \frac{\partial p_3}{\partial \chi} & = 0 \\
\frac{\partial p_3}{\partial m} & = & 0 & \frac{\partial p_3}{\partial T_2} & = 0 \\
\frac{\partial p_3}{\partial u_5} & = & 0 & \frac{\partial p_3}{\partial u_6} & = 0 \\
\frac{\partial p_3}{\partial u_7} & = & 0 & \frac{\partial p_3}{\partial t} & = 0
\end{array} \tag{B.60}$$

Partial Derivative for the Path Constraint on the Euler Angles

$$p_4 = u_5^2 + u_6^2 + u_7^2 \tag{B.61}$$

$$
\begin{array}{llll}
\frac{\partial p_4}{\partial r} & = & 0 & \frac{\partial p_4}{\partial \theta} = 0 \\
\frac{\partial p_4}{\partial \phi} & = & 0 & \frac{\partial p_4}{\partial v} = 0 \\
\frac{\partial p_4}{\partial \gamma} & = & 0 & \frac{\partial p_4}{\partial \chi} = 0 \\
\frac{\partial p_4}{\partial m} & = & 0 & \frac{\partial p_4}{\partial T_2} = 0 \\
\frac{\partial p_4}{\partial u_5} & = & 2u_5 & \frac{\partial p_4}{\partial u_6} = 2u_6 \\
\frac{\partial p_4}{\partial u_7} & = & 2u_7 & \frac{\partial p_4}{\partial t} = 0
\end{array}
\tag{B.62}
$$

B.4 Partial Derivatives for Entry

Partial Derivatives for $\dot{v}$

$$
\dot{v} = -D - g \sin\gamma \tag{B.63}
$$

$$
\begin{array}{llll}
\frac{\partial \dot{v}}{\partial r} & = & -\frac{\partial D}{\partial r} - \frac{\partial g}{\partial r}\sin\gamma & \frac{\partial \dot{v}}{\partial \theta} = 0 \\
\frac{\partial \dot{v}}{\partial \phi} & = & 0 & \frac{\partial \dot{v}}{\partial v} = -\frac{\partial D}{\partial v} \\
\frac{\partial \dot{v}}{\partial \gamma} & = & -g\cos\gamma & \frac{\partial \dot{v}}{\partial \chi} = 0 \\
\frac{\partial \dot{v}}{\partial m} & = & -\frac{\partial D}{\partial m} & \frac{\partial \dot{v}}{\partial \alpha} = -\frac{\partial D}{\partial \alpha} \\
\frac{\partial \dot{v}}{\partial w_2} & = & 0 & \frac{\partial \dot{v}}{\partial u_8} = 0 \\
\frac{\partial \dot{v}}{\partial u_9} & = & 0 & \frac{\partial \dot{v}}{\partial t} = 0
\end{array}
\tag{B.64}
$$

Partial Derivatives for $\dot{\gamma}$

$$
\dot{\gamma} = \frac{Lu_8}{v} - \left(\frac{g}{v} - \frac{v}{r}\right)\cos\gamma \tag{B.65}
$$

$$
\begin{aligned}
\frac{\partial \dot{\gamma}}{\partial r} &= \frac{u_8}{v}\frac{\partial L}{\partial r} - \left(\frac{1}{v}\frac{\partial g}{\partial r} + \frac{v}{r^2}\right)\cos\gamma & \frac{\partial \dot{\gamma}}{\partial \theta} &= 0 \\
\frac{\partial \dot{\gamma}}{\partial \phi} &= 0 & \frac{\partial \dot{\gamma}}{\partial v} &= \frac{u_8}{v}\frac{\partial L}{\partial v} - \frac{Lu_8}{v^2} - \left(-\frac{g}{v^2} - \frac{1}{r}\right)\cos\gamma \\
\frac{\partial \dot{\gamma}}{\partial \gamma} &= \left(\frac{g}{v} - \frac{v}{r}\right)\sin\gamma & \frac{\partial \dot{\gamma}}{\partial \chi} &= 0 \\
\frac{\partial \dot{\gamma}}{\partial m} &= \frac{u_8}{v}\frac{\partial L}{\partial m} & \frac{\partial \dot{\gamma}}{\partial \alpha} &= \frac{u_8}{v}\frac{\partial D}{\partial \alpha} \\
\frac{\partial \dot{\gamma}}{\partial w_2} &= 0 & \frac{\partial \dot{\gamma}}{\partial u_8} &= \frac{L}{v} \\
\frac{\partial \dot{\gamma}}{\partial u_9} &= 0 & \frac{\partial \dot{\gamma}}{\partial t} &= 0
\end{aligned}
\tag{B.66}
$$

Partial Derivatives for $\dot{\chi}$

$$
\dot{\chi} = \frac{Lu_9}{v\cos\gamma} - \frac{v}{r}\cos\gamma\cos\chi\tan\phi \tag{B.67}
$$

$$
\begin{aligned}
\frac{\partial \dot{\chi}}{\partial r} &= \frac{u_9}{v\cos\gamma}\frac{\partial L}{\partial r} + \frac{v\cos\gamma\cos\chi\tan\phi}{r^2} & \frac{\partial \dot{\chi}}{\partial \theta} &= 0 \\
\frac{\partial \dot{\chi}}{\partial \phi} &= -\frac{v\cos\gamma\cos\chi\sec^2\phi}{r} & \frac{\partial \dot{\chi}}{\partial v} &= \frac{u_9}{v\cos\gamma}\frac{\partial L}{\partial v} - \frac{Lu_9}{v^2\cos\gamma} - \frac{\cos\gamma\cos\chi\tan\phi}{r} \\
\frac{\partial \dot{\chi}}{\partial \gamma} &= \frac{Lu_9\tan\gamma}{v\cos\gamma} + \frac{v\sin\gamma\cos\chi\tan\phi}{r} & \frac{\partial \dot{\chi}}{\partial \chi} &= \frac{v\cos\gamma\sin\chi\tan\phi}{r} \\
\frac{\partial \dot{\chi}}{\partial m} &= \frac{u_9}{v\cos\gamma}\frac{\partial L}{\partial m} & \frac{\partial \dot{\chi}}{\partial \alpha} &= \frac{u_9}{v\cos\gamma}\frac{\partial L}{\partial \alpha} \\
\frac{\partial \dot{\chi}}{\partial w_2} &= 0 & \frac{\partial \dot{\chi}}{\partial u_8} &= 0 \\
\frac{\partial \dot{\chi}}{\partial u_9} &= \frac{L}{v\cos\gamma} & \frac{\partial \dot{\chi}}{\partial t} &= 0
\end{aligned}
\tag{B.68}
$$

Partial Derivatives for $\dot{m}$

$$
\dot{m} = 0 \tag{B.69}
$$

$$\begin{aligned}
\frac{\partial \dot{m}}{\partial r} &= 0 & \frac{\partial \dot{m}}{\partial \theta} &= 0 \\
\frac{\partial \dot{m}}{\partial \phi} &= 0 & \frac{\partial \dot{m}}{\partial v} &= 0 \\
\frac{\partial \dot{m}}{\partial \gamma} &= 0 & \frac{\partial \dot{m}}{\partial \chi} &= 0 \\
\frac{\partial \dot{m}}{\partial m} &= 0 & \frac{\partial \dot{m}}{\partial \alpha} &= 0 \\
\frac{\partial \dot{m}}{\partial w_2} &= 0 & \frac{\partial \dot{m}}{\partial u_8} &= 0 \\
\frac{\partial \dot{m}}{\partial u_9} &= 0 & \frac{\partial \dot{m}}{\partial t} &= 0
\end{aligned} \tag{B.70}$$

Partial Derivatives for $\dot{\alpha}$

$$\dot{\alpha} = w_2 \tag{B.71}$$

$$\begin{aligned}
\frac{\partial \dot{\alpha}}{\partial r} &= 0 & \frac{\partial \dot{\alpha}}{\partial \theta} &= 0 \\
\frac{\partial \dot{\alpha}}{\partial \phi} &= 0 & \frac{\partial \dot{\alpha}}{\partial v} &= 0 \\
\frac{\partial \dot{\alpha}}{\partial \gamma} &= 0 & \frac{\partial \dot{\alpha}}{\partial \chi} &= 0 \\
\frac{\partial \dot{\alpha}}{\partial m} &= 0 & \frac{\partial \dot{\alpha}}{\partial \alpha} &= 0 \\
\frac{\partial \dot{\alpha}}{\partial w_2} &= 1 & \frac{\partial \dot{\alpha}}{\partial u_8} &= 0 \\
\frac{\partial \dot{\alpha}}{\partial u_9} &= 0 & \frac{\partial \dot{\alpha}}{\partial t} &= 0
\end{aligned} \tag{B.72}$$

Partial Derivatives for g

$$g = \frac{\mu}{r^2} \tag{B.73}$$

$$\begin{array}{lllllll}
\frac{\partial g}{\partial r} & = & -\frac{2g}{r} & \frac{\partial g}{\partial \theta} & = & 0 \\
\frac{\partial g}{\partial \phi} & = & 0 & \frac{\partial g}{\partial v} & = & 0 \\
\frac{\partial g}{\partial \gamma} & = & 0 & \frac{\partial g}{\partial \chi} & = & 0 \\
\frac{\partial g}{\partial m} & = & 0 & \frac{\partial g}{\partial \alpha} & = & 0 \\
\frac{\partial g}{\partial w_2} & = & 0 & \frac{\partial g}{\partial u_8} & = & 0 \\
\frac{\partial g}{\partial u_9} & = & 0 & \frac{\partial g}{\partial t} & = & 0
\end{array} \tag{B.74}$$

Partial Derivatives for D

$$D = \frac{\rho v^2 S C_D}{2m} \tag{B.75}$$

$$\begin{array}{lllllll}
\frac{\partial D}{\partial r} & = & \frac{v^2 S C_D}{2m}\frac{\partial \rho}{\partial r} & \frac{\partial D}{\partial \theta} & = & 0 \\
\frac{\partial D}{\partial \phi} & = & 0 & \frac{\partial D}{\partial v} & = & \frac{\rho v S C_D}{m} \\
\frac{\partial D}{\partial \gamma} & = & 0 & \frac{\partial D}{\partial \chi} & = & 0 \\
\frac{\partial D}{\partial m} & = & -\frac{\rho v^2 S C_D}{2m^2} & \frac{\partial D}{\partial \alpha} & = & \frac{\rho v^2 S}{2m}\frac{\partial C_D}{\partial \alpha} \\
\frac{\partial D}{\partial w_2} & = & 0 & \frac{\partial D}{\partial u_8} & = & 0 \\
\frac{\partial D}{\partial u_9} & = & 0 & \frac{\partial D}{\partial t} & = & 0
\end{array} \tag{B.76}$$

Partial Derivatives for L

$$L = \frac{\rho v^2 S C_L}{2m} \tag{B.77}$$

$$
\begin{array}{lllllll}
\frac{\partial L}{\partial r} & = & \frac{v^2 S C_L}{2m}\frac{\partial \rho}{\partial r} & \frac{\partial L}{\partial \theta} & = & 0 \\
\frac{\partial L}{\partial \phi} & = & 0 & \frac{\partial L}{\partial v} & = & \frac{\rho v S C_L}{m} \\
\frac{\partial L}{\partial \gamma} & = & 0 & \frac{\partial L}{\partial \chi} & = & 0 \\
\frac{\partial L}{\partial m} & = & -\frac{\rho v^2 S C_L}{2m^2} & \frac{\partial L}{\partial \alpha} & = & \frac{\rho v^2 S}{2m}\frac{\partial C_L}{\partial \alpha} \\
\frac{\partial L}{\partial w_2} & = & 0 & \frac{\partial L}{\partial u_8} & = & 0 \\
\frac{\partial L}{\partial u_9} & = & 0 & \frac{\partial L}{\partial t} & = & 0
\end{array}
\tag{B.78}
$$

Partial Derivatives for ρ

$$
\rho = \rho_0 \exp(-(r - R_e)/H) \tag{B.79}
$$

$$
\begin{array}{lllllll}
\frac{\partial \rho}{\partial r} & = & -\frac{\rho}{H} & \frac{\partial \rho}{\partial \theta} & = & 0 \\
\frac{\partial \rho}{\partial \phi} & = & 0 & \frac{\partial \rho}{\partial v} & = & 0 \\
\frac{\partial \rho}{\partial \gamma} & = & \cos\gamma & \frac{\partial \rho}{\partial \chi} & = & 0 \\
\frac{\partial \rho}{\partial m} & = & 0 & \frac{\partial \rho}{\partial \alpha} & = & 0 \\
\frac{\partial \rho}{\partial w_2} & = & 0 & \frac{\partial \rho}{\partial u_8} & = & 0 \\
\frac{\partial \rho}{\partial u_9} & = & 0 & \frac{\partial \rho}{\partial t} & = & 0
\end{array}
\tag{B.80}
$$

Partial Derivatives for C_D

$$
C_D = C_{D_0} + C_{D_1}\alpha + C_{D_2}\alpha^2 \tag{B.81}
$$

$$
\begin{aligned}
\frac{\partial C_D}{\partial r} &= 0 \quad \frac{\partial C_D}{\partial \theta} = 0 \\
\frac{\partial C_D}{\partial \phi} &= 0 \quad \frac{\partial C_D}{\partial v} = 0 \\
\frac{\partial C_D}{\partial \gamma} &= 0 \quad \frac{\partial C_D}{\partial \chi} = 0 \\
\frac{\partial C_D}{\partial m} &= 0 \quad \frac{\partial C_D}{\partial \alpha} = C_{D_1} + 2C_{D_2}\alpha \\
\frac{\partial C_D}{\partial w_2} &= 0 \quad \frac{\partial C_D}{\partial u_8} = 0 \\
\frac{\partial C_D}{\partial u_9} &= 0 \quad \frac{\partial C_D}{\partial t} = 0
\end{aligned}
\tag{B.82}
$$

Partial Derivatives for C_L

$$
C_L = C_{L_0} + C_{L_1}\alpha \tag{B.83}
$$

$$
\begin{aligned}
\frac{\partial C_L}{\partial r} &= 0 \quad \frac{\partial C_L}{\partial \theta} = 0 \\
\frac{\partial C_L}{\partial \phi} &= 0 \quad \frac{\partial C_L}{\partial v} = 0 \\
\frac{\partial C_L}{\partial \gamma} &= 0 \quad \frac{\partial C_L}{\partial \chi} = 0 \\
\frac{\partial C_L}{\partial m} &= 0 \quad \frac{\partial C_L}{\partial \alpha} = C_{L_1} \\
\frac{\partial C_L}{\partial w_2} &= 0 \quad \frac{\partial C_L}{\partial u_8} = 0 \\
\frac{\partial C_L}{\partial u_9} &= 0 \quad \frac{\partial C_L}{\partial t} = 0
\end{aligned}
\tag{B.84}
$$

Partial Derivatives for the Path Constraint on Bank Angle

$$
p_5 = u_8^2 + u_9^2 \tag{B.85}
$$

$$
\begin{aligned}
\frac{\partial p_5}{\partial r} &= 0 & \frac{\partial p_5}{\partial \theta} &= 0 \\
\frac{\partial p_5}{\partial \phi} &= 0 & \frac{\partial p_5}{\partial v} &= 0 \\
\frac{\partial p_5}{\partial \gamma} &= 0 & \frac{\partial p_5}{\partial \chi} &= 0 \\
\frac{\partial p_5}{\partial m} &= 0 & \frac{\partial p_5}{\partial \alpha} &= 0 \\
\frac{\partial p_5}{\partial w_2} &= 0 & \frac{\partial p_5}{\partial u_8} &= 2u_8 \\
\frac{\partial p_5}{\partial u_9} &= 2u_9 & \frac{\partial p_5}{\partial t} &= 0
\end{aligned}
\tag{B.86}
$$

Partial Derivatives for the Objective Functional

$$
\mathcal{J} = k_1 \frac{\dot{Q}}{Q_{max}} + k_2 \frac{q}{q_{max}} + k_3 \frac{a^2}{a^2_{max}} \tag{B.87}
$$

$$
\begin{aligned}
\frac{\partial \mathcal{J}}{\partial r} &= \frac{k_1}{Q_{max}}\frac{\partial \dot{Q}}{\partial r} + \frac{k_2}{q_{max}}\frac{\partial q}{\partial r} + \frac{k_3}{a^2_{max}}\frac{\partial a^2}{\partial r} & \frac{\partial \mathcal{J}}{\partial \theta} &= 0 \\
\frac{\partial \mathcal{J}}{\partial \phi} &= 0 & \frac{\partial \mathcal{J}}{\partial v} &= \frac{k_1}{Q_{max}}\frac{\partial \dot{Q}}{\partial r} + \frac{k_2}{q_{max}}\frac{\partial q}{\partial r} + \frac{k_3}{a^2_{max}}\frac{\partial a^2}{\partial r} \\
\frac{\partial \mathcal{J}}{\partial \gamma} &= 0 & \frac{\partial \mathcal{J}}{\partial \chi} &= 0 \\
\frac{\partial \mathcal{J}}{\partial m} &= \frac{k_1}{Q_{max}}\frac{\partial \dot{Q}}{\partial r} + \frac{k_2}{q_{max}}\frac{\partial q}{\partial r} + \frac{k_3}{a^2_{max}}\frac{\partial a^2}{\partial r} & \frac{\partial \mathcal{J}}{\partial \alpha} &= \frac{k_1}{Q_{max}}\frac{\partial \dot{Q}}{\partial r} + \frac{k_2}{q_{max}}\frac{\partial q}{\partial r} + \frac{k_3}{a^2_{max}}\frac{\partial a^2}{\partial r} \\
\frac{\partial \mathcal{J}}{\partial w_2} &= 0 & \frac{\partial \mathcal{J}}{\partial u_8} &= 0 \\
\frac{\partial \mathcal{J}}{\partial u_9} &= 0 & \frac{\partial \mathcal{J}}{\partial t} &= 0
\end{aligned}
\tag{B.88}
$$

Partial Derivatives for $\dot{Q}$

$$
\dot{Q} = k_{therm} \left(\frac{\rho}{\rho_0}\right)^{1/2} \left(\frac{v}{v_{circ}}\right)^{3.15} \tag{B.89}
$$

$$
\begin{aligned}
\frac{\partial \dot{Q}}{\partial r} &= \tfrac{1}{2\rho_0} k_{therm} \left(\tfrac{\rho}{\rho_0}\right)^{-1/2} \tfrac{\partial \rho}{\partial r} \left(\tfrac{v}{v_{circ}}\right)^{3.15} & \frac{\partial \dot{Q}}{\partial \theta} &= 0 \\
\frac{\partial \dot{Q}}{\partial \phi} &= 0 & \frac{\partial \dot{Q}}{\partial v} &= \tfrac{3.15}{v_{circ}} k_{therm} \left(\tfrac{\rho}{\rho_0}\right)^{1/2} \left(\tfrac{v}{v_{circ}}\right)^{2.15} \\
\frac{\partial \dot{Q}}{\partial y} &= 0 & \frac{\partial \dot{Q}}{\partial \chi} &= 0 \\
\frac{\partial \dot{Q}}{\partial m} &= 0 & \frac{\partial \dot{Q}}{\partial \alpha} &= 0 \\
\frac{\partial \dot{Q}}{\partial w_2} &= 0 & \frac{\partial \dot{Q}}{\partial u_8} &= 0 \\
\frac{\partial \dot{Q}}{\partial u_9} &= 0 & \frac{\partial \dot{Q}}{\partial t} &= 0
\end{aligned}
\tag{B.90}
$$

Partial Derivatives for q

$$
q = \frac{\rho v^2}{2} \tag{B.91}
$$

$$
\begin{aligned}
\frac{\partial q}{\partial r} &= \tfrac{v^2}{2} \tfrac{\partial \rho}{\partial r} & \frac{\partial q}{\partial \theta} &= 0 \\
\frac{\partial q}{\partial \phi} &= 0 & \frac{\partial q}{\partial v} &= \rho v \\
\frac{\partial q}{\partial y} &= 0 & \frac{\partial q}{\partial \chi} &= 0 \\
\frac{\partial q}{\partial m} &= 0 & \frac{\partial q}{\partial \alpha} &= 0 \\
\frac{\partial q}{\partial w_2} &= 0 & \frac{\partial q}{\partial u_8} &= 0 \\
\frac{\partial q}{\partial u_9} &= 0 & \frac{\partial q}{\partial t} &= 0
\end{aligned}
\tag{B.92}
$$

Partial Derivatives for a^2

$$
a^2 = L^2 + D^2 \tag{B.93}
$$

$$
\begin{array}{llll}
\frac{\partial a^2}{\partial r} & = & 2\frac{\partial L}{\partial r} + 2\frac{\partial D}{\partial r} & \frac{\partial a^2}{\partial \theta} = 0 \\
\frac{\partial a^2}{\partial \phi} & = & 0 & \frac{\partial a^2}{\partial v} = 2\frac{\partial L}{\partial v} + 2\frac{\partial D}{\partial v} \\
\frac{\partial a^2}{\partial y} & = & 0 & \frac{\partial a^2}{\partial \chi} = 0 \\
\frac{\partial a^2}{\partial m} & = & 2\frac{\partial L}{\partial m} + 2\frac{\partial D}{\partial m} & \frac{\partial a^2}{\partial \alpha} = 2\frac{\partial L}{\partial \alpha} + 2\frac{\partial D}{\partial \alpha} \\
\frac{\partial a^2}{\partial w_2} & = & 0 & \frac{\partial a^2}{\partial u_8} = 0 \\
\frac{\partial a^2}{\partial u_9} & = & 0 & \frac{\partial a^2}{\partial t} = 0
\end{array}
\tag{B.94}
$$

Bibliography

[1] Battin, R. H., *An Introduction to the Mathematics and Methods of Astrodynamics, Revised Edition*, American Institute of Aeronautics and Astronautics, Inc., Reston, VA, 1999.

[2] Bauer, T., Betts, J., Hallman, W., Huffman, W., Zondervan, K., "Solving the Optimal Control Problem Using a Nonlinear Programming Technique Part 2: Optimal Shuttle Ascent Trajectories", *Proceedings of the AIAA/AAS Astrodynamics Conference*, AIAA-84-2038, Seattle, WA, 20-22 August 1984.

[3] Bazaraa, M. S., Sherali, H. D., Shetty, C. M., *Nonlinear Programming Theory and Algorithms*, John Wiley and Sons, Inc., New York, NY, 1993.

[4] Belman, R.,Kalaba, R., *Dynamic Programming and Modern Control Theory*, Academic Press, Inc., San Diego, CA, 1965.

[5] Betts, J. T. and Gablonsky, J. M., "A Comparison of Interior Point and SQP Methods on Optimal Control Problems", M&CT-TECH-02-004, Phantom Works Mathematics and Computing Technology, The Boeing Company, Seattle, WA, March 2002.

[6] Betts, J. T., *Practical Methods for Optimal Control Using Nonlinear Programming* Society for Industrial and Applied Mathematics, Philadelphia, PA, 2001.

[7] Betts, J. T., “Survey of Numerical Methods for Trajecotry Optimization,” *Journal of Guidance, Control, and Dynamics*, Vol. 21, No. 2, 1998, pp. 193-207.

[8] Bryson, A., and Ho, Y., *Applied Optimal Control*, Hemisphere Publishing Corporation, New York, 1975.

[9] Calise, A. J., Melamed, N., and Lee, S., “Design and Evaluation of a Three-Dimensional Optimal Ascent Guidance Algorithm,” *Journal of Guidance, Control, and Dynamics*, Vol. 21, No. 6, 1998, pp. 867-875.

[10] Canuto, C., Hussaini, M. Y., Quarteroni, A., and Zang, T. A., *Spectral Methods in Fluid Dynamics*, Springer-Verlag, New York, 1988.

[11] Chapra, S. C. and Canale, R. H., *Numerical Methods for Engineers*, WCB/McGraw-Hill, Boston, MA, 1998.

[12] Clarke, K. A., *Performance Optimization Study of a Common Aero Vehicle Using a Legendre Pseudospectral Method* S. M. Thesis, Department of Aeronautics and Astronautics, MIT, May 2003.

[13] Conway, B. A., and Larson, K. M., “Collocation Versus Differential Inclusion in Direct Optimization,” *Journal of Guidance, Control, and Dynamics*, Vol. 21, No. 5, 1998, pp. 780-785.

[14] Dyckman, T. R., *Benchmark Characterization for Reusable Launch Vehicle Onboard Trajectory Generation Using a Legendre Pseudospectral Optimization Method* S. M. Thesis, Department of Aeronautics and Astronautics, MIT, June 2002.

[15] Elnagar, J., Kazemi, M. A., and Razzaghi, M., “The Pseudospectral Legendre Method for Discretizing Optimal Control Problems,” *IEEE Transactions on Automatic Control,* Vol. 40, No. 10, 1995, pp. 1793-1796.

[16] Fahroo, F., and Ross, I. M., "Costate Estimation by a Legendre Pseudospectral Method," *Journal of Guidance, Control, and Dynamics*, Vol. 24, No. 2, 2001, pp.270-277.

[17] Fahroo, F., and Ross, I. M., "A Spectral Patching Method for Direct Trajectory Optimization," *Journal of Astronautical Sciences*,Vol. 48, Nos. 2 and 3, 2000, pp. 269-286.

[18] Fahroo, F., and Ross, I. M., "Computational Optimal Control by Spectral Collocation with Differential Inclusion," *Proceedings of the 1999 Flight Mechanics Symposium,* NASA CP-1999-209235, 1999, pp. 185-200.

[19] Fornberg, B., *A Practical Guide to Pseudospectral Methods*, Cambridge University Press, New York, 1996.

[20] Franklin, G. F., Powell, J. D, and Emami-Naeini, A., *Feedback Control of Dynamic Systems*, Prentice Hall, Upper Saddle River, NJ, 2002.

[21] Gill, P. E., Murray, W., and Saunders, M. A., "SNOPT: An SQP Algorithm for Large-Scale Constrained Optimization," *SIAM Journal on Optimization*, Vol.12, No.4, 2002, pp. 979-1006

[22] Gill, P. E., Saunders, M. A., and Wright, M. H., "User's Guide for NPSOL 5.0: A Fortran Package for Nonlinear Programming", Technical Report SOL 86-2, Department of Mathematics, University of California, San Diego, 30 July 1998.

[23] Gill, P. E., Murray, W., and Saunders, M. A., "User's guide for SNOPT 5.3: A Fortran package for large-scale nonlinear programming". Technical Report 97-5, Department of Mathematics, University of California, San Diego, La Jolla, CA, February 1999.

[24] Gottlieg, David and Orszag, Steven A., *Numerical Analysis of Spectral Methods: Theory and Applications* Society for Industrial and Applied Mathematics, Philadelphia, PA, 1997.

[25] Greenwood, Donald T., *Principles of Dynamics* Prentice Hall, Upper Saddle River, NJ, 1998.

[26] Harpold, J. C. and Graves, C. A., "Shuttle Entry Guidance," *Journal of the Astronautical Sciences*, Vol. 27, No. 3, 1979, pp. 239-268.

[27] Kirk, Donald E., *Optimal Control Theory: An Introduction*, Prentice-Hall Inc., New Jersey, 1970.

[28] Mease, K. D., Chen, D. T., Teufel, P., Schonenberger, H., "Reduced-Order Entry Trajectory Planning for Acceleration Guidance," *Journal of Guidance, Control, and Dynamics*, Vol. 25, No. 2, 2002, pp. 287-266.

[29] O'Reilly, Oliver M. , *Engineering Dynamics A primer*, Springer, New York, 2001.

[30] Rao, Anil V., "Extension of a Pseudospectral Legendre Method to Multiple-Phase Optimal Control Problems" *Proceedings of the AIAA Guidance, Navigation, and Control Conference and Exhibit*, AIAA-2003-5634, Austin, TX, 11-14 August 2003.

[31] Rao, Anil V., Clarke, K., "Performance Optimization of a Maneuvering Re-entry Vehicle Using a Legendre Pseudospectral Method", *Proceedings of the AIAA Guidance, Navigation, and Control Conference and Exhibit*, AIAA 2002-4885, Monterey, CA, 5-8 August 2002.

[32] Rea, J. R., *A Legendre Pseudospectral Method for Rapid Optimization of Launch Vehicle Trajectories.* S. M. Thesis, Department of Aeronautics and Astronautics, MIT, June 2001.

[33] Rockwell International, *Aerodynamic Design Data Book, Volume 2, Launch Vehicle,* SD72-SH-0600, Vol. 2L, June 1981.

[34] Ross, Michael, Fahroo, Fariba, "A Direct Method for Solving Nonsmooth Optimal Control Problems", *Proceedings of the 2002 World Congress of*

the International Federation on Automatic Control, IFAC 2002, Barcelona, Spain, July 2002.

[35] Space Shuttle Reference Manual, Rev. 1998.

[36] Trefethen, L., *Spectral Methods in MATLAB*, Society for Industrial and Applied Mathematics, Philadelphia, Pennsylvania, 2000.

[37] Vinh, N. X., Busemann, A., and Culp, R. D., *Hypersonic and Planetary Entry Flight Mechanics*, University of Michigan Press, Ann Arbor, MI, 1980.

[38] Vinh, N. X., *Optimal Trajectories In Atmospheric Flight*, Elsevier Scientific Publishing Company, New York, 1981.

[39] Zondervan, K., Bauer, T., Betts, J., Huffman, W., "Solving the Optimal Control Problem Using a Nonlinear Programming Technique Part 3: Optimal Shuttle Reentry Trajectories", *Proceedings of the AIAA/AAS Astrodynamics Conference*, AIAA-84-2039, Seattle, WA, 20-22 August 1984.